

C.1

**ARCHIVE COPY
DO NOT LOAN**

WING LEADING EDGE HEATING AND PRESSURE PROBING,
BODY FLAP HEATING, AND VAPOR SCREEN TESTS ON
THE SPACE SHUTTLE ORBITER CONFIGURATION AT
MACH 8 AND 10



L. A. Ticatch and S. A. Stepanek and
G. D. Wannenwetsch
Calspan Field Services, Inc.

Property of U. S. Air Force
AEDC LIBRARY
F40600-81-C-0004

January 1983

Final Report for Period July 27, 1982 - November 23, 1982

Approved for public release; distribution is unlimited. Per
Mark Amundson (STINFO OFFICER) in letter dated 29 June
1998.

**TECHNICAL REPORTS
FILE COPY**

**ARNOLD ENGINEERING DEVELOPMENT CENTER
ARNOLD AIR FORCE STATION, TENNESSEE
AIR FORCE SYSTEMS COMMAND
UNITED STATES AIR FORCE**

AEDC TECHNICAL LIBRARY



NOTICES

When U. S. Government drawings, specifications, or other data are used for any purpose other than a definitely related Government procurement operation, the Government thereby incurs no responsibility nor any obligation whatsoever, and the fact that the government may have formulated, furnished, or in any way supplied the said drawings, specifications, or other data, is not to be regarded by implication or otherwise, or in any manner licensing the holder or any other person or corporation, or conveying any rights or permission to manufacture, use, or sell any patented invention that may in any way be related thereto.

References to named commercial products in this report are not to be considered in any sense as an endorsement of the product by the United States Air Force or the Government.

APPROVAL STATEMENT

This report has been reviewed and approved.



ALBERT H. BOUDREAU
Reentry Systems Branch
Deputy for Operations

Approved for publication:

FOR THE COMMANDER



JOHN M. RAMPY, Director
Aerospace Flight Dynamics Test
Deputy for Operations

UNCLASSIFIED

SECURITY CLASSIFICATION OF THIS PAGE (When Data Entered)

REPORT DOCUMENTATION PAGE		READ INSTRUCTIONS BEFORE COMPLETING FORM
1. REPORT NUMBER AEDC-TSR-83-V7	2. GOVT ACCESSION NO.	3. RECIPIENT'S CATALOG NUMBER
4. TITLE (and Subtitle) WING LEADING EDGE HEATING AND PRESSURE PROBING, BODY FLAP HEATING, AND VAPOR SCREEN TESTS ON THE SPACE SHUTTLE ORBITER CONFIGURATION AT MACH 8 AND 10		5. TYPE OF REPORT & PERIOD COVERED Final Report July 27, 1982 - Nov. 23, 1982
7. AUTHOR(s) L. A. Ticatch, S. A. Stepanek and G. D. Wannenwetsch Calspan Field Services, Inc.		6. PERFORMING ORG. REPORT NUMBER
9. PERFORMING ORGANIZATION NAME AND ADDRESS Arnold Engineering Development Center Air Force Systems Command Arnold Air Force Station, TN 37389		8. CONTRACT OR GRANT NUMBER(s)
11. CONTROLLING OFFICE NAME AND ADDRESS AFWAL/FIMG Wright-Patterson Air Force Base, OH 45433		10. PROGRAM ELEMENT, PROJECT, TASK AREA & WORK UNIT NUMBERS Program Element 62201F Control No. 2404
14. MONITORING AGENCY NAME & ADDRESS (if different from Controlling Office)		12. REPORT DATE January 1983
		13. NUMBER OF PAGES 95
		15. SECURITY CLASS. (of this report) UNCLASSIFIED
		15a. DECLASSIFICATION/DOWNGRADING SCHEDULE N/A
16. DISTRIBUTION STATEMENT (of this Report) Approved for public release; distribution is unlimited. Per Mark Amundson (STINFO OFFICER) in letter dated 29 June 1998.		
17. DISTRIBUTION STATEMENT (of the abstract entered in Block 20, if different from Report)		
18. SUPPLEMENTARY NOTES Available in Defense Technical Information Center (DTIC).		
19. KEY WORDS (Continue on reverse side if necessary and identify by block number) heat transfer body flap pressure vapor screen leading edge space shuttle orbiter thin-film gage hypersonic testing		
20. ABSTRACT (Continue on reverse side if necessary and identify by block number) Tests were performed on scale models of the Space Shuttle Orbiter at angles of attack from 25 to 40 degrees at Mach 8 and 10. Thin-film instrumentation and testing techniques were used to provide aero-heating measurements on the wing leading edge. Standard techniques were adapted to obtain body flap heating measurements over a range of flap angles (0-20 deg) using a continuous sweep testing mode for various boundary layer transition locations. Pitot pressure probing was conducted in the vicinity of the wing leading edge and vapor screen photographs were obtained at various stations along the entire length of the		

UNCLASSIFIED

SECURITY CLASSIFICATION OF THIS PAGE (When Data Entered)

20. (Continued)

orbiter body. Only sample tabulations of the test results are included in this documentary report.

CONTENTS

	<u>Page</u>
NOMENCLATURE	4
1.0 INTRODUCTION	7
2.0 TEST FACILITIES DESCRIPTION	
2.1 Wind Tunnels	10
2.2 Precision of Measurements	11
3.0 BODY FLAP HEATING (PHASE IA)	
3.1 Test Article	16
3.2 Test Instrumentation	17
3.3 Test Conditions and Procedures	17
3.4 Data Reduction	18
3.5 Data Package Presentation	19
4.0 VAPOR SCREEN (PHASE IB)	
4.1 Test Article	32
4.2 Test Instrumentation	32
4.3 Test Conditions and Procedures	33
4.4 Data Reduction	34
4.5 Data Package Presentation	34
5.0 PITOT PRESSURE PROBING (PHASE II)	
5.1 Test Article	44
5.2 Test Instrumentation	45
5.3 Test Conditions and Procedures	45
5.4 Data Reduction	47
5.5 Data Package Presentation	47
6.0 LEADING EDGE HEATING DEMONSTRATION (PHASE III)	
6.1 Test Article	64
6.2 Test Instrumentation	65
6.3 Test Conditions and Procedures	66
6.4 Data Reduction	66
6.5 Data Package Presentation	68
7.0 WING LEADING EDGE HEATING TEST (PHASE IV)	
7.1 Test Article	81
7.2 Test Instrumentation	81
7.3 Test Conditions and Procedures	82
7.4 Data Reduction	82
7.5 Data Package Presentation	82

APPENDIX I

REFERENCE HEAT-TRANSFER COEFFICIENTS	95
--	----

ILLUSTRATIONS

Figures

2.1 Tunnel B	12
2.2 Tunnel C	13
3.1 Phase IA Test Article in the Tunnel B Test Section	20
3.2 Phase IA Test Article in the Tunnel B Installation Tank	21

	<u>Page</u>
3.3 Sketch of Phase IA Installation in Tunnel B	22
3.4 Sketch of Phase IA Installation in Tunnel C	23
3.5 Basic Dimensions and Coordinates System Definition for the Body Flap Heating Test Article	24
3.6 Photograph of Spherical Ball Trip Band Used to Vary Transition Location During Body Flap Heating Tests	25
3.7 Sketch of Coax Gage Locations for the Body Flap Heating Tests.	26
4.1 Phase IB Test Article in the Tunnel B Test Section	35
4.2 Phase IB Test Article in the Tunnel B Installation Tank	36
4.3 Sketch Phase IB Test Article Installation in Tunnel B	37
4.4 Basic Dimensions and Coordinate System Definition	38
4.5 Sketch of Translating Laser and Camera Platform	39
4.6 Sample Vapor Screen Photograph	40
5.1 Phase II Test Article in the Tunnel B Test Section	48
5.2 Phase II Test Article in the Tunnel B Installation Tank.	49
5.3 Sketch of Phase II Installation.	50
5.4 Bottom View of 94-0 Shuttle Orbiter Model Modified with Probing Hardware	51
5.5 Closeup of Pitot Pressure Rake	52
5.6 Pitot Pressure Rake Dimensions and Probe Identification	53
5.7 Location of Bottom Probe on Each Rake Relative to Wing Surface.	54
5.8 Probing Mechanism on Test Article with Vernier Scale	55
5.9 Vertical Pitot Pressure Survey and Data Repeatability	56
5.10 Lateral Pitot-Pressure Survey - Probe #4 and Probe #104	57
5.11 Model Pitch Angle Sensitivity Summary	58
6.1 Phase III Test Article in the Tunnel B Test Section.	69
6.2 Phase III Test Article Installation in Tunnel B	70
6.3 Closeup of the Leading Edge Heating Demonstration Test Article	71
6.4 Basic Dimensions of the Macor® Substrate and Holder for the Leading Edge Heating Demonstration Test Article	73
6.5 Leading Edge Heating Demonstration Test Article with Flow Shield	74
6.6 Sketch of the Installation Scheme of the Leading Edge Heating Demonstration Test Article Flow Shield in Tunnel B	75
6.7 Instrumentation Location Sketch for the Leading Edge Heating Demonstration Test Article	76
7.1 Phase IV Test Article in the Tunnel C Test Section	83
7.2 Sketch of Phase IV Installation in Tunnel C.	84
7.3 Instrumented Segment of the Orbiter Wing Leading Edge	85
7.4 Basic Dimensions for the Wing Leading Edge Heating Test Article.	86
7.5 Closeup of Wing Leading Edge Macor Insert.	87
7.6 Basic Dimensions of the Wing Leading Edge Instrumented Insert with Gage Numbering Identification	89
7.7 Measured Leading Edge Contours	90

Tables

1.1	Data Transmittal Summary	9
2.1	Estimated Uncertainties for Basic Measurements in Tunnels B and C	14
2.2	Estimated Uncertainties for Calculated Parameters	15
3.1	Coax Gage Coordinates for the Body Flap Heating Test Article	27
3.2	Summary of Photographic Coverage for the Body Flap Heating Test	28
3.3	Run Summary for the Body Flap Heating Tests	29
4.1	Summary of Photographic Coverage for Vapor Screen Test . . .	42
4.2	Summary of Vapor Screen Test	43
5.1	Average Height of Probes above Model Surface	59
5.2	Summary of Photographic Coverage for Pressure Probing Test .	60
5.3	Run Summary for the Pitot Pressure Probing Test	61
6.1	Instrumentation Locations for the Leading Edge Heating Demonstration Test Article	77
6.2	Summary of Photographic Coverage for Leading Edge Heating Demonstration Test	78
6.3	Run Summary for the Leading Edge Heating Demonstration Test	79
7.1	Thin Film Coordinates for the Wing Leading Edge Heating Test Article.	91
7.2	Summary of Photographic Coverage for Wing Leading Edge Heating Test	92
7.3	Summary of Leading Edge Heating Test (Phase IV)	93

Sample Data

3.1	Typical Tabulated Data on Body Flap Heating Test	31
5.1	Typical Tabulated Data on the Pressure Probing Test	63
6.1	Typical Tabulated Data on the Leading Edge Heating Demonstration Test	80
7.1	Typical Tabulated Data on the Wing Leading Edge Heating Test	94

NOMENCLATURE

ALPI	Indicated pitch angle, deg
ALPHA	Angle of attack, deg
B	Wing span, in. (see Figs. 3.5, 4.4 or 7.4)
c	Model material specific heat, Btu/lbm-°R
C(t _n)	Coax gage scale factor, Btu/ft ² -sec ^{1/2} -°R
E	Thin-film output, mv
Flap angle, FA	Body flap deflection angle, deg (see Fig. 3.5)
H(REF)	Reference heat transfer coefficient based on a reference nose radius of 0.0175 ft, assuming a 3-D stagnation point (see Appendix I)
HREF1,2,3	Reference heat transfer coefficient based on reference dimensions R1, R2, or R3. This calculation pertains to 2-D stagnation points (see Appendix I)
H(TT)	Heat transfer coefficient based on TT, QDOT/(TT-TWi), Btu/ft ² -sec-°R
I(TT)	Enthalpy based on TT, Btu/lbm
I(TW)	Enthalpy based on TW, Btu/lbm
k	Model material thermal conductivity, Btu/ft-sec-°R
L	Reference length in. (see Figs. 3.5 and 4.4)
M	Free-stream Mach number
MU	Dynamic viscosity based on free-stream temperature, lbf-sec/ft ²
MUTT	Dynamic viscosity based on TT, lbf-sec/ft ²
ORIFICE	Pressure probe identification number
P	Free-stream static pressure, psia
PP	Pitot probe pressure, psia
PT	Tunnel stilling chamber pressure, psia
PT2	Stagnation pressure downstream of a normal shock, psia

PHII	Indicated roll angle, deg
Q	Free-stream dynamic pressure, psia
QDOT	Heat-transfer rate, Btu/ft ² -sec
R	Leading edge radius, (see Table 6.1), in.
RE	Free-stream unit Reynolds number, ft ⁻¹
RHO	Free-stream density, lbm/ft ³
RN	Reference nose radius used to calculate H(REF). (RN = 0.0175 ft)
RUN	Data set identification number
RX	Where X = 1, 2, or 3 is the reference dimension used to calculate HREF and STREF for 2-D stagnation points. For Phase III, R1 = 0.0117, R2 = 0.0208, and R3 = 0.042. For Phase IV, R1 = 0.0182
S	Surface distance coordinate (Table 6.1)
s	Thin-film sensitivity (°R/mv)
SRCK	Square root of the product of model density specific heat and thermal conductivity; Btu/ft ² -sec ^{1/2} -°R
STREF1,2,3	Referenced Stanton number based on reference dimensions R1, R2, or R3. This calculation pertains to 2-D stagnation points (see Appendix I)
ST(TT)	Stanton number based on total temperature $\frac{QDOT}{(RHO)(V)[I(TT) - I(TW)]}$
T	Free-stream static temperature, °R
t _j	Time of jth data loop, sec
t _n	Time of nth data loop, sec
TI	Initial wall temperature before injection into flow, °R
TIME	Elapsed time from lift-off, sec

TIMEINJ	Elapsed time from lift-off to arrival at tunnel centerline, sec
TT	Tunnel stilling chamber temperature, °R
TW	Model surface temperature, °R
ΔTW	Change in model surface temperature, °R
TW_0	Temperature at which film output zero was set, °R
V	Free-stream velocity, ft/sec
X	Model scale axial coordinate from model nose (See Figs. 3.5 and 4.4), in.
X_ℓ	Wing cross-sectional coordinate (see Fig. 7.7), in.
Y	Model scale lateral coordinate (see Figs. 3.5 and 4.4) in.
Y_ℓ	Wing cross-sectional coordinate (see Fig. 7.7), in.
YPP	Coordinate describing the distance along the leading edge survey line from the model centerline, in.
YPPCLI, YPPCLO	Distance along survey line from the model centerline to the right stack of the inboard (I) or outboard (O) probe rake, in.
Z	Model scale vertical coordinate (See Figs. 3.5 and 4.4)
ZPP	Pitot-pressure probe height above model, distance to probe centerline along normal to model surface, in.
α	Model angle of attack, deg
ρ	Model material density, lbm/ft ³

1.0 INTRODUCTION

The work reported herein was performed by the Arnold Engineering Development Center (AEDC), Air Force Systems Command (AFSC), under Program Element 62201F, Control Number 2404, at the request of the Air Force Wright Aeronautical Laboratory (AFWAL/FIMG). The AFWAL project manager was J. R. Hayes. The results were obtained by Calspan Field Services, Inc./AEDC Division, operating contractor for the Aerospace Flight Dynamics testing effort at the AEDC, AFSC, Arnold Air Force Station, Tennessee. The tests were performed in the Hypersonic Wind Tunnels B and C in the von Karman Gas Dynamics Facility (VKF) during the period from July 27 through November 23, 1982, under AEDC Project Number C407VB (Calspan No. V--B-1L).

The primary test objective was to provide data for aero-heating code verification and development. A secondary objective was to demonstrate new heat transfer testing techniques which will increase productivity and provide data in critical design areas on future reentry body projects. The shuttle body was chosen as being representative of winged re-entry bodies since its shape is well documented and vast amounts of previous ground and flight test data are available for comparison. A brief description of the various phases and objectives follows:

<u>Phase</u>	<u>Test</u>	<u>Report Section*</u>
IA	Body Flap Heating	3.0
IB	Vapor Screen	4.0
II	Pitot Pressure Probing	5.0
III	Leading Edge Heating Demonstration	6.0
IV	Wing Leading Edge Heating	7.0

The objectives of the body flap heating test, Phase IA, were to measure the variations in body flap heating at different deflection angles as a function of boundary layer transition location, and to verify that valid continuous sweep data could be taken on the flap. Two entries were made, one at Mach 8 and one at Mach 10. Free-stream Reynolds number ranged from 0.55 million to 1.9 million per foot and orbiter angle of attack (α) ranged from 25 to 40 deg. The flap angle ranged from 0 to 20 degrees. Phase IB, the vapor screen test, was performed in order to visualize the flow around the model. It was conducted at Mach 8 with α ranging from 25 to 40 degrees.

*In this report each phase is described in a separate section.

The objectives of Phase II, the Leading Edge Pressure Probing Phase, were to characterize the flow field in the strake leading edge region of the Space Shuttle Orbiter and to locate the impingement of the bow shock on the wing. Pitot pressure surveys were obtained at Mach 8 and a free-stream Reynolds number of 1.0 million per foot with the orbiter angle-of-attack ranging from 25 to 40 degrees.

Phase III, the Leading Edge Instrumentation Demonstration Phase, demonstrated a leading edge heating measurement technique that would accurately measure heat transfer on small radius leading edges and could be applied to a shuttle orbiter model. This test was run at Mach 8 and Reynolds number from 1.0 to 3.4 million per foot.

The objective of Phase IV, the Wing Leading Edge Heating Phase, was to measure the orbiter wing leading edge heating in the bow shock interaction region using the technique demonstrated in Phase III. This test was conducted at Mach 10 with free-stream Reynolds number from 0.56 to 1.5 million per foot and model angle of attack from 25 to 40 degrees.

As mentioned above, new testing techniques were involved in Phases I, III and IV. In Phase I, coax gage heat transfer data were obtained on the body flap as it was swept from 0 to 20 degrees. In Phases III and IV, a new technique was used to make heating measurements on small radius, leading-edge sections. This report describes the testing techniques used for these phases in a general manner and the test data which accompany this report were reduced using existing methods. In a future AEDC Technical Report (TR), details of these new testing techniques will be presented along with an analysis of the application of specialized data reduction techniques to improve data quality.

All test data, including photographs, logs and other information required to use the data have been transmitted to the sponsor as described in Table 1.1. Inquiries to obtain copies of the test data should be directed to AFWAL/FIMG, Wright-Patterson Air Force Base, Ohio 45433. A microfilm record of the tabulated data has been retained at AEDC.

TABLE 1.1 Data Transmittal Summary

The following items were transmitted to the Sponsors:

Mr. R. D. Neumann
Mr. J. R. Hayes
AFWAL/FIMG
Wright-Patterson AFB,
OH 45433

<u>Item</u>	<u>No. of Copies</u>
Test Summary Report	3
Final Tabulated Data	3
Body Flap Heat Test (Phase I)	
Pressure Probing Test (Phase II)	
Leading Edge Heating Development Test (Phase III)	
Wing Leading Edge Heating Test (Phase IV)	
Magnetic Tape of Final Data	1
Photographs	1
Installation	
Vapor Screen	
Shadowgraphs	

2.0 TEST FACILITIES DESCRIPTION

2.1 WIND TUNNELS

The AEDC Tunnels B and C (Figs. 2.1 and 2.2) are closed circuit, continuous flow, variable density wind tunnels. Each tunnel is equipped with a model injection system which allows removal of the model from the test section while the tunnel remains in operation.

Tunnels B and C have axisymmetric contoured nozzles and a 50-in.-diam test section. Tunnel B has two interchangeable nozzles to provide Mach numbers 6 and 8, Tunnel C has a Mach number 10 nozzle. Tunnel B operates over a range of stagnation pressure levels from 20 to 300 psia at Mach 6, and 50 to 900 psia at Mach number 8. The Tunnel C pressure range is 200 to 2000 psia. A natural-gas-fired combustion heater provides stagnation temperatures up to 1350°R in Tunnel B, and in series with an electric resistance heater provides temperatures up to 2260°R in Tunnel C. Each tunnel (throat, nozzle, test section, and diffuser) is cooled by integral, external water jackets. A description of the tunnels may be found in the Test Facilities Handbook*.

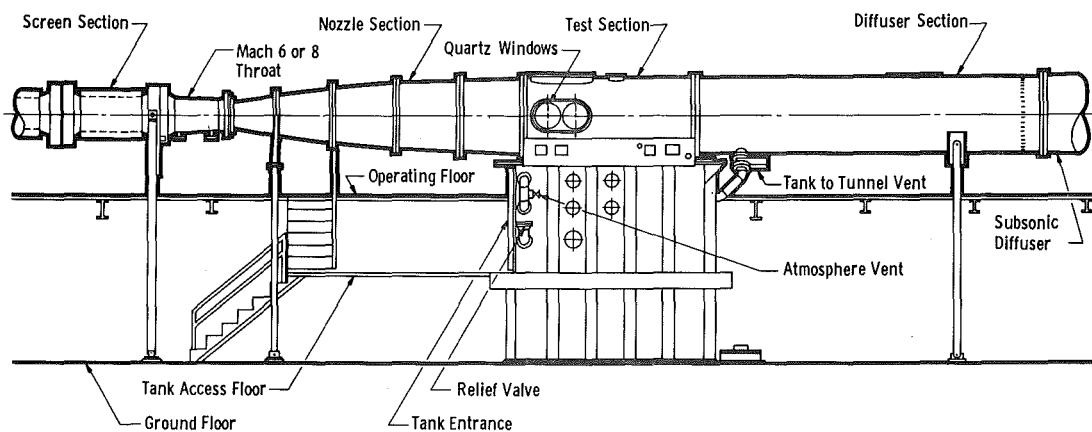
In the continuous flow wind tunnels (A, B, C), the model is mounted on a sting support mechanism in an installation tank directly underneath the tunnel test section. The tank is separated from the tunnel by a pair of fairing doors and a safety door. When closed, the fairing doors, except for a slot for the pitch sector, cover the opening to the tank and the safety door seals the tunnel from the tank area. After the model is prepared for a data run, the personnel access door to the installation tank is closed, the tank is vented to the tunnel flow, the safety and fairing doors are opened, the model is injected into the airstream, and the fairing doors are closed. After the data are obtained, the model is retracted into the tank and the sequence is reversed with the tank being vented to atmosphere to allow access to the model in preparation for the next injection. The sequence is repeated for each configuration change. When required, the model was cooled in the tank between injections to maintain initial wall temperatures within approximately 100 °F of room temperature.

*Test Facilities Handbook (Eleventh Edition). "von Karman Gas Dynamics Facility, Vol. 3." Arnold Engineering Development Center, April 1981.

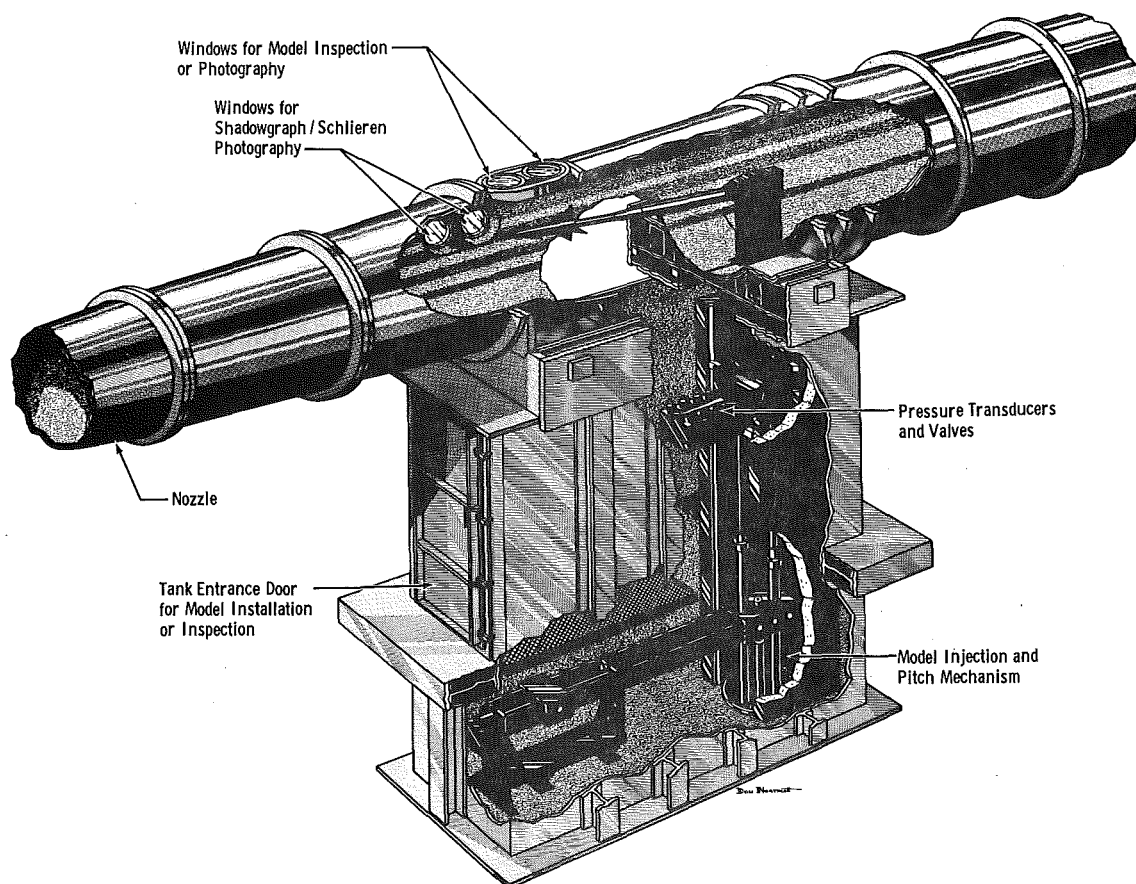
A given injection cycle is termed a run, and all data obtained are identified by run number.

2.2 PRECISION OF MEASUREMENTS

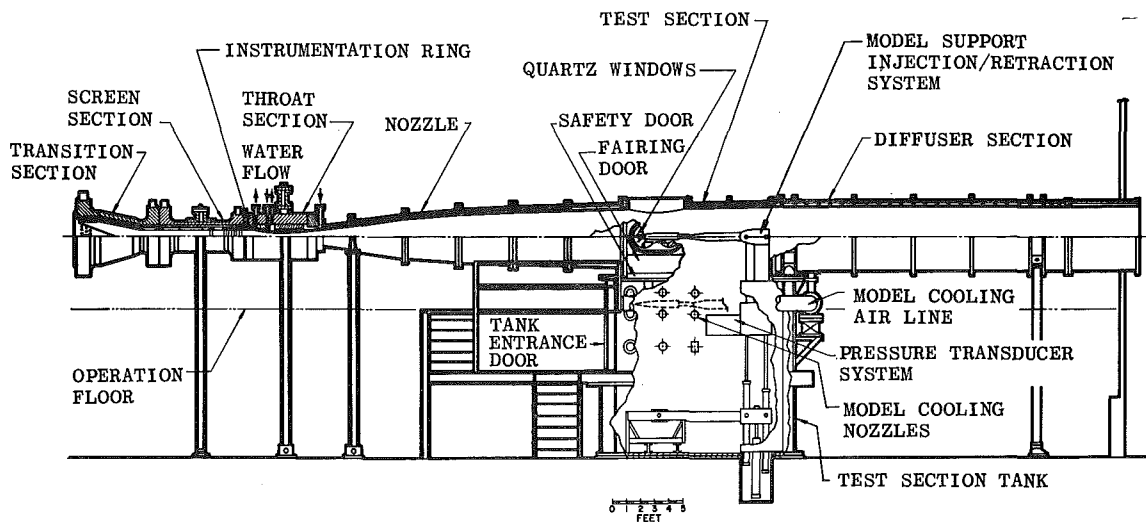
The instrumentation, recording devices, and calibration methods used to measure the primary tunnel parameters are listed in Table 2.1 along with estimated measurement uncertainties. The range and estimated uncertainties for primary parameters that were calculated from the measured parameters are listed in Table 2.2. In the Vapor Screen phase, there were no calculated parameters.



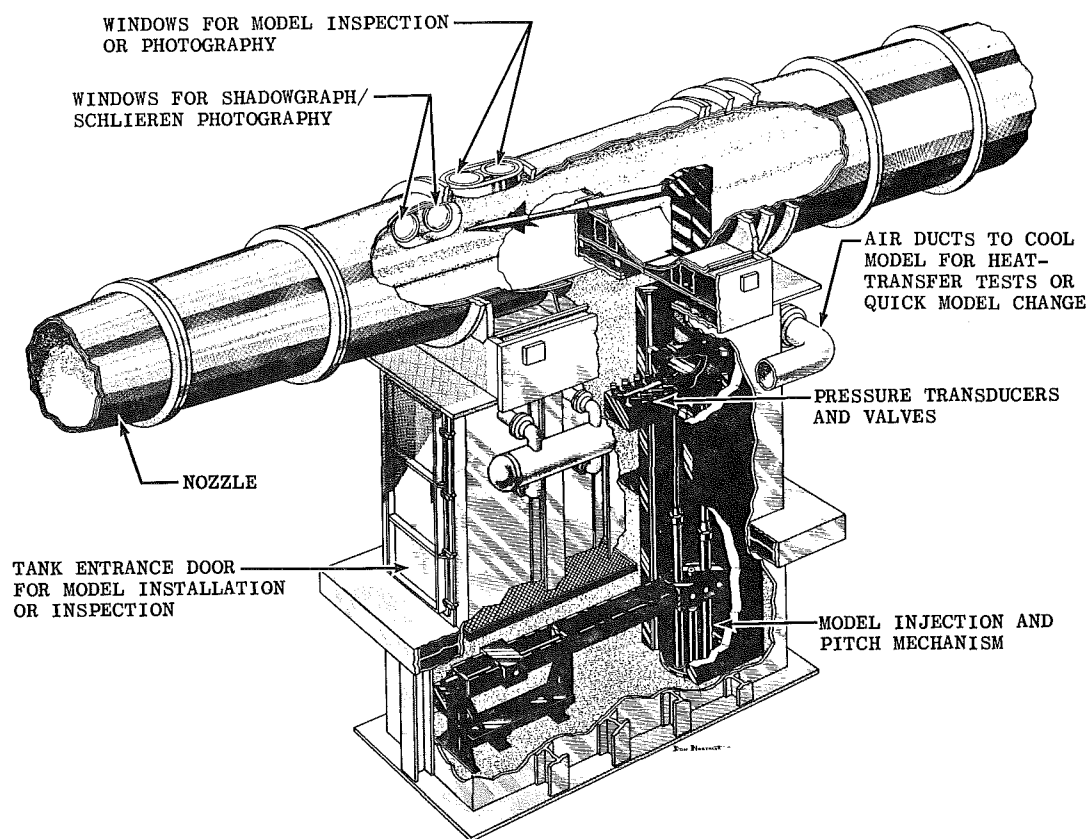
a. Tunnel assembly



b. Tunnel test section
Fig. 1. Tunnel B



a. Tunnel assembly



b. Tunnel test section
Fig. 1 Tunnel C

TABLE 2.1 Estimated Uncertainties for Basic Measurements
in Tunnels B and C

Parameter Designation	STEADY STATE ESTIMATED MEASUREMENT*							Range	Type of Measuring Device	Type of Recording Device	Method of System Calibration
	Precision Index ±(S)			Bias ±(B)		Uncertainty ±(B + t95S)					
	Percent of Reading	Unit of Measurement	Degree of Freedom	Percent of Reading	Unit of Measurement	Percent of Reading	Unit of Measurement				
PT, psia, (Tun. B)		0.02 0.11 0.11	30	0.25 0.25	 0.58	(0.25% + 0.04) (0.25% + 0.22)		104 to 200 200 to 232 232 to 1000	Bell & Howell Force and Pressure Transducer	Digital Data Acquisition System/Analog-to-Digital Converter	In-place application of Multiple Pressure Levels Measured with a Pressure Measuring Device Calibrated in the Standards Laboratory
(Tun. C)		0.62		0.16		(0.16% + 1.24)		>500 <2500			
TT, °F		1.0 1.0		 0.375	2.0	 (0.375% + 2.0)		32 to 530 530 to 2300	Chromel®-Alumel® Thermocouple	Doric Temperature Instrument/Digital Multiplexer	Thermocouple Verification of NPS Conformity by Voltage Substitution Calibration
ALPI, deg PHI, deg		0.025 0.20			0+ 0+		0.05 0.40	±13 ±180	Potentiometer	Digital Data Acquisition System/Analog-to-Digital Converter	Heidenhain Rotary Encoder ROD 700 Resolution 0.0006° Overall Accuracy 0.001°
PP, psia		4x10 ⁻³	2		0.01		0.03	0.2 < P < 15	Pressure Systems Incorporated ESP32 Pressor Sensor	Analog to Digital Converter/Digital Data Acquisition System	In-place application of Multiple Pressure Levels Measured with a Pressure Measuring Device Calibrated in the Standards Laboratory
TW, °F, coax gages		1.0			2.0		4.0	80 to 300	Chromel®-Constantan® Thermocouple	Digital Data Acquisition System/Analog-to-Digital Converter	Voltage Substitution Calibration (Secondary Standard)
Δ TW, °F, thin-film						5%	1	0 to 20 > 20	Thin-film platinum resistance thermometer		
Flap Angle, FA, deg		0.1			0.1		0.3	-1 to 21			

*REFERENCE: Thompson, J. W. and Abernethy, R. B. et al. "Handbook Uncertainty in Gas Turbine Measurements." AEDC-TR-73-5, February 1973

NOTES:

+Assumed to be zero

15

*Abernethy, R. B. et al. and Thompson, J. W. "Handbook Uncertainty in Gas Turbine Measurements." AEDC-TR-73-5 (AD 755356), February 1973.
+Assumed to be zero

3.0 BODY FLAP HEATING (PHASE IA)

3.1 TEST ARTICLE

A 0.0175-scale version of the Space Shuttle Orbiter, designated the 92-0 model, was used for the Body Flap Heating Phase (IA). A photograph of the test article in the Tunnel B test section is shown in Fig. 3.1. A photograph of the test article in the Tunnel B installation tank is shown in Fig. 3.2 which illustrates the positioning of the air manifolds used to provide cooling between injections. Figure 3.3 is a sketch of the installation of the test article in Tunnel B which identifies positioning in the test section and the standard sting components used during the test entry.

Testing at Mach 8 was originally to have been accomplished using a continuous body flap sweep mode for data acquisition. However, due to unforeseen noise generated during automatic flap movement, data were obtained during the Mach 8 entry using discrete flap angle positioning. After the Mach 8 tests were completed, additional shielding was provided for instrumentation leads within the model and through the sting to reduce these noise levels. Due to tunnel availability, the test phase which was subsequently run to verify the continuous sweep test mode was performed in Tunnel C at Mach 10, rather than in Tunnel B at Mach 8. The installation sketch for the Mach 10 entry is shown in Fig. 3.4.

To permit remotely-controlled, continuous sweeping of the body flap, the basic 92-0 model was modified to accommodate an on-board Superior Electric SLO-SYN electric motor. Changes to the basic orbiter external contour were confined to the lee-ward body region only. A shaft-drive system was used to allow the motor to move the body flap via a bell crank arrangement. The position of the motor, shaft, and crank drive system is illustrated in Fig. 3.5, along with the basic dimensions and coordinate system definitions for the model.

The SLO-SYN motor is a stepping device which produces a small angular drive shaft rotation when commanded by an input electrical impulse. A remote control system, supplied by AFWAL, was used to provide a continuous stream of command signals to the motor and thus provide flap motion as desired. This system also provided an analog voltage signal which was proportional to the number of step commands sent to the motor. This signal was recorded with the test data and, via pretest calibration, body flap angle could thereby be determined.

As mentioned previously, one objective of this test phase was to obtain heat-transfer data for the body flap for various locations of boundary layer transition along the orbiter body. To control the location of transition, a series of spherical-ball trip bands were fabricated which could be quickly applied to various stations along the windward surface of the orbiter. A photograph of one of these trip bands installed on the Orbiter is

shown in Fig. 3.6. Dimensions of the trips and an installation of the trip locations used during testing are shown in Fig 3.7.

To accommodate reduction of the co-ax gage outputs to incident heat flux, the body flap used during this phase was not to scale. More specifically, it was a constant thickness (0.2 in.) slab with a planform shape which approximates the actual orbiter body flap (see Fig. 3.5).

3.2 TEST INSTRUMENTATION

Heat-transfer rate measurements were obtained on the 92-0 model using 1/8 in. coaxial (or coax) gages. A coax gage is a surface thermocouple formed by a Chromel[®] wire fixed coaxially with a Constantan[®] cylinder and separated by a very thin electrically-insulating bonding compound. Coax gage locations are shown in Fig. 3.7. Table 3.1 shows the coordinates of each gage.

Two Chromel[®]-Alumel[®] thermocouples were attached to the lee-side of the body flap. The temperature histories from these thermocouples will be used to assess the coax gage data obtained during continuous sweep testing (Section 3.3).

During these entries, high speed, black and white, 16mm, shadowgraph movies were obtained on several runs. For the majority of testing, shadowgraph still photographs were taken. A summary of the photographic coverage for these entries is presented in Table 3.2.

3.3 TEST CONDITIONS AND PROCEDURES

The nominal free stream test conditions for the Body Flap Heating Phase are given below:

<u>M</u>	<u>PT, psia</u>	<u>TT, °R</u>	<u>Q, psia</u>	<u>P, psia</u>	<u>RE x 10⁻⁶, ft⁻¹</u>
8	180	1220	0.90	0.020	1.0
8	410	1310	1.96	0.044	1.9
10	375	1750	0.63	0.009	0.55
10	960	1840	1.52	0.022	1.3

A test summary describing all test runs for this phase is presented in Table 3.3.

The body flap heating phase was conducted using either a constant body flap angle or a sweep flap angle history. For constant body flap angle runs, the orbiter model was positioned to the desired angle of attack and the body flap was set to the desired flap angle, using the flap motor (see Section 3.1). The

model was then injected into the tunnel flow, and retracted after approximately 2 seconds of exposure. For the body flap sweep runs, the orbiter model was positioned to the desired angle of attack and the model was injected with the body flap angle set at -1 degree. When the model reached the tunnel centerline, the body flap was driven through 20 degrees of flap angle and then returned to -1 deg. The model was then retracted with an approximate total exposure time of seven seconds.

The coax gage outputs were recorded using a digital data scanner in conjunction with the analog subsystem. Data acquisition from all instruments, including the SLO-SYN controller status signal, was under the control of a Digital Equipment Corporation (DEC) PDP 11/40 computer, utilizing the Random Access Data System (RADS). The data system was started just prior to injection, while the model was still in the tank. All transducer outputs were recorded continuously at the rate of 95 times per second during the sweep flap mode and 17 times a second during the discrete flap mode. Data acquisition terminated when the model was retracted from the tunnel centerline.

3.4 DATA REDUCTION

The coax gage heat flux was computed for each time point (t_n) from the measured surface temperature by the following equation:

$$QDOT(t_n) = \frac{2C(t_n)}{\sqrt{\pi}} \sum_{j=2}^n \frac{TW(t_j) - TW(t_{j-1})}{\sqrt{t_n - t_j} + \sqrt{t_n - t_{j-1}}}$$

Coax gage surface temperature, $TW(t_j)$, was computed using a curve fit of the Thermocouple Reference Tables published by the National Bureau of Standards (1974).

For data obtained using the discrete flap angle mode (see Section 3.3), 15 consecutive QDOT values were averaged starting with the second value obtained after the test article reached tunnel centerline. This averaging technique was used to reduce the effects of any noise in the gage outputs. Gage surface temperature was also averaged.

For data obtained using the sweep flap angle mode, single values of QDOT and TW are used for tabulation and further calculations. This is due to the rapidly changing convective environment associated with the sweep mode.

The surface heat-transfer coefficient at each gage was calculated using values of QDOT and TW as follows:

$$H(TT) = \frac{QDOT}{TT - TW}$$

The heat transfer coefficient calculated above was normalized using the Fay-Riddell stagnation point coefficient (H(REF)) based on a radius of 0.0175 ft, see Appendix I.

3.5 DATA PACKAGE PRESENTATION

A presentation of typical tabulated data included in a separate data package is presented in Sample 3.1. This consists of a listing of the tunnel conditions and model attitude information for each run, followed by the heat transfer data for each coax gage.

Further analysis of the data will be presented in a future AEDC Technical Report.

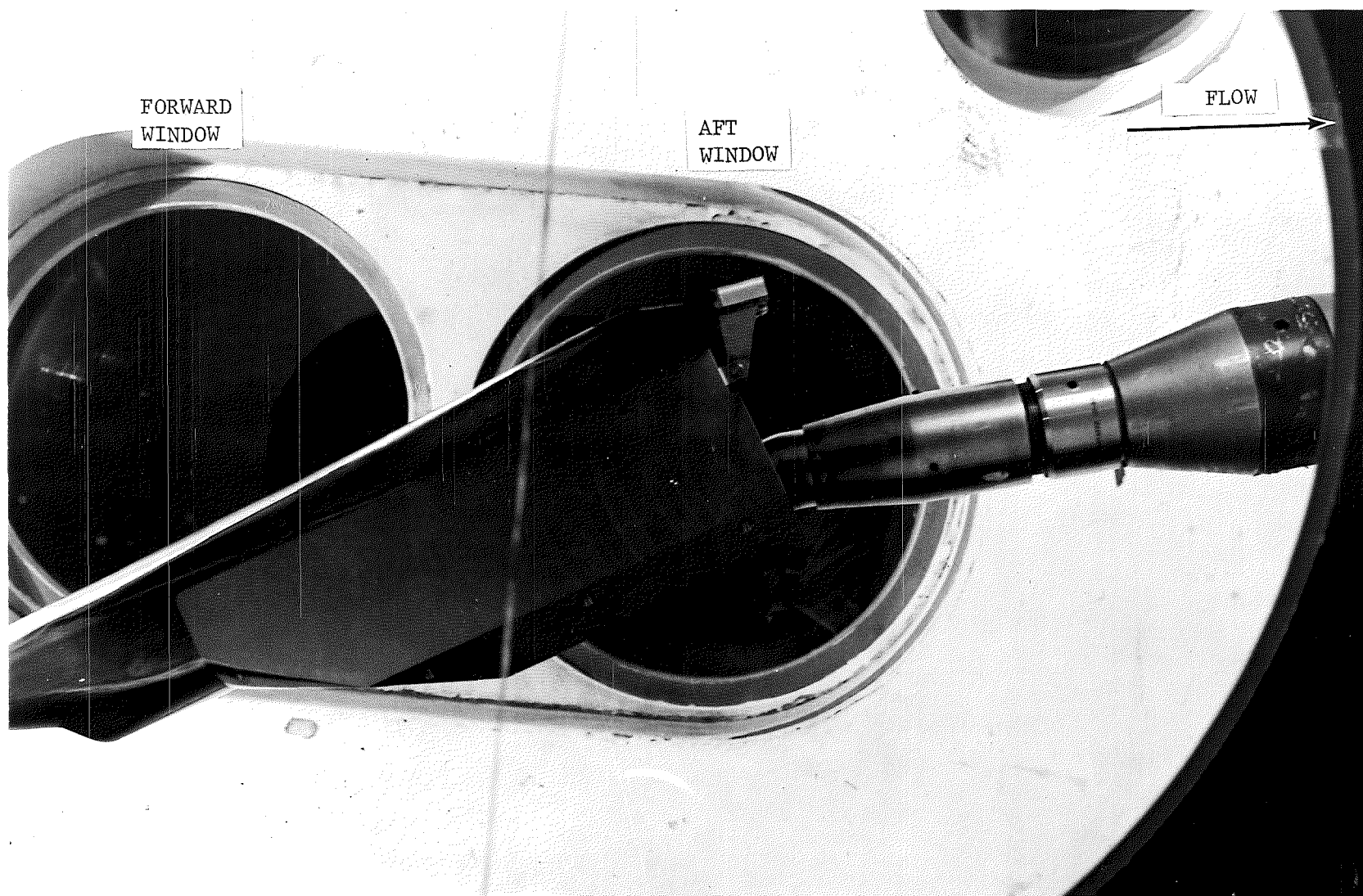


Figure 3.1 Phase IA Test Article in the Tunnel B Test Section

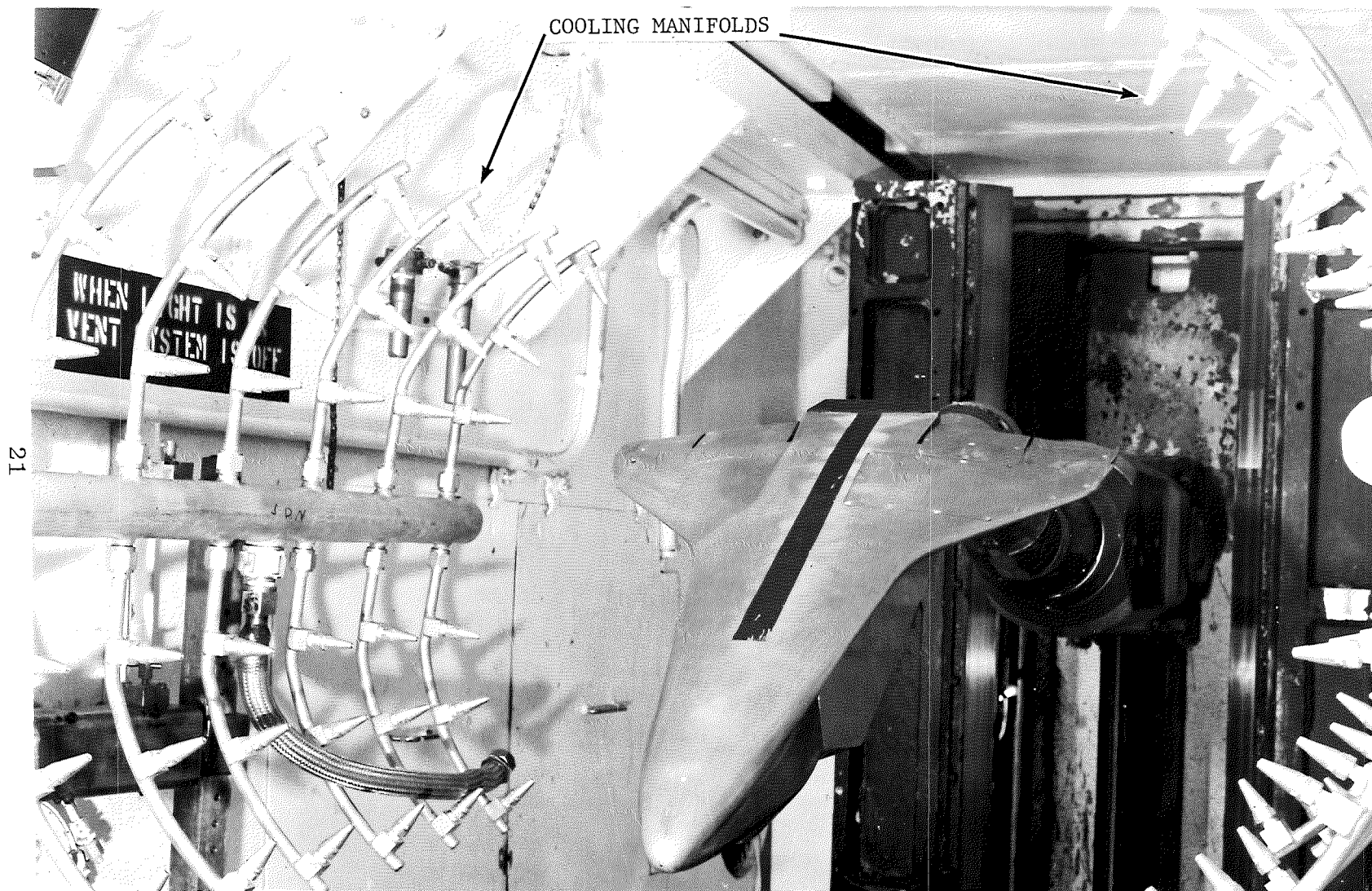


Figure 3.2 Phase IA Test Article in the Tunnel B Installation Tank

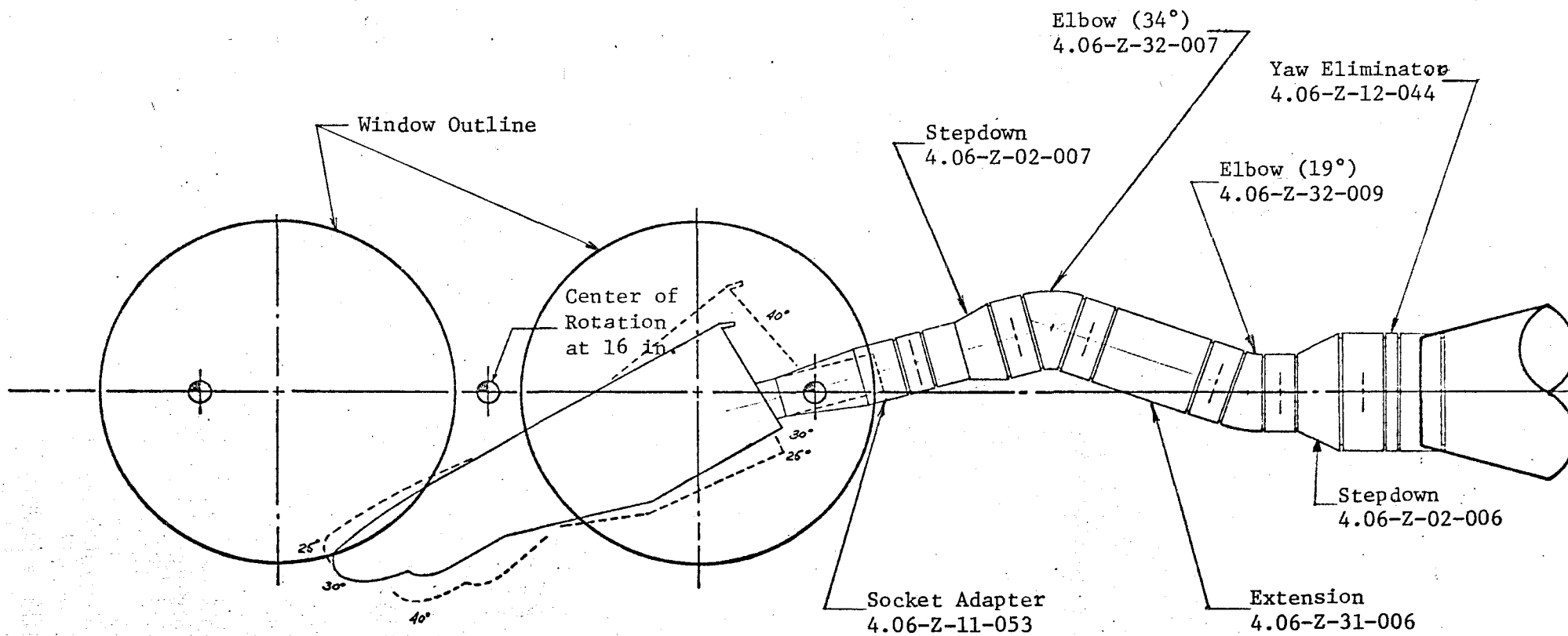


Figure 3.3 Sketch of Phase IA Installation in Tunnel B

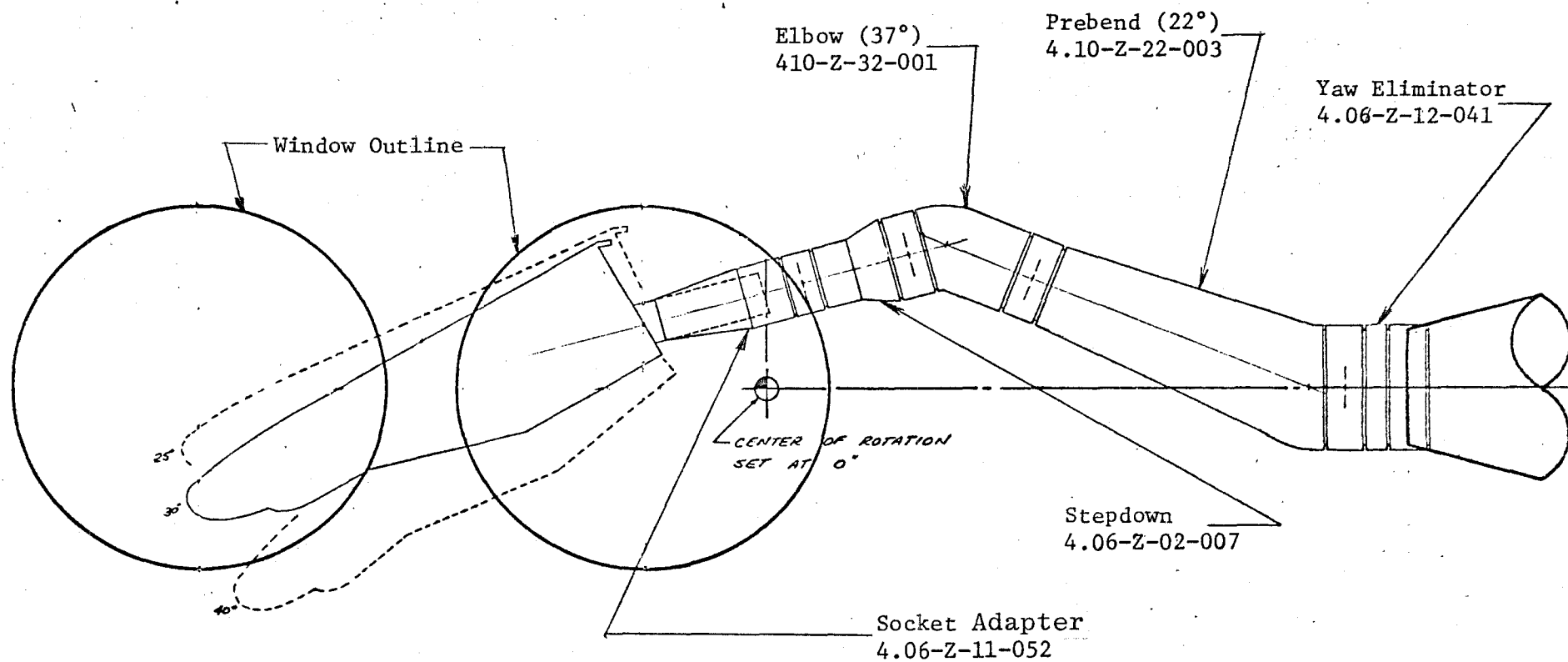
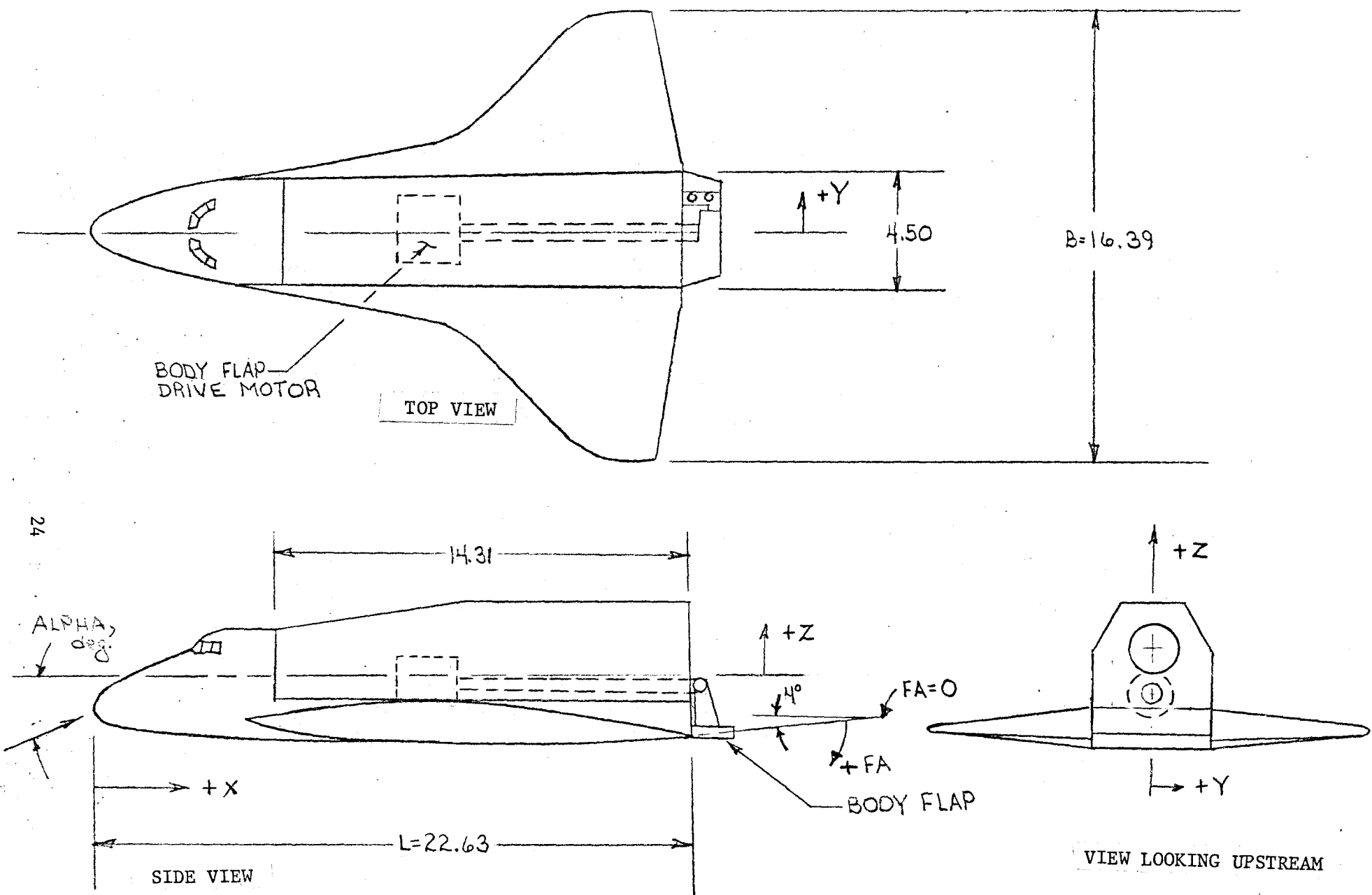


Figure 3.4 Sketch of Phase IA Installation in Tunnel C



All Dimensions in Inches

Figure 3.5 Basic Dimensions and Coordinate System Definition for the Body Flap Heating Test Article



Figure 3.6 Photograph of Spherical Ball Trip Band Used to Vary Transition Location During Body Flap Heating Tests

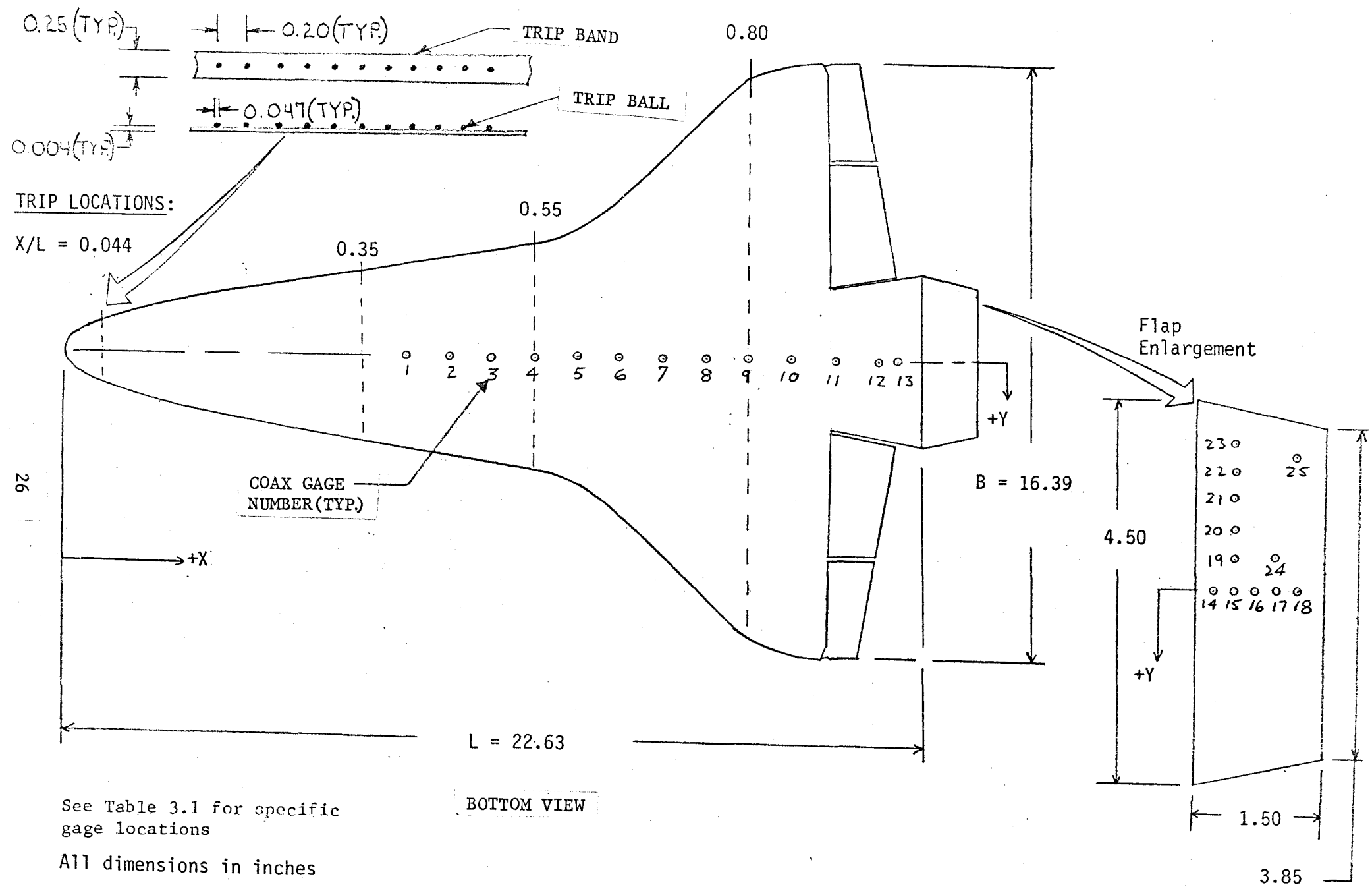


Figure 3.7 Sketch of Coax Gage Locations for the Body Flap Heating Tests

TABLE 3.1 Coax Gage Coordinates for the Body Flap Heating
Test Article

WINDWARD CENTERLINE GAGES	COAX GAGE #	X/L	2Y/B
	1	0.40	0
	2	0.45	
	3	0.50	
	4	0.55	
	5	0.60	
	6	0.65	
	7	0.70	
	8	0.75	
	9	0.80	
	10	0.85	
	11	0.90	
	12	0.95	
	13	0.975	
BODY FLAP GAGES	14	1.01	
	15	1.02	
	16	1.03	
	17	1.04	↓
	18	1.05	0
	19	1.02	-0.05
	20	↓	-0.10
	21		-0.15
	22	↓	-0.20
	23	1.02	-0.235
	24	1.04	-0.10
	25	1.054	-0.21

L = 22.63 in.

B = 16.39 in.

TABLE 3.2 Summary of Photographic Coverage for the Body Flap Heating Test

	Camera Number	Camera Type	Camera View	Frame Rate	Run Number	Film ID
Phase I - Body Flap Heating (M=8)	1	Varitron 70 mm Shadowgraph stills	Side view of flow field through forward window	1 per run	1-111	463
	2	↓	Side view of flow field through aft window	1 per run	1-111	464
Phase I - Body Flap Heating (M=10)	1	Varitron 70 mm Shadowgraph stills	Side view of flow field through forward window	1 per run	201-254	917
	2	↓	Side view of flow field through aft window	1 per run	201-254	918

TABLE 3.3 Run Summary for the Body Flap Heating Tests

a. Summary of Body Flap Test in Tunnel B (Phase I)

REx10 ⁻⁶ /ft	TRIP at X/L =	BODY ANGLE OF ATTACK, α , deg	FLAP ANGLE, deg						
			0	5	10	15	20	**SWEEP	
1.0	0.044	25	2	3					1
2.0		25	5	6	7	9	8		4
		30	10	11	12	13	14		
		35	15	16	17	18	19		
	0.044	40	20	21	22	23	24		
	No Trip	25	25,36,37	26	27	28	29,30		
		30	31	32	33	34	35		
		35	38	39	40	41	42		
	No Trip	40	43	44	45	46	47		
	0.55	25	48	49	50	51	52		
		30	53	54	55	56	57,58		
		35	59	60	61	62	63,64		
	0.55	40	*65,67	*66,68	69	70	71		
	0.35	25	72	73	74	75	76		
		30	77	78	79	80	81		
		35	82	83	84	85	86		
	0.35	40	87	88	89	90	91		Run Number (TYP.)
	0.80	25	92	93	94	95	96		
		30	97	98	99	100	101		
		35	102	103	104	105	106		
2.0	0.80	40	107	108	109	110	111		

* Trip was not mounted properly to model. Use data with caution.

** Data were obtained at a rate of 95 loops per second. For all other runs, the data rate was 17 loops per second.

TABLE 3:3 Concluded

b. Summary of Body Flap Test in Tunnel C (Phase I)

$RE \times 10^{-6}/ft$	TRIP at X/L =	BODY ANGLE OF ATTACK, α , deg	FLAP SPEED	FLAP ANGLE, deg					SWEEP
				0	5	10	15	20	
0.55 ↓ 0.55 ↓ 1.3 ↓ 1.3 ↓ 0.55 ↓	0.044 ↓ ↓ ↓ ↓ ↓ ↓ ↓ ↓ ↓ ↓ ↓	25	High	202	203	204	205	206	201, 207
		40	↓	209	210	211	212	213	208, 214, 215
		25	↓	217	218	219	220	221	216, 223
		40	↓	225	226	227	228	229	224, 230, 231
		25	High						232
		25	Low						233
		40	Low						234
		25	High	236	237	238	239	240	235, 241
		40	High	243	244	245	246	247	242, 248
		25	Low						249
		25	High	251		252		253	254
		40	Low						250
		40	High						255

Note: The following data were acquired at a rate of 95 loops per second; all sweep runs (except Runs 202, 214 and 215), and constant flap angle Runs 207 and 209. The data for the other runs were obtained at 17 loops per second.

ARVIN/CALSPAN FIELD SERVICES, INC.
AEDC DIVISION
VON KARMAN GAS DYNAMICS FACILITY
ARLORD AIR FORCE STATION, TENNESSEE
AFFOL STRAKE HEATING INVESTIGATION

DATE COMPUTED 27-SEP-82
TIME COMPUTED 19:16:12
DATE RECORDED 27-SEP-82
TIME RECORDED 19:13:17
PROJECT NUMBER V 8-1L

RUO	RUO TYPE	TRIP LOCATION	M	PT, PSIA	TT, DEGR	ALPHA, DEG	ALPI, DEG
1201	DISCRETE FLAP ANGLE	X/L = 0.044	7.93	409.1	1312.7	29.94	-0.06

T	P	PT2	Q	V	RHO	MU	RE	H(REF)	CENTERLINE
DEGR	PSIA	PSIA	PSIA	FT/SEC	LB/FT3	LB-SEC/FT2	FT-1	(RR=0.0175FT)	TIME(SEC)
96.8	4.453E-02	3.622	1.96	3822.3	1.242E-03	7.788E-08	1.894E+06	3.456E-02	0.000

FLAP ANGLE = 10.01 DEG TIME = 2.047 SEC

GAGE NO	X/L	21/B	TW DEG R	QDOT BTU/FT2-SEC	H(TT) BTU/FT2-SEC-R	H(TT)/H(REF)
FOREBODY						
1	0.400	0.0	571.0	5.01	6.756E-03	0.196
2	0.450	0.0	567.9	4.18	5.613E-03	0.162
3	0.550	0.0	564.3	4.74	6.339E-03	0.183
4	0.550	0.0	562.0	5.46	7.278E-03	0.211
5	0.600	0.0	556.4	4.73	6.248E-03	0.181
6	0.650	0.0	553.8	4.63	6.101E-03	0.177
7	0.700	0.0	551.1	4.95	6.503E-03	0.188
8	0.750	0.0	548.4	4.92	6.434E-03	0.186
9	0.800	0.0	546.4	4.95	6.462E-03	0.187
10	0.850	0.0	542.4	4.31	5.591E-03	0.162
11	0.900	0.0	538.8	3.48	4.493E-03	0.130
12	0.950	0.0	537.0	1.78	2.291E-03	0.066
13	0.975	0.0	518.7	2.19	2.199E-03	0.064
FLAP						
14	1.010	0.0	560.1	5.36	7.126E-03	0.206
15	1.020	0.0	560.1	5.70	7.572E-03	0.219
16	1.030	0.0	560.2	5.58	7.418E-03	0.215
17	1.040	0.0	560.1	5.44	7.225E-03	0.209
18	1.050	0.0	560.2	5.60	7.441E-03	0.215
19	1.020	-0.0	559.6	5.56	7.379E-03	0.214
20	1.020	-0.1	560.2	5.58	7.414E-03	0.215
21	1.020	-0.2	557.0	4.47	5.917E-03	0.171
22	1.020	-0.2	562.9	5.89	7.859E-03	0.227
23	1.020	-0.2	562.6	5.59	7.456E-03	0.216
24	1.040	-0.1	560.1	5.48	7.287E-03	0.211
25	1.054	-0.2	564.9	6.29	8.405E-03	0.243

Sample 3.1 Typical Tabulated Data on Body Flap Heating Test

4.0 VAPOR SCREEN (PHASE IB)

4.1 TEST ARTICLE

The 92-0 model of the Space Shuttle Orbiter used in the Body Flap Heating Phase was also used in the Vapor Screen Phase (IB). The model was restored to its original configuration prior to vapor screen testing. Photographs of the test article in the Tunnel B test section and installation tank are shown in Figs. 4.1 and 4.2, respectively. As seen in these photographs, the model was painted black to reduce the reflection of the laser beam. Figure 4.3 is a sketch of the installation of the test article in Tunnel B, identifying the standard sting components used during the test entry. Basic dimensions of the 92-0 model are conveyed in Fig. 4.4, as well as coordinate system definition.

4.2 TEST INSTRUMENTATION

During vapor screen testing, the tunnel pressure and temperature were manipulated to produce fog in the test section flow, which resulted from air liquefaction and water vapor condensation (see Section 4.3). Since the liquefaction and condensation processes are both affected by changes in pressure and temperature, the density of the fog in the flow field about the test article is a function of the local pressure and temperature. By observing the variation in fog density, information about the local flow structure can be ascertained. The fog density variations are observed and documented by illuminating the flow field in a given plane using a laser light source and photographing the light from this source which is reflected by the fog.

In this test series, a Lexel Model 95 Ion Laser was used to illuminate the fog. This laser is a Class IV-Argon type with 8 watts of available power. The power level used on this entry never exceeded 1-1/2 watts. A cylindrical lens with a 12.5mm focal length was used. The beam thickness was approximately 1.5mm wide in a plane parallel to the free-stream flow and had a dispersion angle of approximately 20 degrees in a plane normal to the flow.

Two 70mm cameras were used to take both black and white and color still photographs of the illuminated flow field. The laser and the cameras were fixed in position atop a translating platform located just outside the tunnel side windows. This enabled the cameras to be in constant focus with the laser beam plane for every planar position. Figure 4.5 shows a sketch of the arrangement of the cameras and the laser relative to the model and the tunnel.

On several occasions, a 16mm movie camera was also used to photograph the flow field as the platform was translated downstream. Table 4.1 presents a summary of the photographic data obtained during this entry.

The platform was equipped with an indexing system which could be related to the laser beam location along the tunnel centerline. Although the platform also could be vertically translated, vertical position was not recorded. Vertical position changes did not affect the location of the illuminated plane, but did allow relative changes in the angle at which photographs were taken. Therefore, vertical changes were used merely to allow photographs to be taken on both the windward and leeward side of the orbiter wing.

4.3 TEST CONDITIONS AND PROCEDURES

The nominal tunnel stilling chamber conditions for the Vapor Screen Phase are given below:

<u>PT, psia</u>	<u>TT, °R</u>
190	590
120	650

To obtain the proper flow conditions to enhance the laser illumination technique, the tunnel was operated without heaters or driers. Because this relatively wet, cold air was expanded through the Mach 8 nozzle, a portion of the water vapor in the air condensed and a portion of the air liquefied. The condensed vapor and liquefied air produced a fog in the free stream flow, and the fog level could be adjusted somewhat by varying the stilling chamber density (i.e., pressure).

The expansion of the flow from the stilling chamber to the test section is nonisentropic at these conditions, therefore, free-stream parameters usually calculated assuming isentropic expansion were not presented with the data.

A test summary describing the test runs for this phase is presented in Table 4.2. Besides the photographs taken during the test, this summary includes all pertinent data for the Vapor Screen Phase. No other data were presented in the final data package for this phase.

After the desired amount of fog was obtained, the laser was activated and the orbiter model injected into the test section. For each angle of attack, the following procedure was followed:

1. The laser beam was aligned with the intersection of the body flap and the orbiter fuselage on the windward surface. This position of the translating platform (see Section 4.2) was recorded. This provided the basis for locating the illuminated plane relative to the orbiter for all photographs obtained at that angle of attack.

2. A series of photographs was obtained by translating the laser-camera platform, taking a photograph of the illuminated flow field, recording the platform position indicator reading, and taking a loop of data with the digital data system to document the stilling chamber conditions.
3. The model was then repositioned to the next angle of attack and the process repeated.

For this entire entry, the body flap was set at 12 degrees.

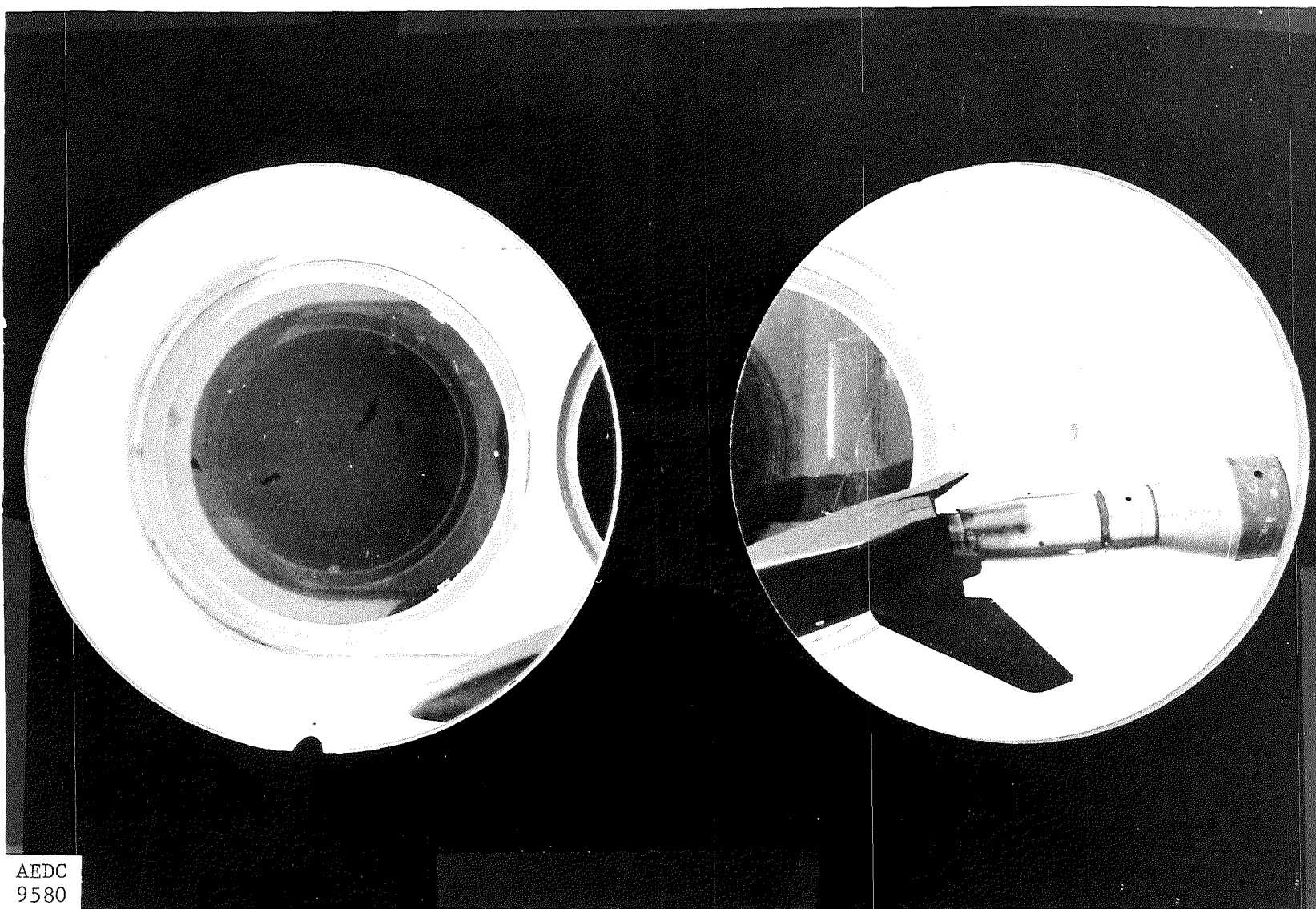
4.4 DATA REDUCTION

Due to the nonisentropic nature of the flow expansion from the stilling chamber to the test section, the only tunnel parameters presented with these data are the nominal stilling chamber pressure and temperature. Any other free-stream parameters (including Mach number) calculated for this flow based on standard isentropic assumptions are invalid.

As discussed in Section 4.3, the plane illuminated by the laser is initially located with reference to the body flap-fuselage intersection. Therefore, for the complete vapor screen test data supplied in Table 4.2, the values of X/L shown indicate the intersection of the laser beam plane with a line which is parallel to the orbiter X axis and intersects the body flap-fuselage intersection. Note that regardless of all other parameters, the illuminated plane remains normal to the free-stream flow direction.

4.5 DATA PACKAGE PRESENTATION

A typical vapor screen photograph is shown in Fig. 4.6. A listing of the stilling chamber pressure and temperature is given in the Run Summary, Table 4.2.



AEDC
9580

Figure 4.1 Phase IB Test Article in the Tunnel B Test Section

AEDC
9581

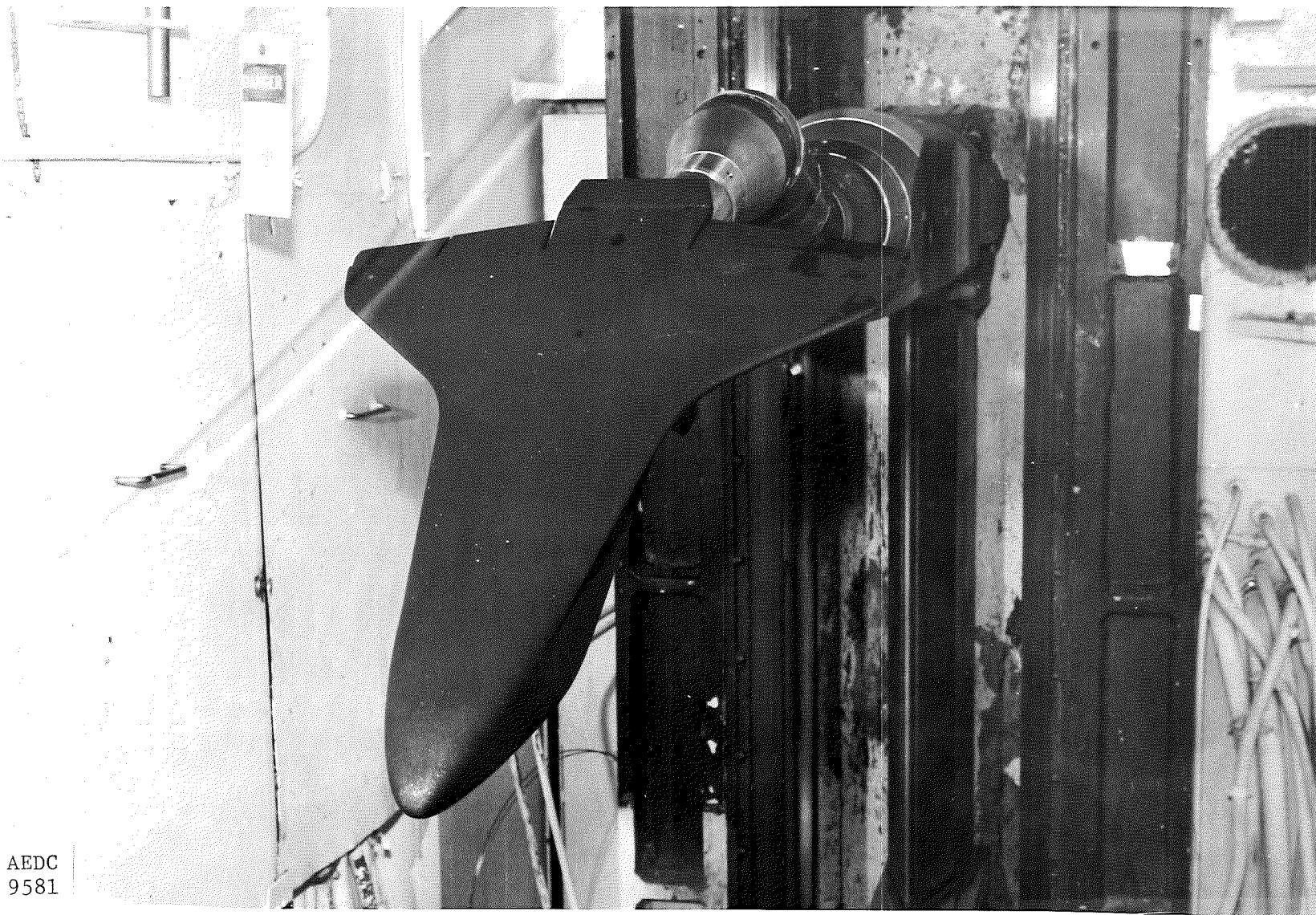
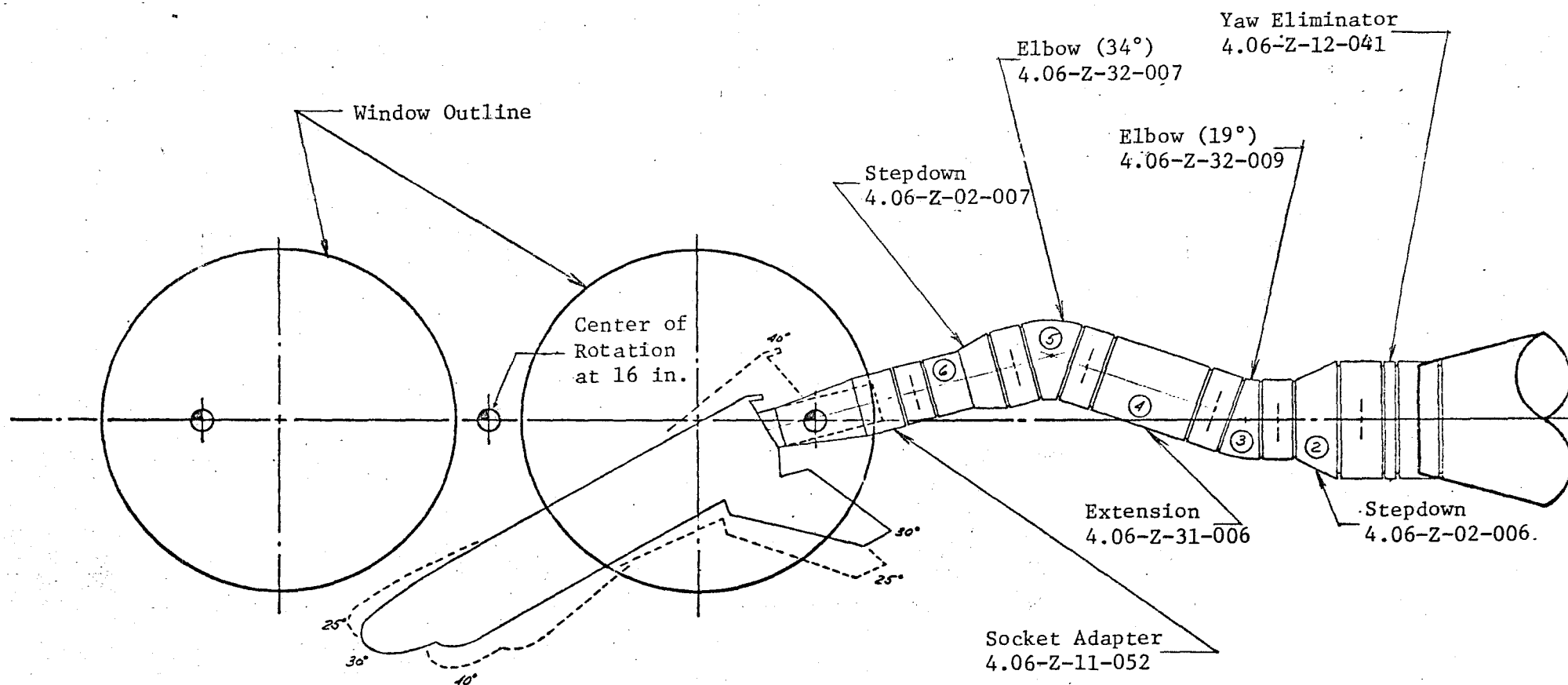


Figure 4.2 Phase IB Test Article in the Tunnel B Installation Tank

50-INCH HYPERSONIC TUNNEL B M = 8

TUNNEL WALL



TUNNEL WALL

Figure 4.3 Sketch of Phase IB Installation in Tunnel B

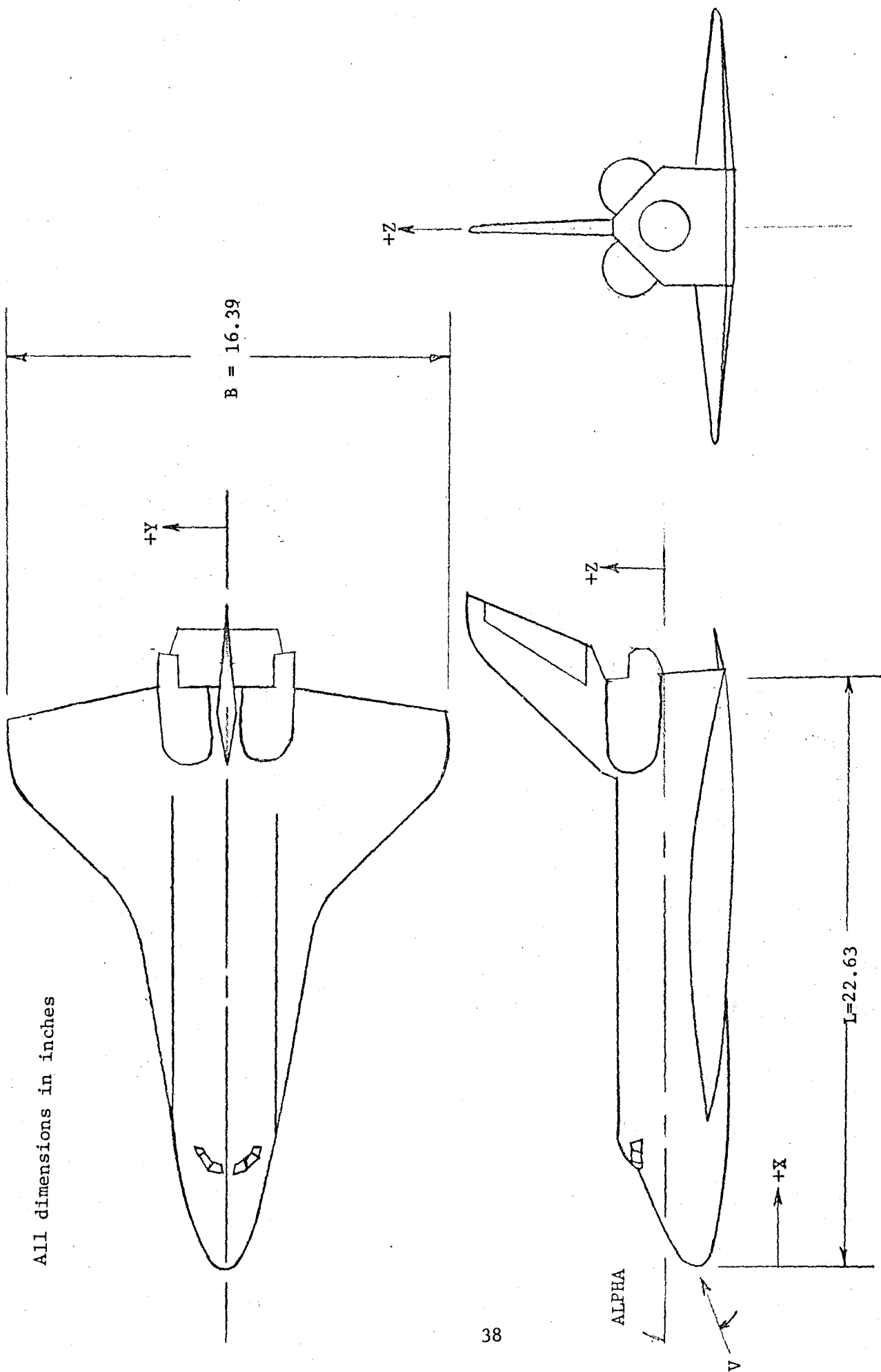


Figure 4.4 Basic Dimensions and Coordinate System Definition

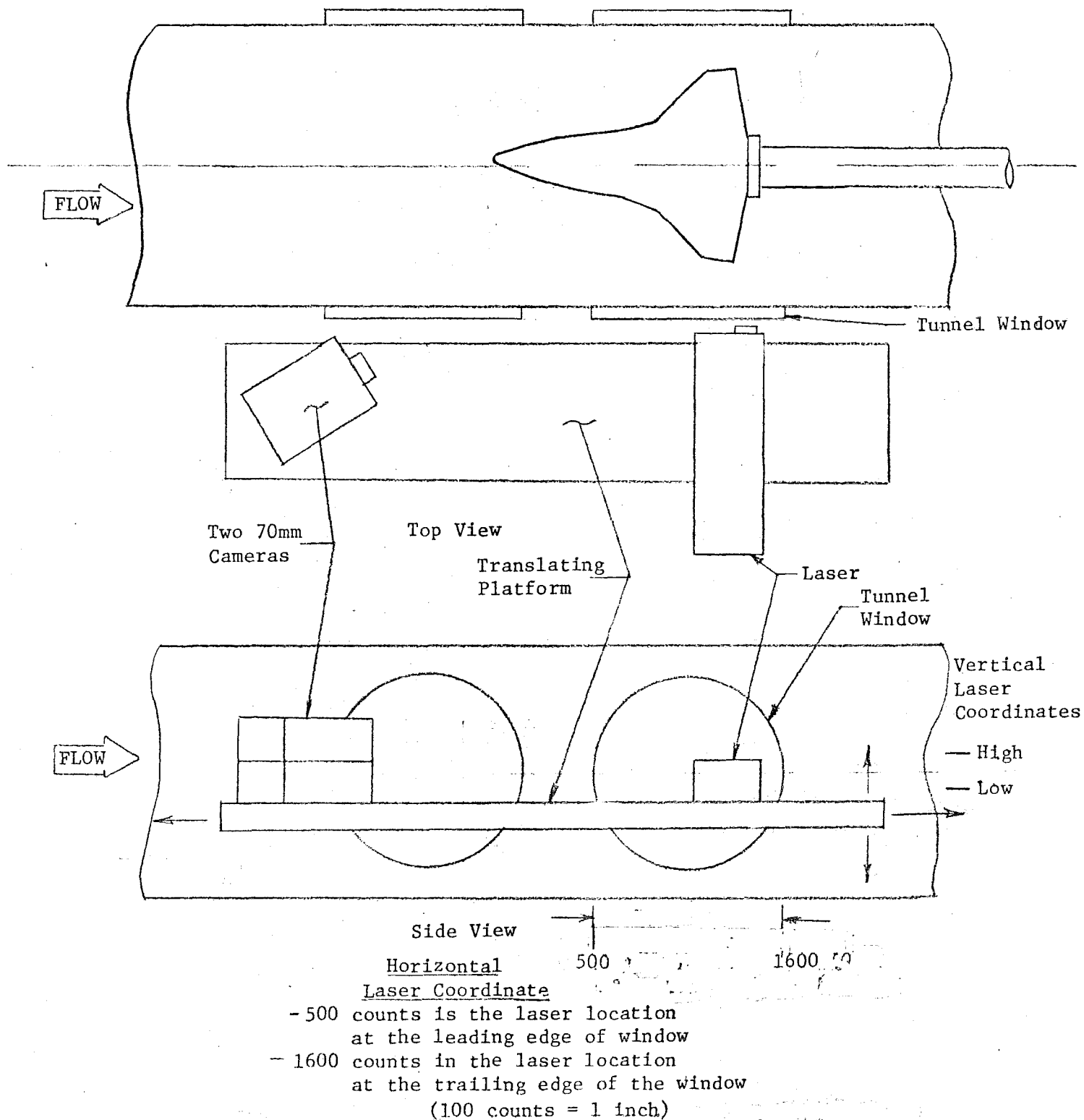
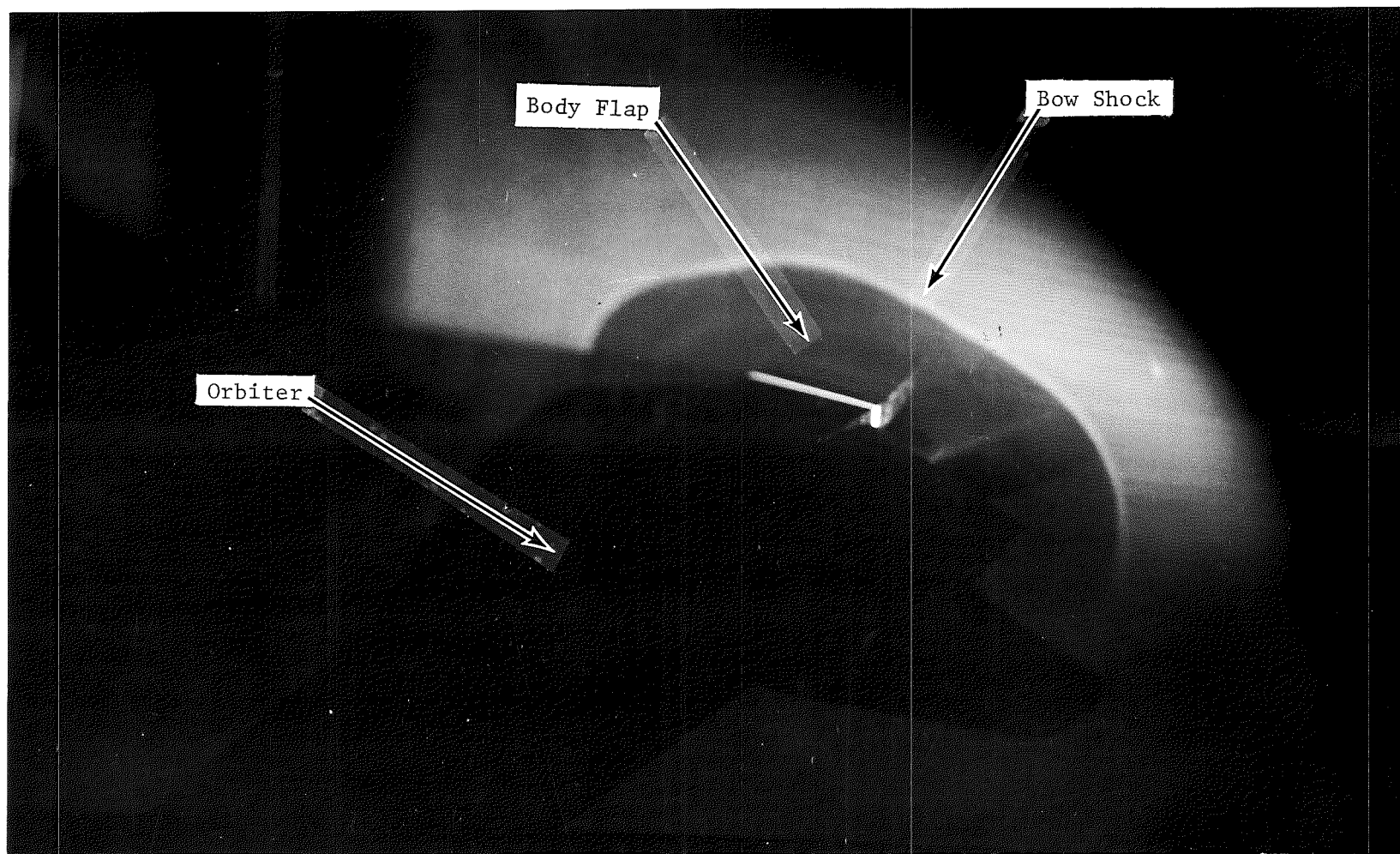


Figure 4.5 Sketch of Translating Laser and Camera Platform



a. Run 64
Figure 4.6 Sample Vapor Screen Photographs



b. Run 93
Figure 4.6 Concluded

TABLE 4.1 Summary of Photographic Coverage for Vapor Screen Test

	Camera Number	Camera Type	Camera View	Frame Rate	Run Number	Film ID
Phase IB - Vapor Screen	1	Hasselblad 70 mm sequence stills (color)	Side view at model on centerline	1 per run	1-60 61-111	367 368
	2	Hasselblad 70 mm sequence stills (B&W)	↓	1 per run	1-60 61-111	368 382
	3	Mitchell 16 mm motion picture	↓	24 per sec	112-114	1

TABLE 4.2 Summary of Vapor Screen Test

PT, psia	TT, °R	Laser ▲ Location	ALPHA=25 deg			ALPHA=30 deg			ALPHA=35 deg			ALPHA=40 deg		
			High*	Low*	X/L	High*	Low*	X/L	High*	Low*	X/L	High*	Low*	X/L
			Run No.			Run No.			Run No.			Run No.		
180-185 ↓	590-610 ↓	500										24	1	0.61
		600										23	2	0.65
		700										22	3	0.70
		800										21	4	0.74
		900										20	5	0.78
		1000										19	6	0.83
		1100										18	7	0.87
		1200										17	8	0.92
		1300										16	9	0.96
		1400										15	10	1.01
		1500										14	11	1.05
		1600										13	12	1.09
119-127 ↓	625-650 ↓	500	111	88	0.62	72	49, 73	0.64	48	25	0.63			
		600	110	89	0.67	71	50, 74	0.68	47	26	0.67			
		700	109	90	0.71	70	51, 75, 87	0.73	46	27	0.72			
		800	108	91	0.76	69	52, 76, 85, 86	0.77	45	28	0.76			
		900	107	92	0.80	68	53, 77	0.81	44	29	0.81			
		1000	106	93	0.84	67	54, 78	0.86	43	30	0.85			
		1100	105	94	0.89	66	55, 79	0.91	42	31	0.89			
		1200	104	95	0.93	65	56, 80	0.95	41	32	0.94			
		1300	103	96	0.98	64	57, 81	0.99	40	33	0.98			
		1400	102	97	1.02	63	58, 82	1.03	39	34	1.03			
		1500	101	98	1.06	62	59, 83	1.08	38	35	1.07			
		1600	100	99	1.11	61	60, 84	1.12	37	36	1.11			

▲ Horizontal Laser Location

* Vertical Laser Location is either High or Low

See Figure 4.5

Runs 112-114 are movie runs; laser sweep from X/L = 0.61 to 1.1.

5.0 PITOT PRESSURE PROBING (PHASE II)

5.1 TEST ARTICLE

A 0.025-scale version of the Space Shuttle Orbiter, designated as the 94-0 model by the supplier, Rockwell International, was modified with a manually positioned on-board probing mechanism for use on the Pitot Pressure Probing Phase (II). Photographs of the test article in the Tunnel B test section and tank are shown in Figs. 5.1 and 5.2, respectively. A sketch of the test article in the test section, shown in Fig. 5.3, identifies the standard sting components used during the test entry. Basic model dimensions and probing mechanism characteristics are shown in Fig. 5.4.

The probing mechanism consisted of two wedge-shaped rakes free to slide parallel to the straight wing leading edge section and guided in a T-slot milled into the bottom surface of the model. Figure 5.5 shows a closeup view of a pitot rake and Fig. 5.6 identifies individual probes and pertinent rake and tube dimensions.

Each rake used in the manual on-board probing mechanism contained 13-0.042 in. O.D. x 0.027 in. I.D. rounded, stainless steel pitot tubes. The tubes were arranged in two stacks, as pictured in Fig. 5.6, laterally spaced 0.2 inches apart such that 0.4-inch rake movement provided 0.2-in. increments in lateral survey stations. Tubes in a particular stack were spaced 0.1 in. apart vertically. The tubes extended 1.57 in. forward of the rake tips to allow sufficient upstream clearance of any rake-body shock wave interaction. Additional support stiffeners were added 0.5 in. from the probe tips to help them withstand the aerodynamic stress and to help maintain relative probe tip spacing. The adjacent probe stacks were aligned perpendicular to the model axial centerline to further enhance the odds against adjacent probe flow interference.

The height of the lowest probes (#1 and 101) above the wing surface was measured at each survey location with the appropriate rake flush mounted. These values are plotted in Fig. 5.7 indicating the effect of the model contour on vertical probe locations in the flow field. A probe diameter is imposed on this plot to help characterize the effects of model contour on the vertical probe height.

The probe heights tabulated in Table 5.1 for probes #1 and 101 represent average values obtained from the survey station measurements over the 8-inch span of each respective rake (Fig. 5.7). The measured, vertical spacing of the other pitot tube in each probe stack was combined with the lowest-probe averages to obtain the values in Table 5.1.

Each rake was installed to extend over one-half of the 16-inch long survey line. The T-slot was continued past the model

centerline where it eventually ran out over the model fuselage. This enabled removal of the inboard rake so it could be attached to the cut-wing side for interference-free probing with the outboard rake alone. The outboard rake was well offset from its T-slot slider to allow the survey to extend all the way to the wing tip. To facilitate the manual positioning of the survey rakes, a vernier scale was etched onto the model surface in 0.4-inch increments (see Figs. 5.4 and 5.8). Positioning the rake(s) was accomplished by simply loosening the set screws and sliding the entire body along the slot until the lowest probe on the right stack was aligned with the desired vernier scale tick mark.

5.2 TEST INSTRUMENTATION

Beyond the probe rakes, the pressure tubes were soldered to larger (0.063-in.) diameter tubes and routed through a hole in the sting, through the Tunnel B model inject/retract mechanism and to the ESP-32 module located in the tank floor below the wind tunnel test section. This miniaturized transducer package permitted the simultaneous measurement of up to 32 pressures, and its relative proximity to the probe tips kept to a minimum the pressure measurement stabilization time. Thus, all pressure measurements taken were equilibrium pressures, eliminating the need for advanced pressure-stabilization prediction data reduction methods and further enabling the quick and accurate testing and data-taking procedures required to meet the test objectives.

To record the position of the probe rakes aligned to the vernier scale, still photographs, as shown in Fig. 5.8, were taken from above the model at 25 deg angle of attack. A TV camera also recorded that same view onto video tape. Shadowgraph still photographs were taken for each run (angle of attack) to record the shock wave pattern about the model and the surface-mounted rakes. A summary of the photographic coverage of the pressure probing test is given in Table 5.2.

5.3 TEST CONDITIONS AND PROCEDURES

The nominal free-stream test conditions for the Pitot Pressure Probing Phase are given below.

<u>M</u>	<u>PT, psia</u>	<u>TT, °R</u>	<u>Q, psia</u>	<u>P, psia</u>	<u>RE x 10⁻⁶, ft⁻¹</u>
8	190	1220	0.92	0.021	1.0

A test summary describing all test runs for this phase is presented in Table 5.3.

The model was injected into the tunnel at an angle of attack of 25 degrees. Upon insuring that the measured pitot pressure had reached equilibrium, 5 loops of data were recorded over a period of 1 second. During this time, photographs were taken from the top and side window mounted cameras to provide probe

rake positioning documentation. The model was then pitched sequentially to 30, 35 and 40 degrees angle of attack where data were obtained in a similar manner. Each angle of attack is termed a run, and all tabulated and photographic data are identified by the run number.

To produce the desired pitch angles, the Model Attitude Control System (MACS) was used. The MACS is a computer based controller which issues preselected drive commands to the model positioning mechanisms. The model was returned to its "home" position of 25 degrees angle of attack upon retraction into the tank for manual rake repositioning.

Instrumentation outputs were recorded using the digital data scanner in conjunction with the analog subsystem. Data acquisition from all instruments was under the control of a DEC-PDP 11/40 computer, utilizing the Random Access Data System (RADS). The data system was started after a sufficient time was allowed prior to each run (angle of attack) for pressure stabilization. Monitoring the transducer output during the early test injections revealed that a reasonable delay time was 5 seconds, and this was used for the remainder of the test.

To investigate the potential for using both survey rakes simultaneously without the outboard pitot probe experiencing flow interference effects from the inboard probes, an interference study was implemented at the beginning of the test. The outboard rake was positioned at the extremities of its survey range (the wing tip and the midpoint of the survey line) both with and without the inboard rake positioned 8 in. inboard along the survey line. Each of 4 injections included all 4 angles of attack. Sufficient repeat data were obtained to distinguish probe interference effects from normal pressure measurement and probe rake positioning uncertainties. Interference was positively identified. These identified probe interference effects, combined with the relative ease and quickness of rake positioning, dictated that the majority of testing be performed with one rake at a time. The inboard rake was subsequently removed and the outboard rake was used to survey from the wing tip to the survey line midpoint. The inboard rake was then used to continue the survey to completion at the model centerline.

To investigate the sensitivity of the pressure measurements to small variations in pitch angle, measurements were taken at 24.9, 25, and 25.1 degrees angle of attack. Repeatability within the uncertainty of the pressure measurements was obtained. Similar results for similar pitch angle variations at the 40 degree angle-of-attack attitude verify that the pitot pressure measurements were relatively insensitive to small variations in pitch angle.

On-line analysis of the pitot pressure profiles obtained at 0.2 in. increments along the leading edge allowed the bow shock interaction region to be readily identified. Therefore, additional measurements were made to provide 0.1 in. profile spacing along an approximate 3 in. span which encompassed this interference zone.

The ESP-32 modules were calibrated prior to the test with pressures measured by secondary standards traceable to the National Bureau of Standards. The calibration calculates the best linear curve fit from up to ten pressure loadings that determine a resultant scale factor for each transducer. Prior to each test run the modules were referenced to a hard vacuum to obtain zero output values for each transducer.

5.4 DATA REDUCTION

Prior to each operational shift, and as required, the ESP-32 module with a total of 32, 15-psid transducers was calibrated as described in Section 5.3. From these data scale factors for each transducer are calculated. After reaching pressure equilibrium, 5 loops of data were taken over a period of 1 second. The appropriate scale factor and zero reading were used to determine the pressure on each transducer. These 5 pressures were averaged to obtain the pressure sensed by the pitot tube.

5.5 DATA PACKAGE PRESENTATION

A presentation of typical tabulated data included in a separate data package is presented in Sample 5.1.

Representative plotted pitot pressure data for vertical surveys from both stacks of the outboard rake at a single survey station are shown in Fig. 5.9. Two runs are plotted in that figure, illustrating rake positioning and pressure measurement repeatability.

A summary of the measured pressures for one probe over the entire survey is presented in Fig. 5.10. Figure 5.11 illustrates the insensitivity of the pressure measurements to small (0.1 degree) variations in model angle of attack.

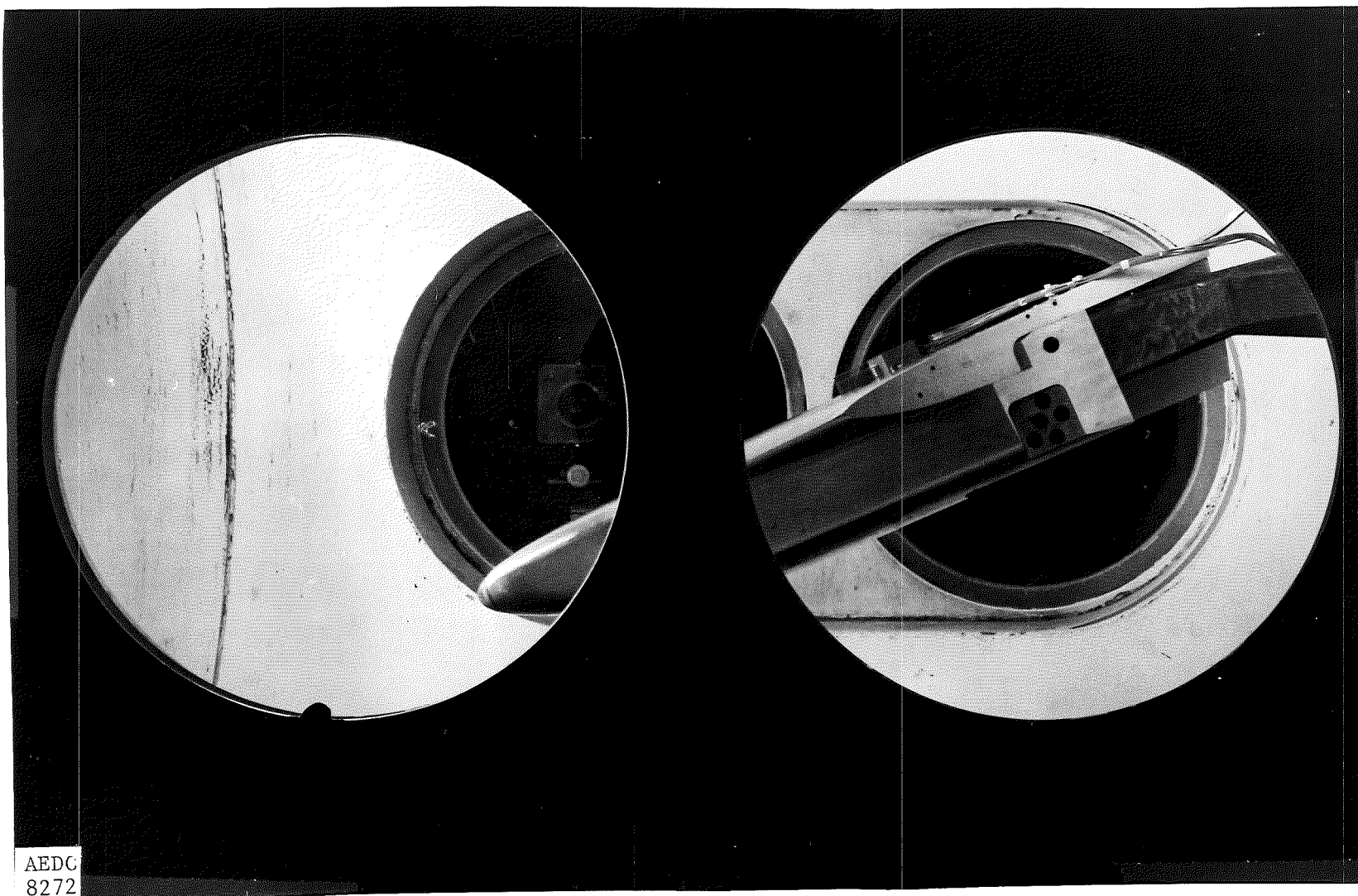


Figure 5.1 Phase II Test Article in the Tunnel B Test Section

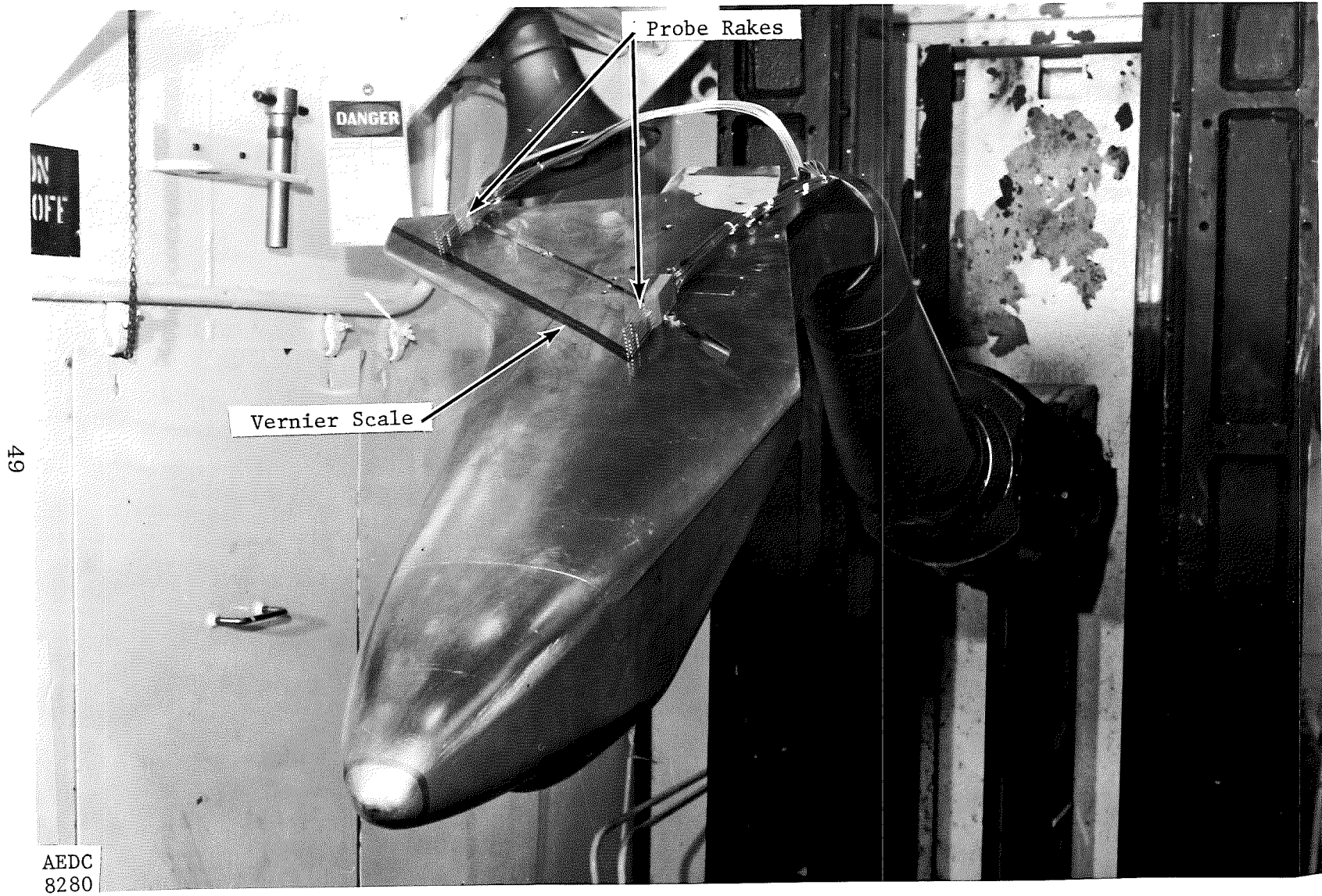


Figure 5.2 Phase II Test Article in the Tunnel B Installation Tank

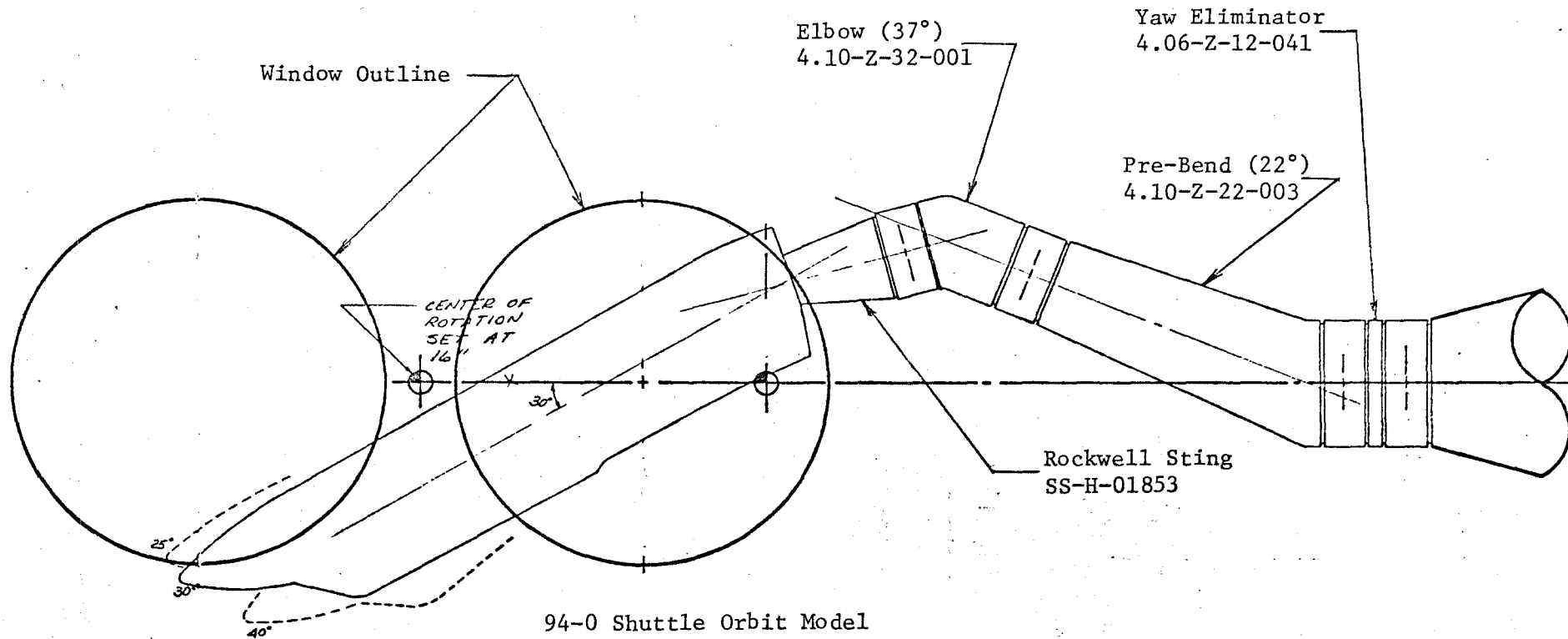


Figure 5.3 Sketch Phase II Installation

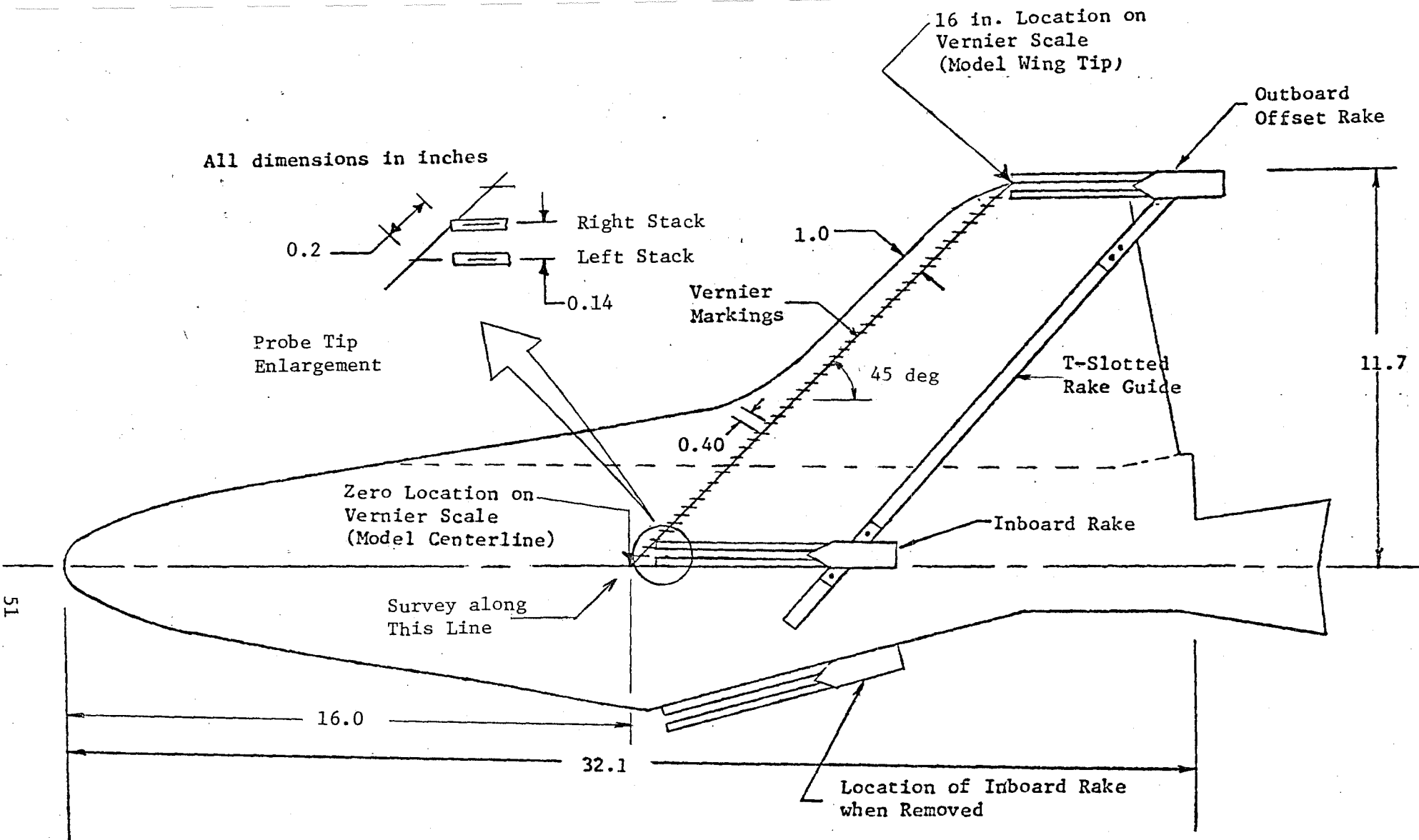


Figure 5.4 Bottom View of 94-0 Shuttle Orbiter Model Modified with Probing Hardware

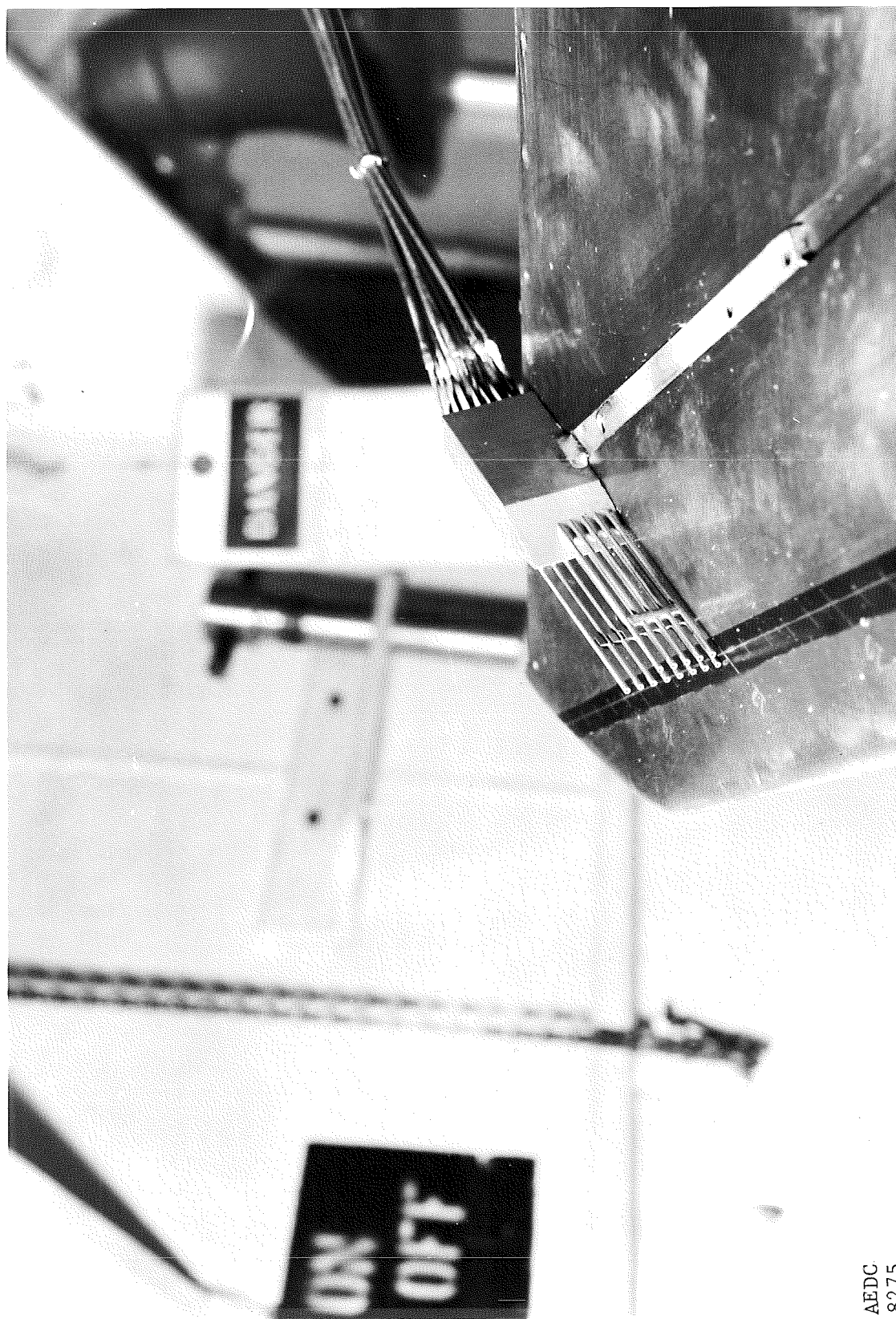
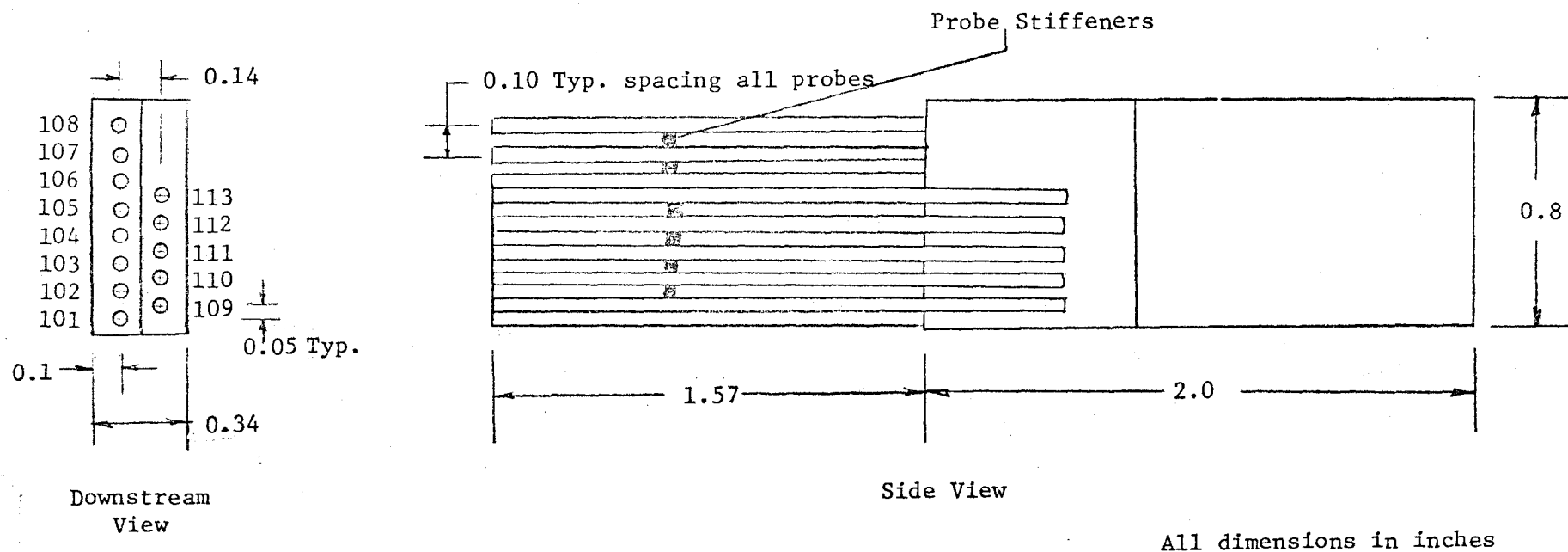


Figure 5.5 Closeup of Pitot Pressure Rake

AE DC
8275



The inboard rake is the same as the outboard rake. The inboard identification numbers are merely the last 2 digits of the representative outboard probe

Figure 5.6 Pitot Pressure Rake Dimensions and Probe Identification

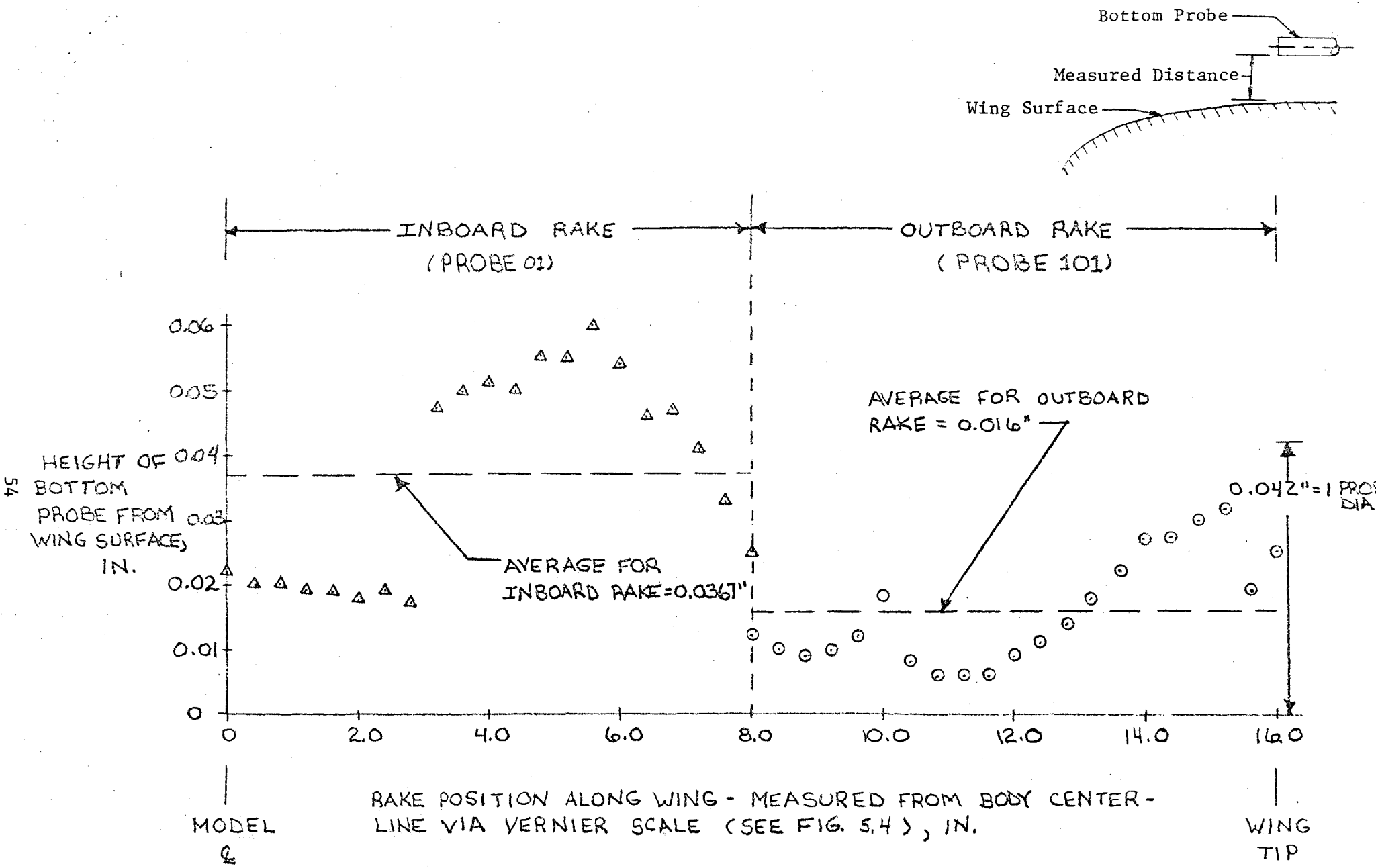


Figure 5.7 Location of Bottom Probe on Each Rake Relative to Wing Surface

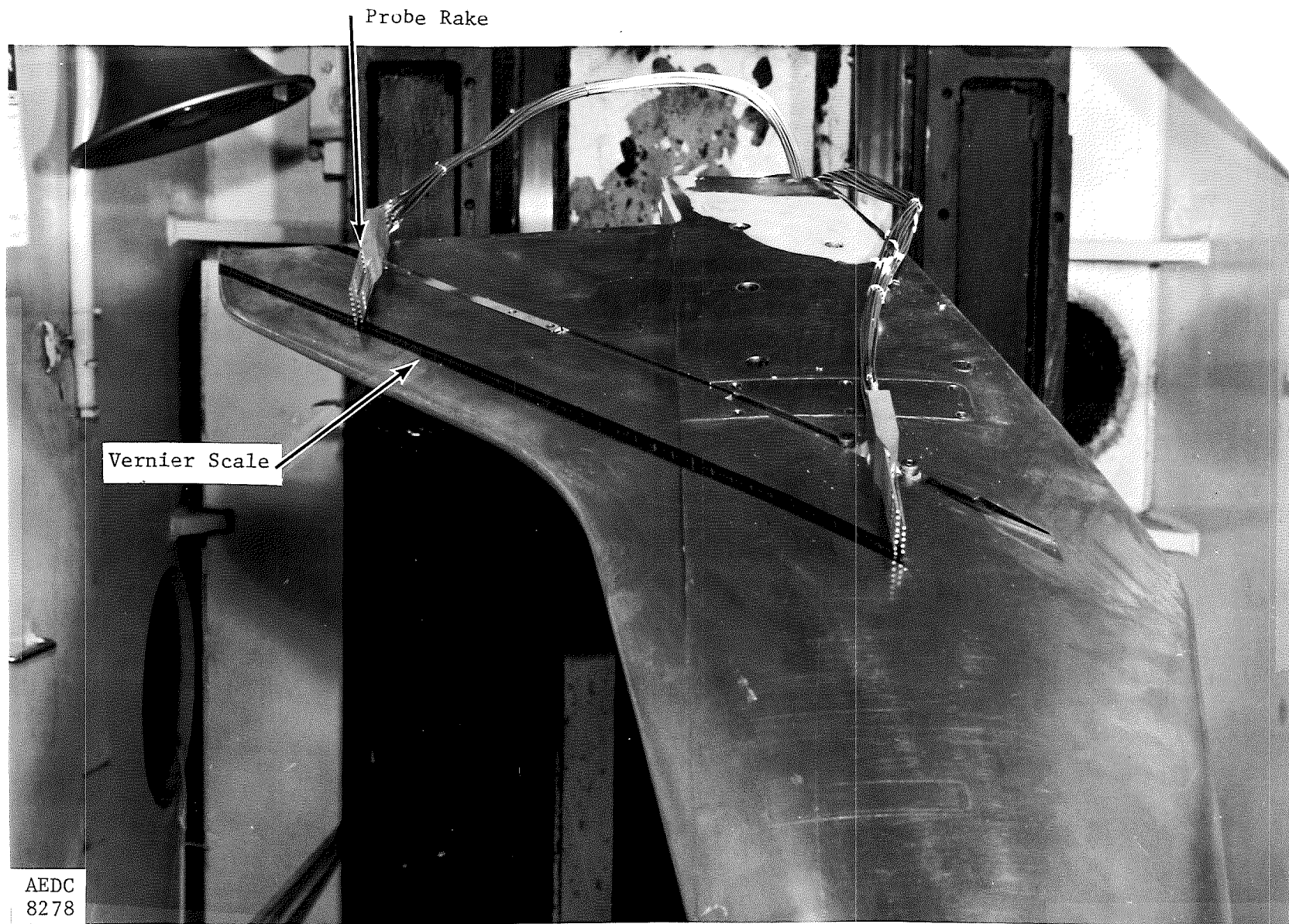


Figure 5.8 Probing Mechanism on Test Article with Vernier Scale

\triangle Run 105 \circ Run 109

OUTBOARD YPPCLI = 8.40

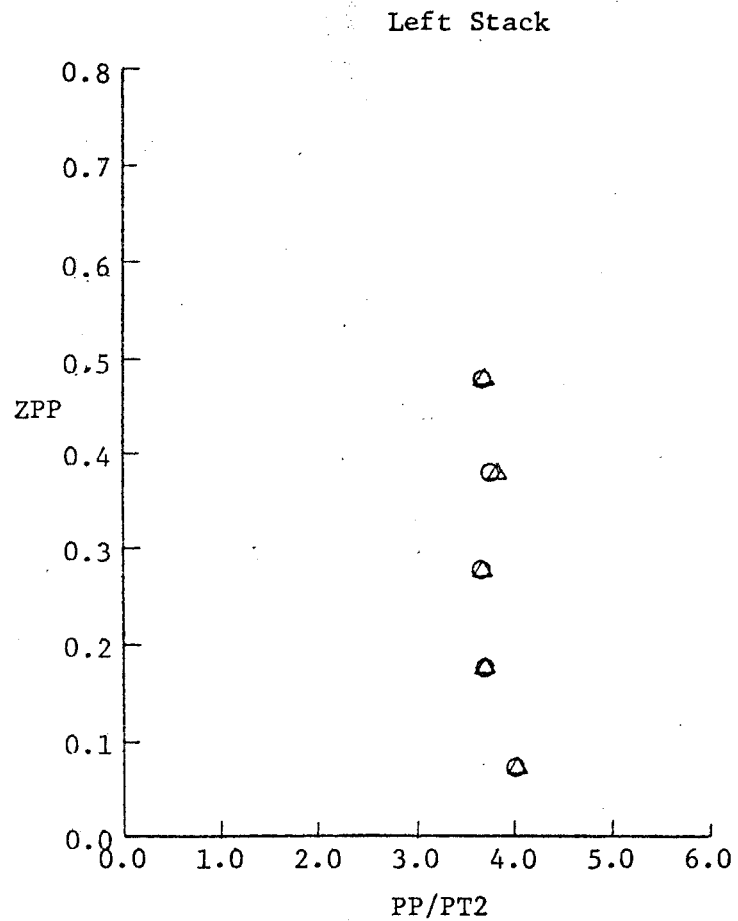
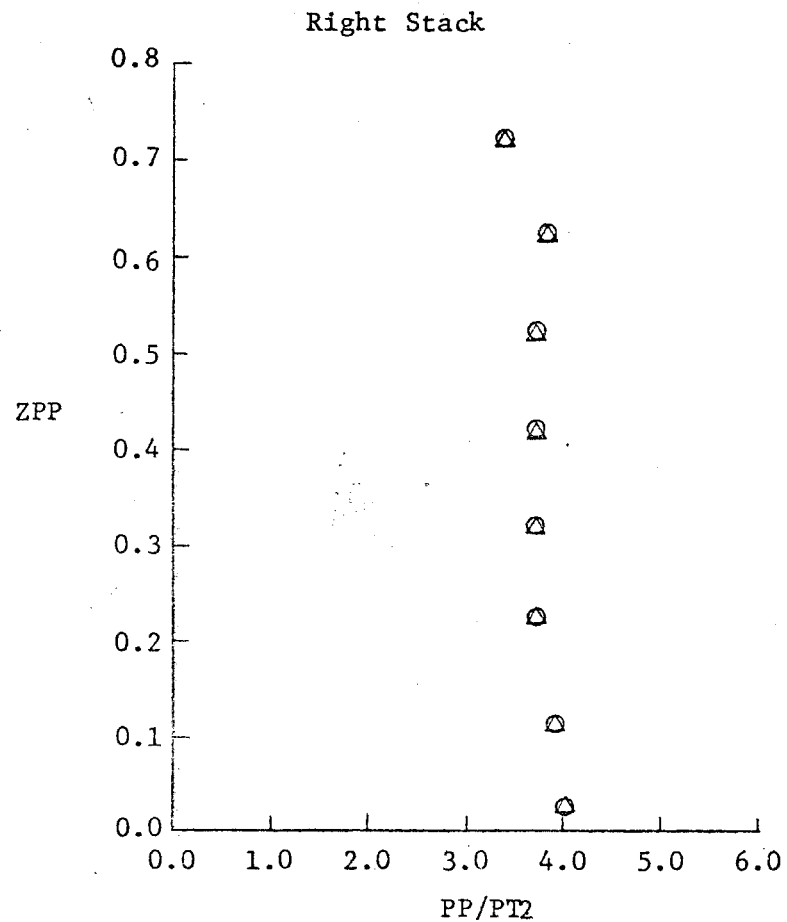
 $\alpha = 35^\circ$

Figure 5.9 Vertical Pitot-Pressure Survey and Data Repeatability

ANGLE OF ATTACK = 25 deg.

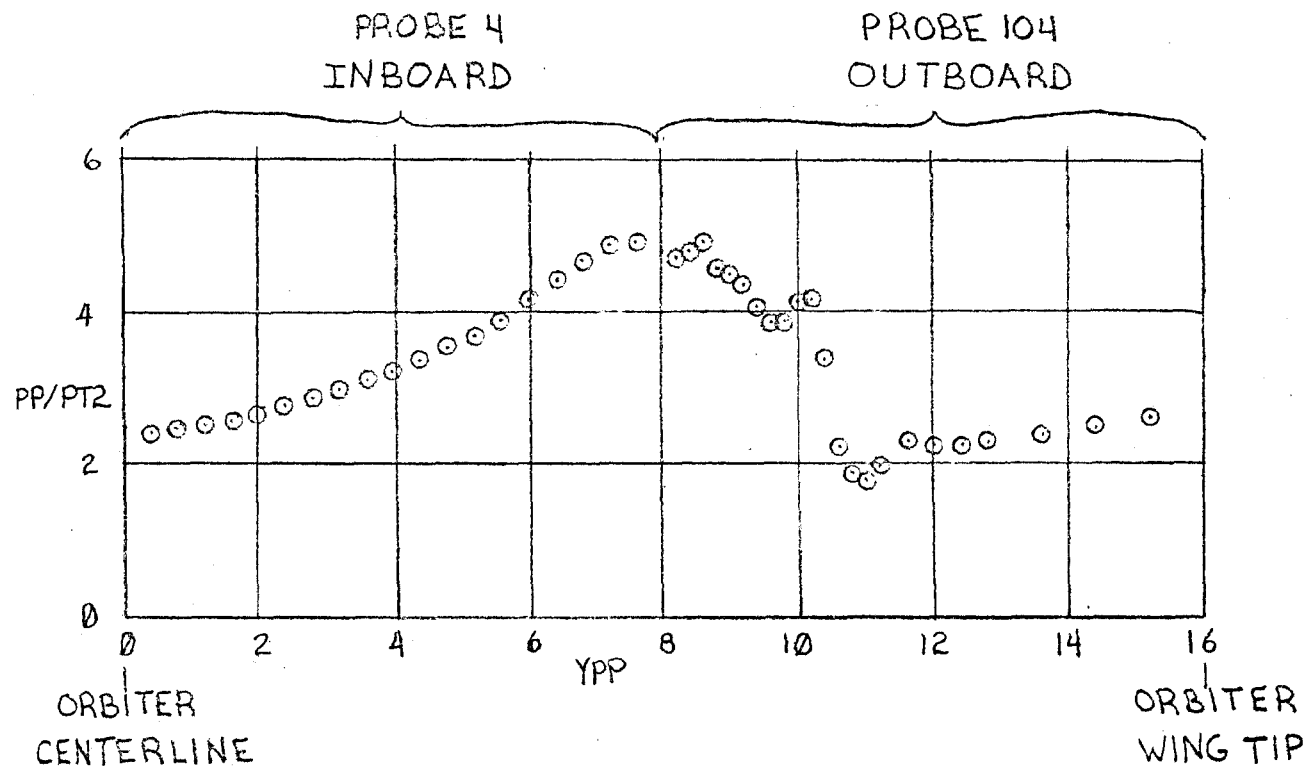
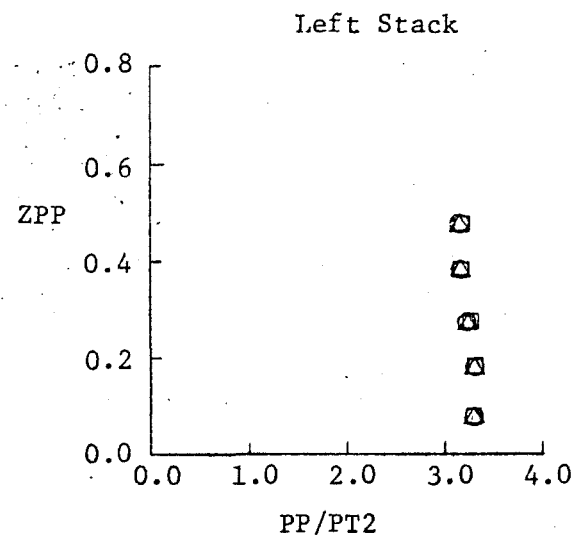
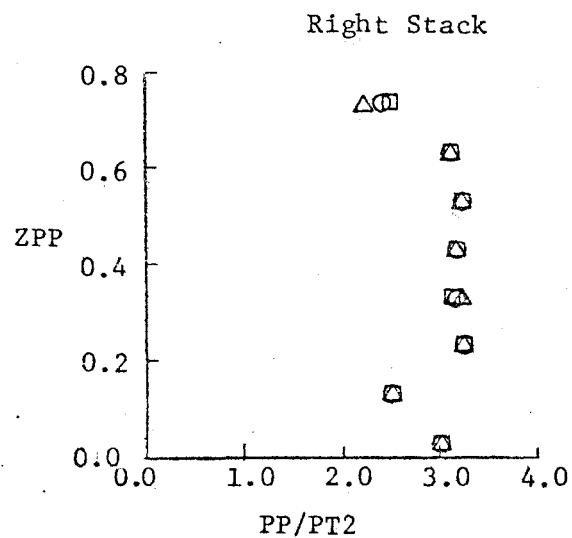


Figure 5.10 Lateral Pitot-Pressure Survey - Probe # 4 and Probe # 104

Run 20 $\alpha = 39.9$
 Run 21 $\alpha = 40.0$
 Run 22 $\alpha = 40.1$

Inboard YPPCLI = 8.0



Outboard YPPCLO = 16.0

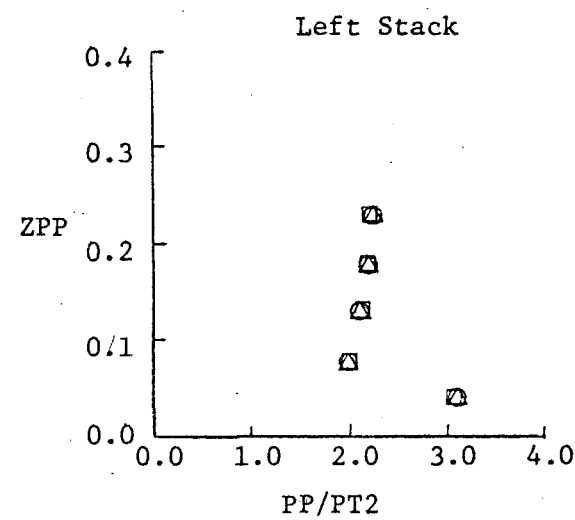
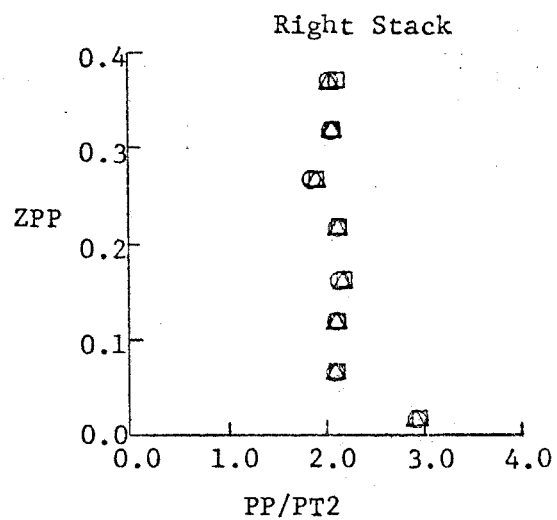


Figure 5.11 Model Pitch Angle Sensitivity Summary

TABLE 5.1 Average Height of Probes above Model Surface

RAKE	PROBE NUMBER	HEIGHT ABOVE MODEL SURFACE, in.*
Inboard ↓	1	0.037 ±0.005
	2	0.137
	3	0.238
	4	0.338
	5	0.436
	6	0.537
	7	0.637
	8	0.737
	9	0.087
	10	0.189
	11	0.289
	12	0.387
	13	0.488
Outboard ↓	101	0.016
	102	0.114
	103	0.214
	104	0.313
	105	0.413
	106	0.513
	107	0.615
	108	0.714
	109	0.066
	110	0.166
	111	0.266
	112	0.365
	113	0.466

*Note: See Fig. 5.7 for variations in heights of Probe 1 and Probe 101 as determined by posttest measurements.

TABLE 5.2 Summary of Photographic Coverage for Pressure Probing Test

	Camera Number	Camera Type	Camera View	Frame Rate	Run Number	Film ID
Phase II - Pressure Probing	1	Varitron 70 mm sequence stills (B&W)	Looking down from top on probe region	1 per run	1-242	408
	2	↓	Side view of probe region (flow from right to left)	1 per run	1-242	409
	3	Varitron 70 mm shadowgraph stills	Side view of flow field through forward window	1 per run	1-242	405
	4	↓	Side view of flow field through aft window	1 per run	1-242	406

TABLE 5.3 Run Summary for the Pitot Pressure Probing Test

Survey Location Right Stack* (in. from Q_L)	Rake	Model Angle of Attack, deg				Pitch Sensitivity (angle of attack)
		25	30	35	40	
16.0	Outboard	1	2	3	4	17 (24.4) 18 (25.0) 19 (25.1) 20 (39.9) 21 (40.0) 22 (40.1)
8.0	↓	5	6	7	8	
0.0	In-Outboard	9	10	11	12	
8.0	↓	13	14	15	16	
↓	↓					
7.6	↓	23	24	25	26	
15.2	Outboard	27	28	29	30	
14.8	↓	31	32	33	34	
14.4	↓	35	36	37	38	
14.0	↓	39	40	41	42	
13.6		43	44	45	46	
13.2		47	48	49	50	
12.8		51	52	53	54	
12.4		55	56	57	58	
12.0		59,63	60,64	61,65	62,66	
11.6		67	68	69	70	
11.2		71	72	73	74	
10.8		75	76	77	78	
10.4		79	80	81	82	
10.0		83	84	85	86	
9.6	↓	87	88	89	90	
		91	92	93	94	

Run Number
(TYP.)

*Note: See Fig. 5.4 for the survey location of the left stack.

TABLE 5.3 Concluded

Survey Location Right Stack* (in. from C_L)	Rake	Model Angle of Attack, deg				Pitch Sensitivity (angle of attack)
		25	30	35	40	
9.2	Outboard ↓	95	96	97	98	
8.8		99	100	101	102	
8.4		103	104	105	106	
↓		107	108	109	110	
8.0		111	112	113	114	
15.6	Inboard ↓	115	116	117	118	
8.0		119	120	121	122	
7.6		123	124	125	126	
7.2		127	128	129	130	
6.8		131	132	133	134	
6.4		135	136	137	138	
6.0		139	140	141	142	
5.6		143	144	145	146	
5.2		147	148	149	150	
4.8		151	152	153	154	
4.4		155, 159	156, 160	157, 161	158, 162	
4.0		163	164	165	166	
3.6		167	168	169	170	
3.2		171	172	173	174	
2.8		175	176	177	178	
2.4	Outboard ↓	179	180	181	182	
2.0		183	184	185	186	
1.6		187	188	189	190	
1.2		191	192	193	194	
0.8		195	196	197	198	
0.4		199, 203	200, 204	201, 205	202, 206	
8.2		207	208	209	210	
8.6		211	212	213	214	
9.0		215	216	217	218	
9.4		219	220	221	222	
9.8		223	224	225	226	
10.2		227, 231	228, 232	229, 233	230, 234	
10.6		235	236	237	238	
11.0		239	240	241	242	

ARVIA/CALSPAN FIELD SERVICES, INC.
 ARDC DIVISION
 VON KARMAN GAS DYNAMICS FACILITY
 ARDC AIR FORCE STATION, TENN
 ARFOL SHUTTLE WING LEADING EDGE PITOT SURVEY(PHASE II)

DATE COMPUTED 23-AUG-82
 DATE RECORDED 23-AUG-82
 TIME RECORDED 17: 9:52
 TIME COMPUTED 17:09
 PROJECT NO V B-1L

INBOARD RAKE YPPCLI = 0.00 IN.

RIGHT STACK YPP= 0.000 (IN.)				LEFT STACK YPP= -0.196 (IN.)			
ORIFICE	ZPP(IN.)	PP(PSIA)	PP/PT2	ORIFICE	ZPP(IN.)	PP(PSIA)	PP/PT2
1	0.027	0.125E+01	0.740E+00	9	0.077	0.279E+01	0.166E+01
2	0.127	0.538E+01	0.320E+01	10	0.179	0.435E+01	0.258E+01
3	0.228	0.465E+01	0.277E+01	11	0.277	0.480E+01	0.265E+01
4	0.328	0.502E+01	0.299E+01	12	0.377	0.475E+01	0.283E+01
5	0.426	0.532E+01	0.316E+01	13	0.478	0.540E+01	0.321E+01
6	0.527	0.552E+01	0.328E+01				
7	0.627	0.557E+01	0.331E+01				
8	0.727	0.532E+01	0.316E+01				

OUTBOARD RAKE YPPCLO = 8.00 IN.

RIGHT STACK YPP= 8.000 (IN.)				LEFT STACK YPP= 7.814 (IN.)			
ORIFICE	ZPP(IN.)	PP(PSIA)	PP/PT2	ORIFICE	ZPP(IN.)	PP(PSIA)	PP/PT2
101	0.027	0.521E+01	0.310E+01	109	0.077	0.645E+01	0.383E+01
102	0.125	0.679E+01	0.404E+01	110	0.177	0.640E+01	0.381E+01
103	0.225	0.642E+01	0.382E+01	111	0.277	0.632E+01	0.376E+01
104	0.324	0.617E+01	0.367E+01	112	0.376	0.610E+01	0.363E+01
105	0.424	0.632E+01	0.376E+01	113	0.477	0.621E+01	0.369E+01
106	0.524	0.617E+01	0.367E+01				
107	0.626	0.609E+01	0.362E+01				
108	0.725	0.593E+01	0.353E+01				

I	P	PT2	Q	V	RHO	MU	KE
DEG,R	PSIA	PSIA	PSIA	FPS	LBH/FT3	LB-SEC/FT2	FT-1
91.7	0.021	1.682	0.91	3696.	0.617E-03	0.738E-07	0.960E+06

MUN	ALPHA DEG	PT PSIA	TT DEG,R	M
11	35.00	184.27	1228.67	7.87

Sample 5.1 Typical Tabulated Data on the Pressure Probing Test

6.0 LEADING EDGE HEATING DEMONSTRATED (PHASE III)

6.1 TEST ARTICLE

To demonstrate test techniques for aerodynamic heating measurements on small-radius model geometries (such as wing leading edges), an unswept, cylindrical leading edge test article was fabricated. This article was tested in Tunnel B at Mach 8 and a photograph of its installation in the test section is shown in Fig. 6.1. An installation sketch is presented in Fig. 6.2.

Two closeup photographs of the demonstration test article are shown in Fig. 6.3 and a drawing with pertinent dimensions is presented in Fig. 6.4. The leading edge piece was fabricated from MACOR[®], a machinable glass ceramic (CODE 9658). It was fabricated in three sections of varying leading edge radii (0.07, 0.125, 0.25 in.). Each constant radius section consisted of three 0.5 in. wide filler pieces with two instrumented pieces interspersed. One instrumented piece in each section was 0.165 in. wide, the other instrumented piece was 0.300 in. wide. Each of these two pieces was instrumented with thin-film gages as discussed in Section 6.2. All of the MACOR sections were held together by a steel clamping mechanism to form one unit.

Figure 6.5 is a photograph of the leading edge test article with the flow shield which was also fabricated for this entry. The shield was made from a wire mesh substrate covered with RTV. The shield was held in place via the following:

Overlength screws in the downstream cover of the leading edge clamping mechanism (see Fig 6.4) prevented the shield from translating downstream.

Rubber stoppers along the forward, inside surface provided support required to keep the shield away from the instrumented leading edge.

Rubber bands were placed around the MACOR pieces and the clamp to keep the shield in place until it was removed.

A sketch of the shield installation in the tunnel is shown in Fig. 6.6. A cable, attached to the inside of the tunnel installation tank and to the forward surface of the shield, was used to separate the shield from the leading edge just prior to the arrival of the leading edge on tunnel centerline. In this manner, it was hoped that the shield would provide instantaneous exposure to the free-stream flow, thereby eliminating the effects of translating through the interaction region between the installation tank and the test section.

6.2 TEST INSTRUMENTATION

The six metric sections of the leading edge development model were instrumented with seventy-two thin-film resistance gages and three thin-foil thermocouples. Due to gage lead wire space limitations, test data were obtained for the three thermocouples and only twenty-nine of the thin-film gages. Figure 6.7 illustrates the location of each gage used during testing and Table 6.1 lists the measured location of each gage. For reference, the close-up photographs of Fig. 6.3 show the arrangement of the gages on the model. The thin-film gages and foil thermocouples were used to measure the surface temperature history at discrete locations on the leading edge. These temperature histories were then used to calculate the local heating rate.

To apply the thin films to the MACOR pieces, the following procedure was followed:

SURFACE PREPARATION - The edges of each MACOR piece were slightly rounded to eliminate any difficulties associated with maintaining electrical continuity of the films as they were routed around the corner from the exposed (aerodynamic) surface to the sides of the leading edge metric sections. In addition, the MACOR surface was polished to less than 5 microinch roughness.

FILM APPLICATION - Hanovia Liquid Bright Platinum #05 (Engelhard Industries, Inc.) was hand painted on the MACOR pieces at room temperature. Liquid gold was then hand painted over the platinum film starting on the exposed surface near the edge of the MACOR piece and extending beyond the rounded corners to the side surfaces to a point where copper lead wires could be attached. The gold film served to electrically short the platinum film near the corners of the MACOR piece and thereby leave only that part of the platinum film painted on the flat, exposed surface sensitive to temperature changes.

FIRING - The MACOR pieces were oven fired to bond permanently the painted films to the MACOR. Successive firing and cooling cycles were used to anneal the films and thereby virtually eliminate changes in film calibration with repeated temperature cycling.

GAGE LEAD ATTACHMENT AND CALIBRATION - Following annealing of the films, copper lead wires were soldered to the gold film at a point on the side of the leading edge. Temperature versus resistance calibrations for all films were then obtained by oven heating the instrumented MACOR piece in preset temperature steps.

The thin-film gage application and calibration techniques used in this test program will be fully documented in a follow-on AEDC Technical Report.

The three thin-foil thermocouples were copper-constantan foils (0.0002 in. thick and 0.0033 in. wide) bonded to the MACOR surface using strain gage cement.

During testing, the thin-film gages were electrically configured as one arm of a Wheatstone bridge circuit with external excitation provided by a 5 volt precision power supply.

One black and white shadowgraph still photograph was obtained on each leading edge test run, and high speed shadowgraph movies were obtained for those runs on which the flow shield (see Section 6.1) was employed. A summary of the photographic data obtained during the entry is presented in Table 6.2.

6.3 TEST CONDITIONS AND PROCEDURES

The nominal free stream test conditions for the Leading Edge Heating Demonstration Phase are given below:

<u>M</u>	<u>PT, psia</u>	<u>TT, °R</u>	<u>Q, psia</u>	<u>P, psia</u>	<u>RE x 10⁻⁶, ft⁻¹</u>
8	200	1260	0.95	0.021	0.97
8	800	1340	3.66	0.082	3.5

A test summary describing all test runs for this phase is presented in Table 6.3. All data were obtained at zero angle of attack.

Data were obtained for the thin-film gages and thin-foil thermocouples at a rate of 95 points per second, starting at the initiation of the injection sequence and ending when the model left the tunnel centerline during the retraction sequence. Data acquisition was controlled automatically by a Digital Equipment Corporation PDP 11/40 computer, utilizing the Random Access Data System with thin-film gage and thermocouple signals preprocessed by a digital data scanner operating in conjunction with an analog subsystem.

On several runs, a flow shield was used to screen the leading edge from tunnel flow during the inject sequence until just prior to arrival at the tunnel centerline. The details of the design and use of this shield are presented in Section 6.1.

6.4 DATA REDUCTION

The resistance of a thin-film gage is a linear function of the temperature of the film. Therefore, if the film is excited by a constant voltage source (as was done for these tests), the output voltage from each film can be used to calculate the surface temperature of the substrate to which the film is attached. The sensitivity of each thin-film gage used in these tests was determined by pretest measurements of resistance at

various substrate temperatures. Prior to the start of testing, the output of each gage was set to zero, therefore the surface temperature could be calculated from the output of the thin-film gages as follows:

$$TW = s \times E + TW_0$$

where:

$$\begin{aligned} s &= \text{gage sensitivity } (^{\circ}\text{R/mv}) \\ E &= \text{gage output (mv)} \\ TW_0 &= \text{temperature at which gage output zero was set, } ^{\circ}\text{R} \end{aligned}$$

For the thin-foil thermocouples, surface temperature was calculated from the thermocouple output voltage via a curve fit of the Thermocouple Reference Tables published by the National Bureau of Standards (1974).

For the data presented with this report, the heat flux at each instrumented location was computed for each time point (t_n) from the measured surface temperature via the following equation derived from semi-infinite solid considerations:

$$QDOT(t_n) = \frac{2C(t_n)}{\sqrt{\pi}} \sum_{j=2}^n \frac{TW(t_j) - TW(t_{j-1})}{\sqrt{t_n - t_j} + \sqrt{t_n - t_{j-1}}}$$

The parameter $C(t_n)$, representing the value of $\sqrt{\rho c k}$ for the substrate material corresponding to the temperature at time t_n , was calculated from the following equation based on pretest measurements of MACOR thermal response data:

$$C(t_n) = 2.692 \times 10^{-5} \left(\frac{TW(t_n) + TW(t_1)}{2} \right) + 0.0827 \left[\text{Btu/ft}^2\text{-sec}^{\frac{1}{2}}\text{-}^{\circ}\text{R} \right]$$

Since the small radius leading edges investigated during these tests cannot be expected to respond thermally as semi-infinite solids, there is some undefined error associated with reducing the surface temperature to heat flux in this manner. An analysis of the magnitude of these errors and presentation of the data corrected for these effects will be included in the analysis of an AEDC Technical Report to be prepared in the future.

The tabulated data in the data package which is associated with this report are based on values of QDOT and TW obtained at a single time point occurring approximately 0.5 seconds prior to the time that the model reached tunnel centerline. The data for runs on which the flow shield was used correspond to values calculated for a time of approximately 0.1 seconds after shield removal. No filtering or averaging techniques have been used to date on these data.

The surface heat-transfer coefficient at each instrumented location was calculated using the values of QDOT and TW obtained as discussed above via the following:

$$H(TT) = \frac{QDOT}{(TT-TW)}$$

The Stanton number was then calculated as follows:

$$ST(TT) = \frac{H(TT) [TT-TW]}{(\rho)(V) [I(TT)-I(TW)]}$$

Both the heat transfer coefficient and the Stanton numbers were normalized using stagnation point predictions from the method of Fay and Riddell (HREF and STREF, respectively). The reference values were each calculated for the appropriate leading edge radius, and leading edge diameter was used in place of the radius in the Fay-Riddell calculations to account for the fact that this is a 2-D rather than a 3-D stagnation point flow situation. The specific equations used to calculate H(REF) and ST(REF) are presented in Appendix I.

6.5 DATA PACKAGE PRESENTATION

A presentation of typical tabulated data included in a separate data package is presented in Sample 6.1. This consists of a listing of tunnel conditions and test article configurations information for each run, followed by the heat-transfer data for each gage.

Further analysis of the data will be presented in a future AEDC Technical Report.

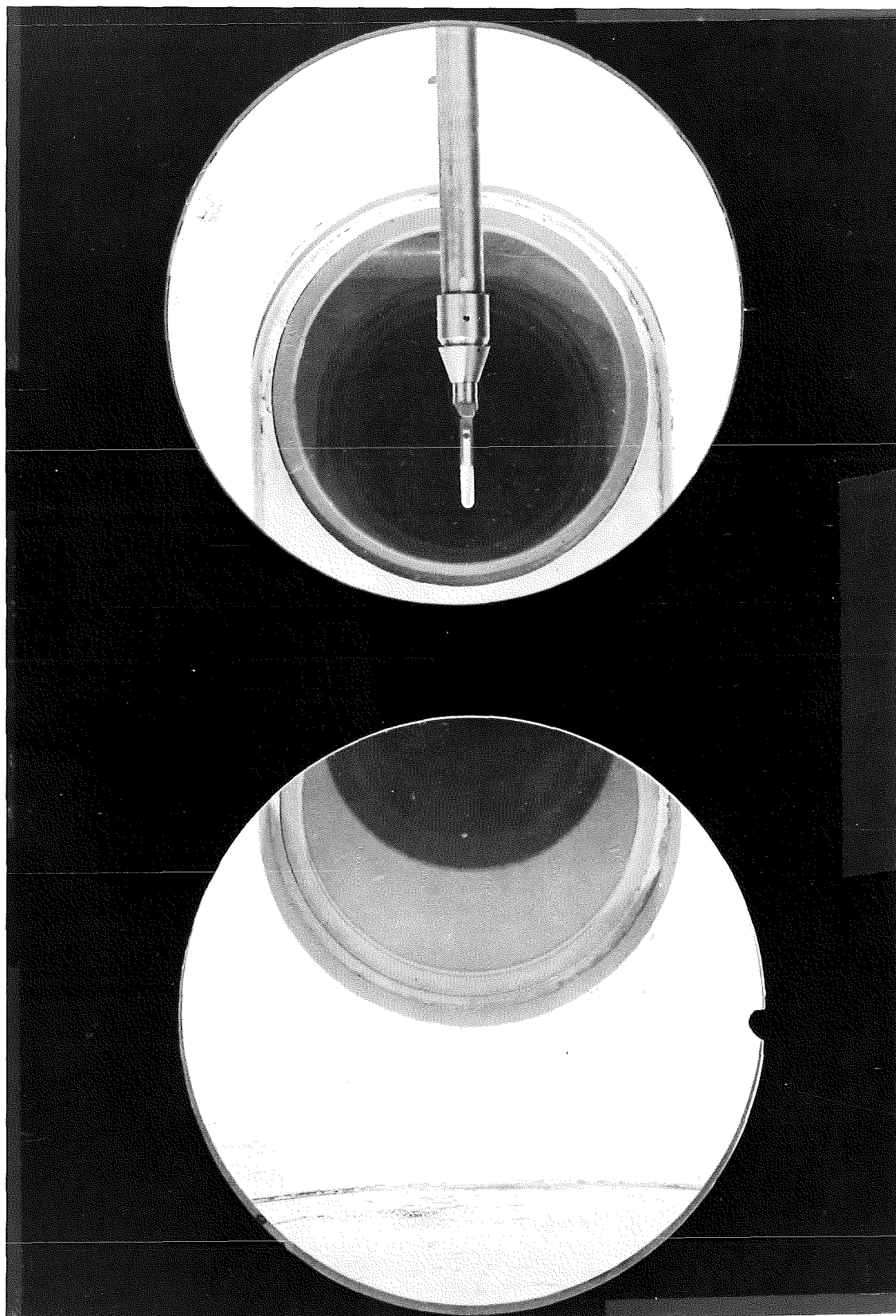
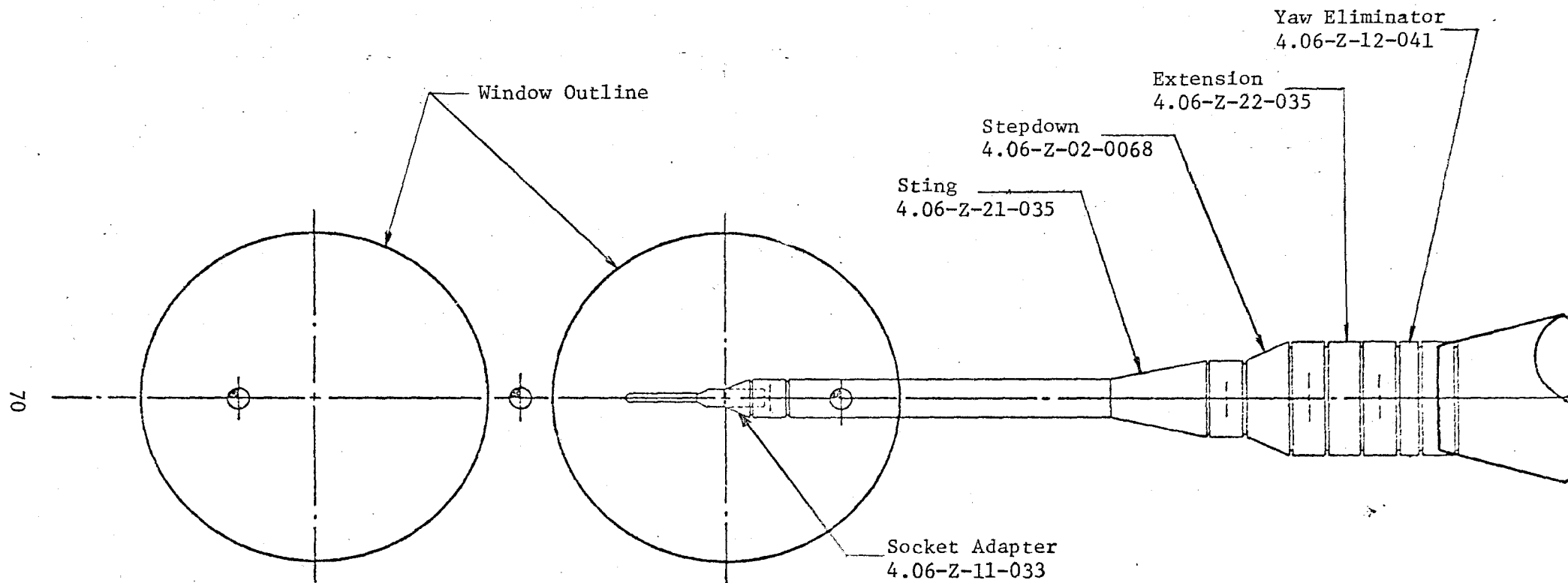


Figure 6.1 Phase III Test Article in the Tunnel B Test Section

50-INCH HYPERSONIC TUNNEL -B M = 8

TUNNEL WALL



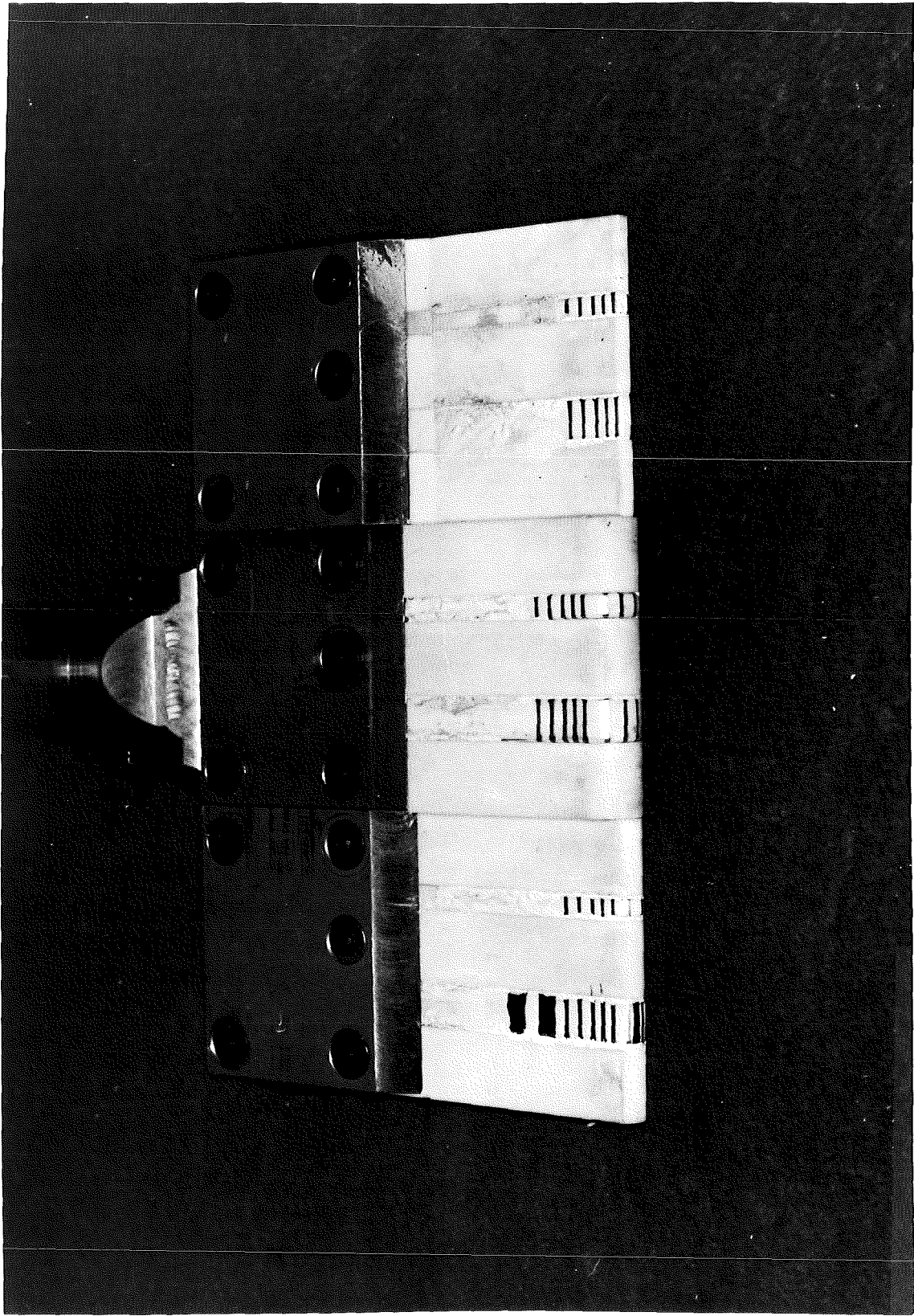
TUNNEL WALL

Figure 6.2 Phase III Test Article Installation in Tunnel B



a. Leading Edge View

Figure 6.3 Closeup of the Leading Edge Heating Demonstration Test Article



b. Planform View
Figure 6.3 Concluded

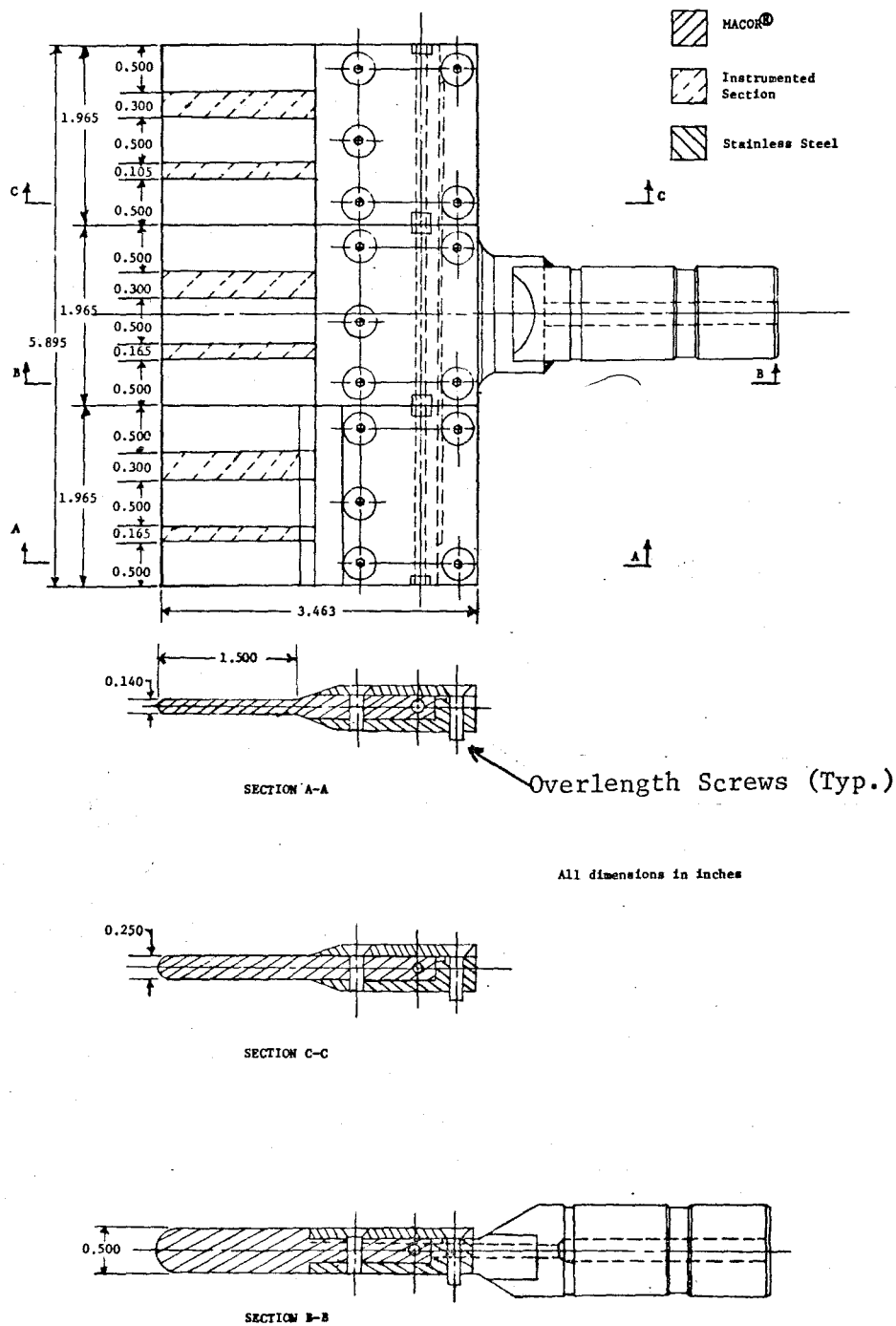


Figure 6.4 Basic Dimensions of the MACOR® Substrate and Holder for the Leading Edge Heating Demonstration Test Article

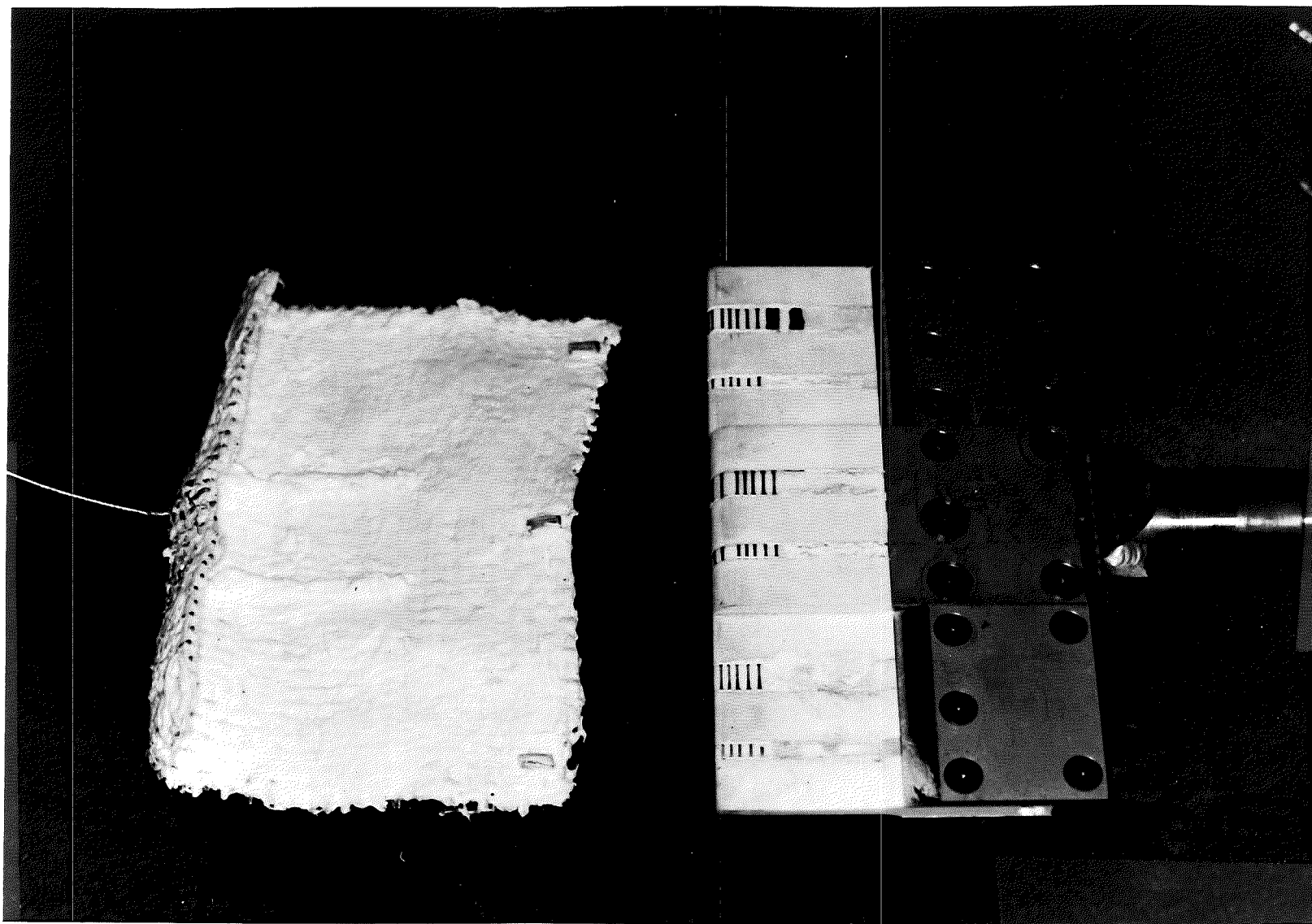


Figure 6.5 Leading Edge Heating Demonstration Test Article with Flow Shield

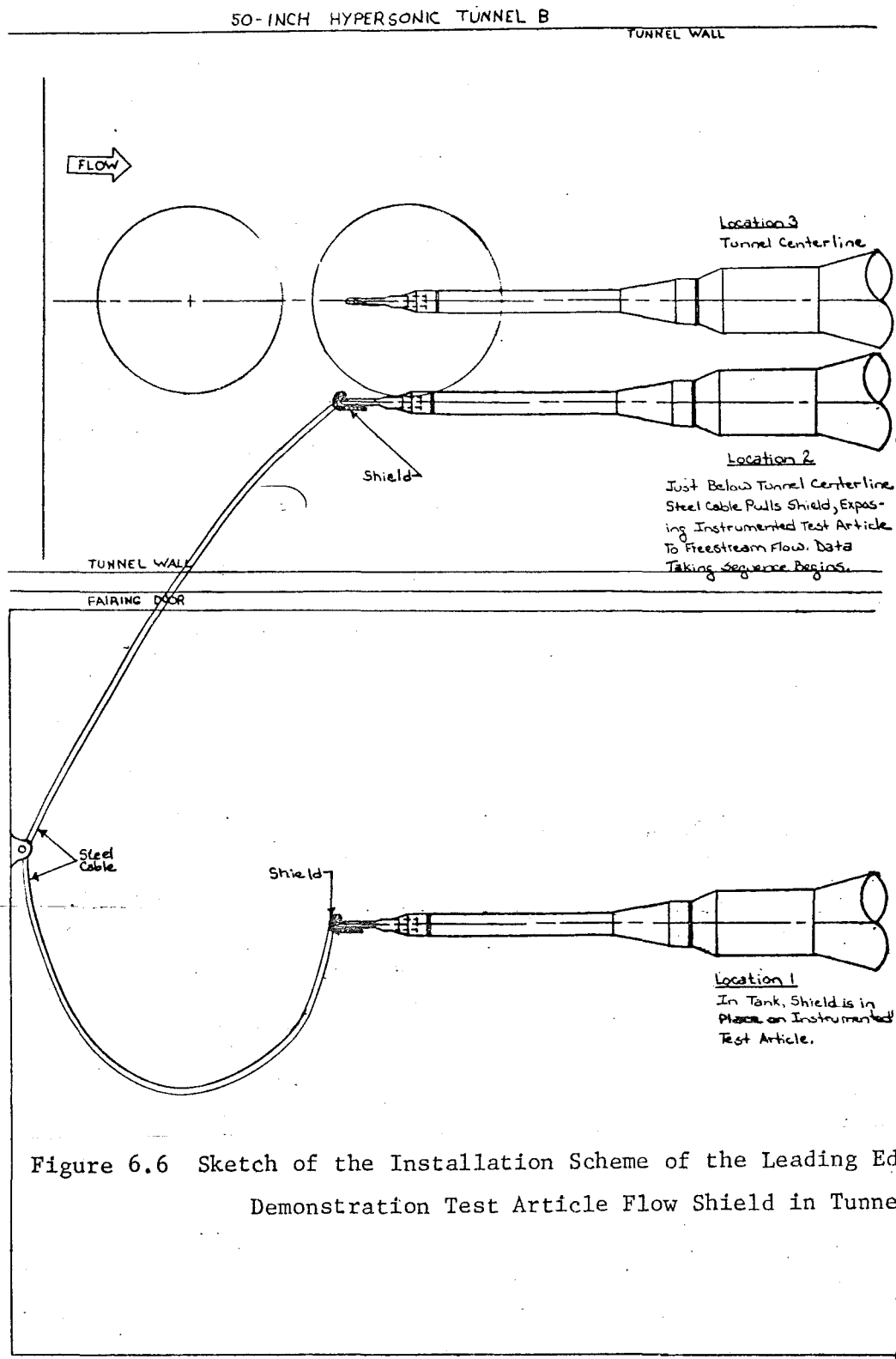
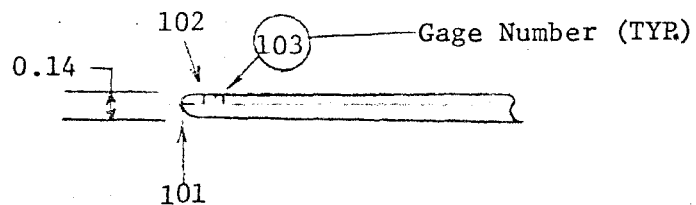
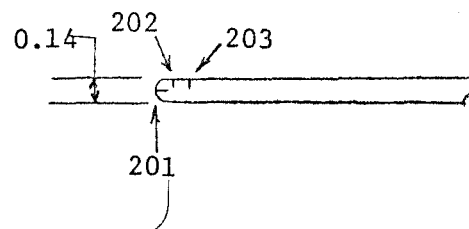


Figure 6.6 Sketch of the Installation Scheme of the Leading Edge Heating Demonstration Test Article Flow Shield in Tunnel B

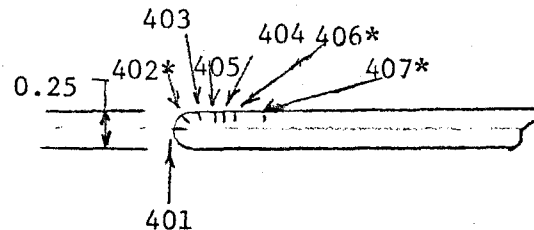
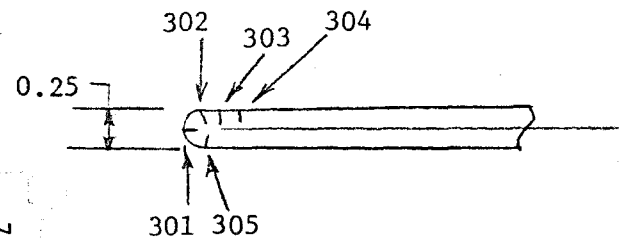
0.3 in. Width



0.165 in. Width



All dimensions in inches



*Indicates thin-foil thermocouple rather than thin-film gage

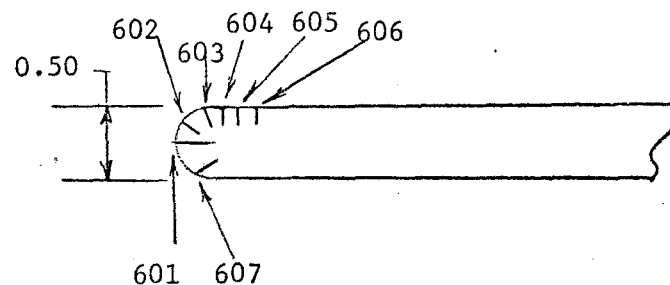
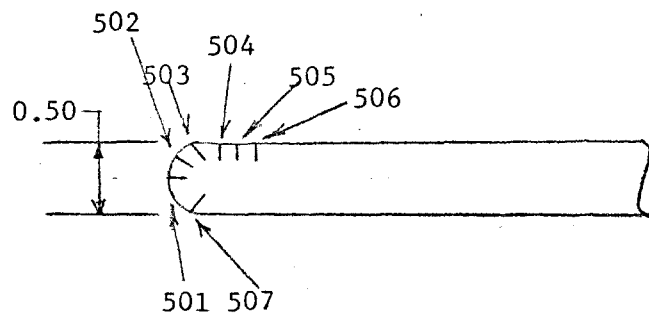


Figure 6.7 Instrumentation Location Sketch for the Leading Edge Heating Demonstration Test Article

TABLE 6.1 Instrumentation Locations for the Leading Edge Heating
Demonstration Test Article

GAGE #	S/R	R	WIDTH OF INSTRUMENTED PIECE, in.
101	0.0	0.07	0.30
102	1.571	↓	↓
103	2.699		
201	-0.075		0.165
202	1.614	↓	↓
203	3.714		
301	-0.057	0.125	0.30
302	0.934	↓	↓
303	1.763		
304	2.395		
305	-0.903		↓
401	0.042		0.165
402*	0.520	↓	↓
403	0.989		
404	1.795		
405	2.395		
406*		↓	↓
407*	2.571		
501	0.0	0.250	0.30
502	0.537	↓	↓
503	0.967		
504	1.591		
505	1.895		
506	2.195		
507	-0.842		↓
601	0.0		0.165
602	0.480	↓	↓
603	0.999		
604	1.607		
605	1.899		
606	2.203		
607	-0.833	↓	↓

* Indicates thin-foil thermocouple rather than thin-film gage.
See Figure 6.7.

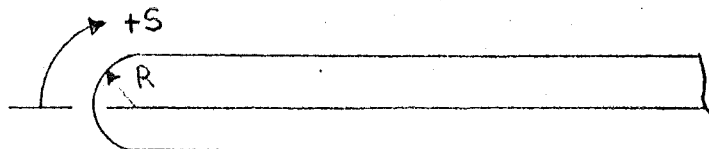


TABLE 6.2 Summary of Photographic Coverage for Leading Edge Heating Demonstration Test

	Camera Number	Camera Type	Camera View	Frame Rate	Run Number	Film ID
Phase III-Leading Edge Instrumentation Development	1	DBM-55 16 mm motion picture	Top view of model on centerline	24 400	1-7 8-10	4762 ↓
	2	↓	Side view of model on centerline	24	1-10	4763
	3	HYCAM 16 mm motion picture	Side view of flow field through aft window	24 400	1-7 8-10	4764 ↓

TABLE 6.3 Run Summary for the Leading Edge Heating
Demonstration Test

RUN	RE/ft $\times 10^{-6}$	ALPHA, deg	PHII, deg	Nominal Time on Centerline	Shield
1	0.97	0	0	2 sec.	Not Used
2	↓	↓	↓	↓	↓
3	↓	↓	180	↓	↓
4	3.5	↓	0	↓	↓
5	↓	↓	↓	↓	↓
6	↓	↓	180	↓	↓
7	↓	↓	0	↓	Used
8	↓	↓	↓	↓	↓
9	↓	↓	↓	2 min.	Not Used
10	↓	↓	↓	2 sec.	↓
11	↓	↓	↓	2 min.	↓

ARVIN/CALSPAN FIELD SERVICES, INC.
AEDC DIVISION
VON KARMAN GAS DYNAMICS FACILITY
ARNOLD AIR FORCE STATION, TENNESSEE

DATE COMPUTED 26-JAN-83
TIME COMPUTED 14:48:07
DATE RECORDED 27-JUL-82
TIME RECORDED 6:10:57
PROJECT NUMBER V 8-1L

RUN CONFIG ALPHA PHII TIME
8 SHIELDED 0.01 0.01 2.01

HREF1 HREF2 HREF3 STREF1 STREF2 STREF3
(R= 0.0117) (R= 0.0208) (R= 0.0416) (R= 0.0117) (R= 0.0208) (R= 0.0416)
5.804E-02 4.346E-02 3.073E-02 2.652E-02 1.986E-02 1.404E-02

N PT TT T P Q V RHO MU RE PT2
PSIA DEG R DEG R PSIA PSIA FT/SEC LBM/FT3 LBF-SEC/FT2 FT-1 PSIA
7.97 783.35 1335.7 97.5 8.227E-02 3.66 3857.2 2.278E-03 7.844E-08 3.481E+06 6.765E+00

GAGE NO S/R TI TW SRCK QDOT H(TT) ST(TT) H(TT)/HREF ST(TT)/STREF
DEG R DEG R BTU/FT2-SEC BTU/FT2-SEC-R

101	0.000	608.674	789.492	0.102	3.620E+01	6.627E-02	2.991E-02	1.142E+00	1.128E+00
102	1.570	542.582	581.484	0.098	8.187E+00	1.085E-02	4.954E-03	1.870E-01	1.868E-01
103	3.000	547.165	573.406	0.098	4.708E+00	6.177E-03	2.820E-03	1.064E-01	1.063E-01
201	0.000	806.526	956.053	0.106	2.857E+01	7.526E-02	3.366E-02	1.297E+00	1.269E+00
202	1.570	558.702	584.692	0.098	3.932E+00	5.236E-03	2.389E-03	9.021E-02	9.009E-02
203	4.140	540.325	550.963	0.097	1.906E+00	2.429E-03	1.111E-03	4.186E-02	4.188E-02
301	0.000	620.467	718.351	0.101	2.013E+01	3.262E-02	1.478E-02	7.505E-01	7.441E-01
302	0.790	583.715	680.931	0.100	1.896E+01	2.896E-02	1.315E-02	6.664E-01	6.621E-01
303	1.570	536.319	562.174	0.097	4.656E+00	6.019E-03	2.750E-03	1.385E-01	1.385E-01
304	2.370	540.062	540.052	0.097	-1.659E-02	-2.085E-05	-9.538E-06	-4.798E-04	-4.803E-04
305	-0.790	540.483	540.443	0.097	-2.367E-02	-2.977E-05	-1.362E-05	-6.850E-04	-6.857E-04
401	0.000	625.323	808.623	0.102	3.615E+01	6.859E-02	3.093E-02	1.578E+00	1.557E+00
402	0.000	586.956	706.246	0.100	2.049E+01	3.255E-02	1.475E-02	7.489E-01	7.431E-01
403	0.440	539.858	539.829	0.097	-1.769E-02	-2.223E-05	-1.017E-05	-5.114E-04	-5.120E-04
404	0.790	540.242	540.171	0.097	-9.532E-02	-1.198E-04	-5.481E-05	-2.757E-03	-2.760E-03
405	1.570	540.152	540.109	0.097	-9.660E-02	-1.214E-04	-5.554E-05	-2.794E-03	-2.797E-03
406	5.970	591.791	591.756	0.099	1.818E-02	2.444E-05	1.115E-05	5.625E-04	5.615E-04
407	7.970	585.554	611.784	0.099	1.451E+00	2.004E-03	9.132E-04	4.612E-02	4.599E-02
501	0.000	583.843	681.319	0.100	1.789E+01	2.734E-02	1.241E-02	8.897E-01	8.839E-01
502	0.520	585.479	677.158	0.100	1.734E+01	2.633E-02	1.195E-02	8.567E-01	8.513E-01
503	1.050	547.486	582.957	0.098	6.338E+00	8.420E-03	3.843E-03	2.740E-01	2.737E-01
504	0.570	544.036	562.088	0.098	1.964E+00	2.539E-03	1.160E-03	8.261E-02	8.260E-02
505	2.170	541.246	556.119	0.097	1.288E+00	1.652E-03	7.551E-04	5.376E-02	5.377E-02
506	2.370	539.165	557.382	0.097	1.451E+00	1.864E-03	8.520E-04	6.067E-02	6.068E-02
507	0.000	558.458	610.209	0.098	1.014E+01	1.396E-02	6.372E-03	4.550E-01	4.534E-01
601	0.000	584.183	710.219	0.100	2.336E+01	3.730E-02	1.693E-02	1.216E+00	1.206E+00
602	0.520	577.520	692.988	0.100	2.091E+01	3.254E-02	1.476E-02	1.059E+00	1.051E+00
603	1.050	543.125	576.345	0.098	5.575E+00	7.343E-03	3.352E-03	2.389E-01	2.387E-01
604	1.570	534.799	561.224	0.097	3.014E+00	3.892E-03	1.778E-03	1.267E-01	1.267E-01
605	1.970	537.193	559.158	0.097	1.884E+00	2.426E-03	1.109E-03	7.894E-02	7.895E-02
606	2.370	533.379	557.532	0.097	2.179E+00	2.801E-03	1.280E-03	9.115E-02	9.116E-02
607	-0.790	570.518	634.878	0.099	1.265E+01	1.804E-02	8.212E-03	5.872E-01	5.848E-01

Sample 6.1 Typical Tabulated Data on the Leading Edge Heating Demonstration Test

7.0 WING LEADING EDGE HEATING TEST (PHASE IV)

7.1 TEST ARTICLE

The thin-film gages on MACOR technique demonstrated in Phase III was used on Phase IV. A MACOR insert was fabricated in the shape of the wing leading edge of the Shuttle Orbiter to attach to the 94-0 (0.025 scale) model. This test article was tested in Tunnel C at Mach 10 and a photograph of its installation in the test section is shown in Fig. 7.1. An installation sketch is presented in Fig. 7.2.

To attach this MACOR insert to the 94-0 Model, an existing copper leading-edge, which was fabricated for this model during earlier testing, was modified. A photograph of the MACOR/copper assembly is shown in Fig. 7.3 and a drawing of the pertinent dimensions is shown in Fig. 7.4. Note that a Novamide filler block was present strictly to maintain uniform flow over the wing (Fig. 7.3).

The MACOR insert was basically 6 in. long with the exterior contoured to the shuttle wing leading edge. The back side was cut away to attach instrumentation leads. Figure 7.5 shows two closeup views and Fig. 7.6 gives the details and dimensions of the insert.

7.2 TEST INSTRUMENTATION

The MACOR insert was instrumented with twenty-seven thin-film gages. The gages were arranged in two spanwise rows along the wing leading edge. Figure 7.6 illustrates the location of each gage and Table 7.1 lists the measured location of the center of each gage.

The thin-film gages were installed in a slightly different manner on the wing insert than in Phase III. Fifty-four small holes (0.0135 in. diam) were drilled into the MACOR leading edge through to the back side channel (two holes for each of the 27 gages). This enabled the attachment of the lead wires through the back, thus eliminating the need to make small inserts as was necessary to do in Phase III for lead wire routing. The procedures used to apply the films, attach the leads, and calibrate were identical to the procedures described in Section 6.2.

Precision measurements were obtained of the contour of the leading edge of the MACOR insert. A plot of the leading edge radius at each end of the insert (the radius of the leading edge varies along its length) is presented in Fig. 7.7 with the chordwise location of the two rows of thin-film gages.

One black and white shadowgraph still photograph was obtained on each run. A summary of the photographic data obtained during this entry is presented in Table 7.2.

7.3 TEST CONDITIONS AND PROCEDURES

The nominal free-stream test conditions for the Wing Leading Edge Heating Test Phase are given below:

<u>M</u>	<u>PT, psia</u>	<u>TT, $^{\circ}$R</u>	<u>Q, psia</u>	<u>P, psia</u>	<u>RE x 10^{-6}, ft$^{-1}$</u>
10	380	1750	0.63	0.009	0.56
10	1150	1850	1.82	0.026	1.5

A test summary describing all test runs for this phase is presented in Table 7.3.

7.4 DATA REDUCTION

The data reduction procedures used in this phase were identical to that discussed in Section 6.4, page 70.

7.5 DATA PACKAGE PRESENTATION

A presentation of typical tabulated data included in a separate data package is presented in Sample 7.1. This consists of a listing of tunnel conditions and model attitude information for each run, followed by the heat-transfer data from each thin-film gage.

Further analysis of the data will be presented in a future AEDC Technical Report.

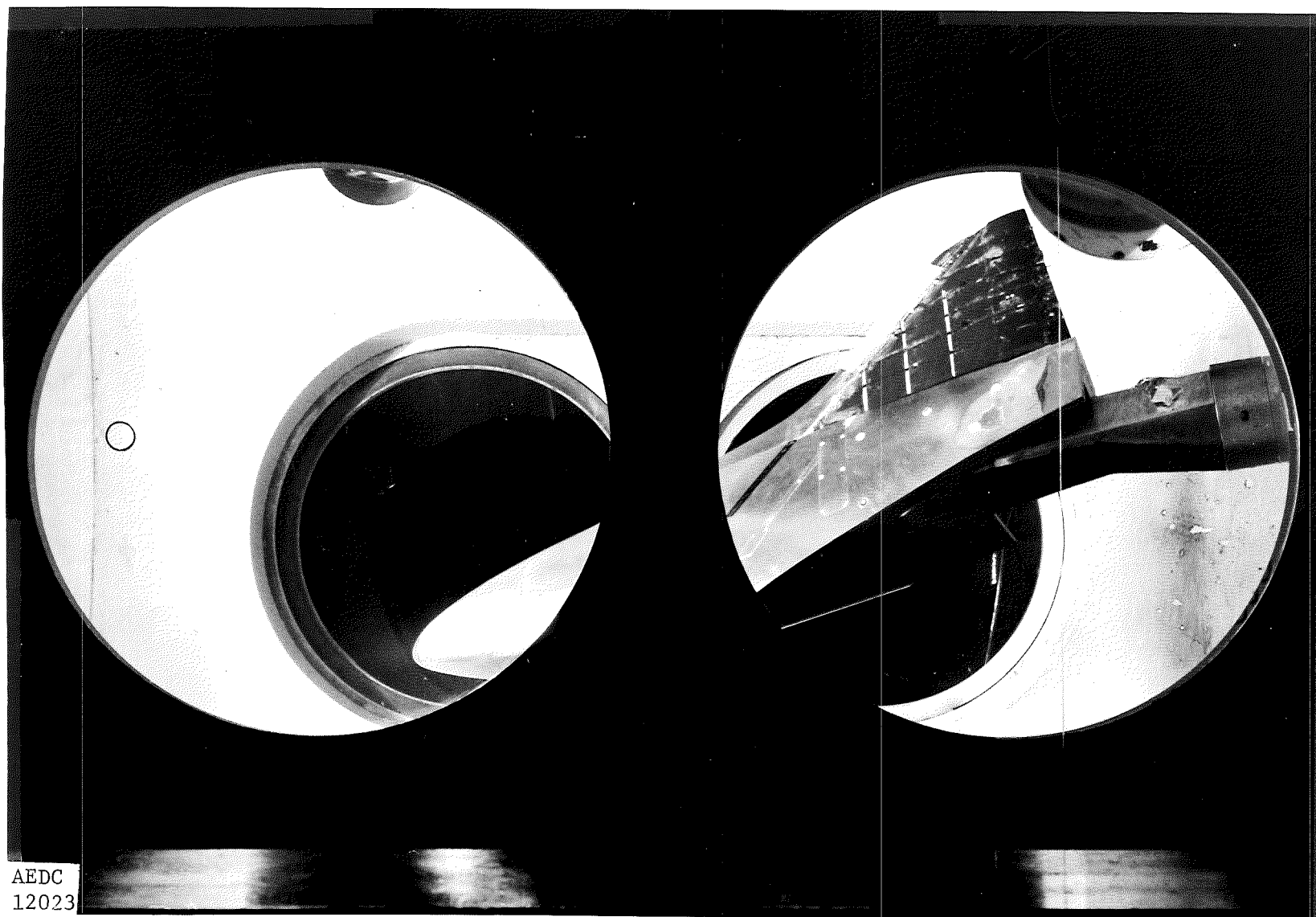
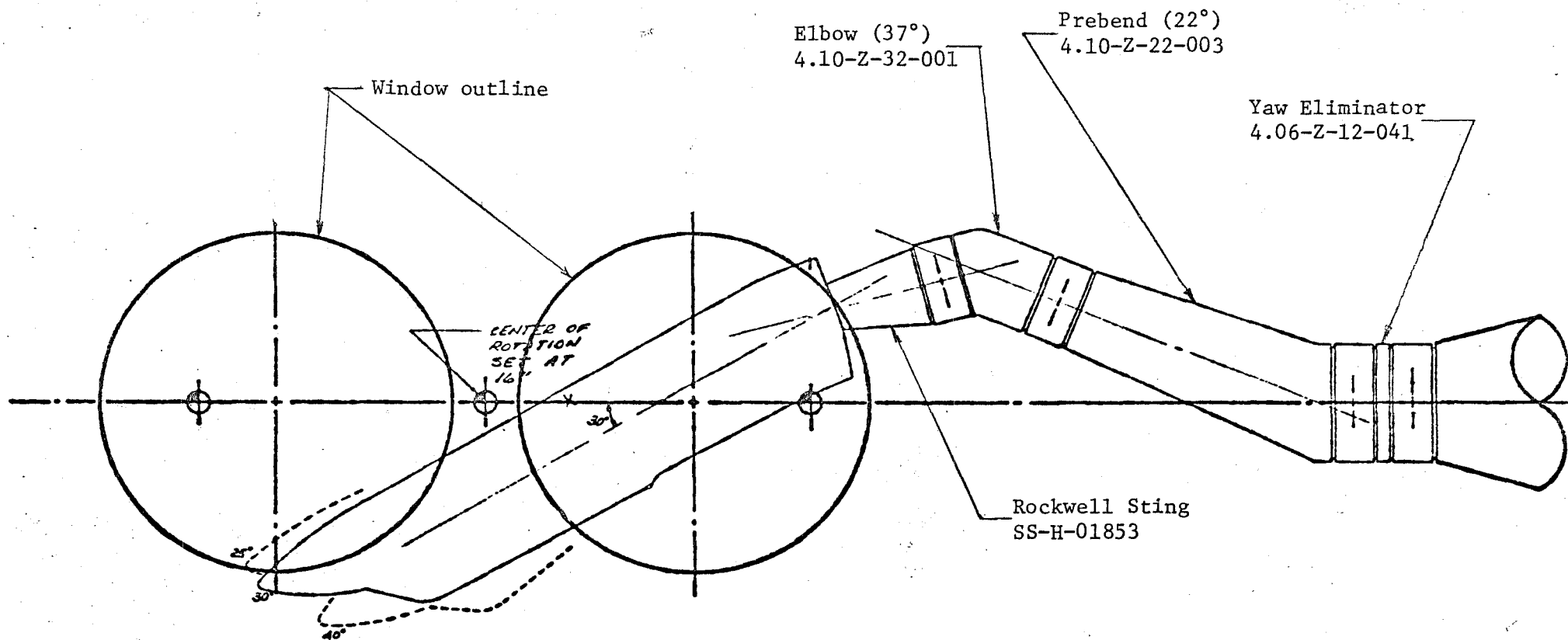


Figure 7.1 Phase IV in the Tunnel C Test Section

50-INCH HYPERSONIC TUNNEL C $M = 10$

TUNNEL WALL



TUNNEL WALL

Figure 7.2 Sketch of Phase IV Installation in Tunnel C

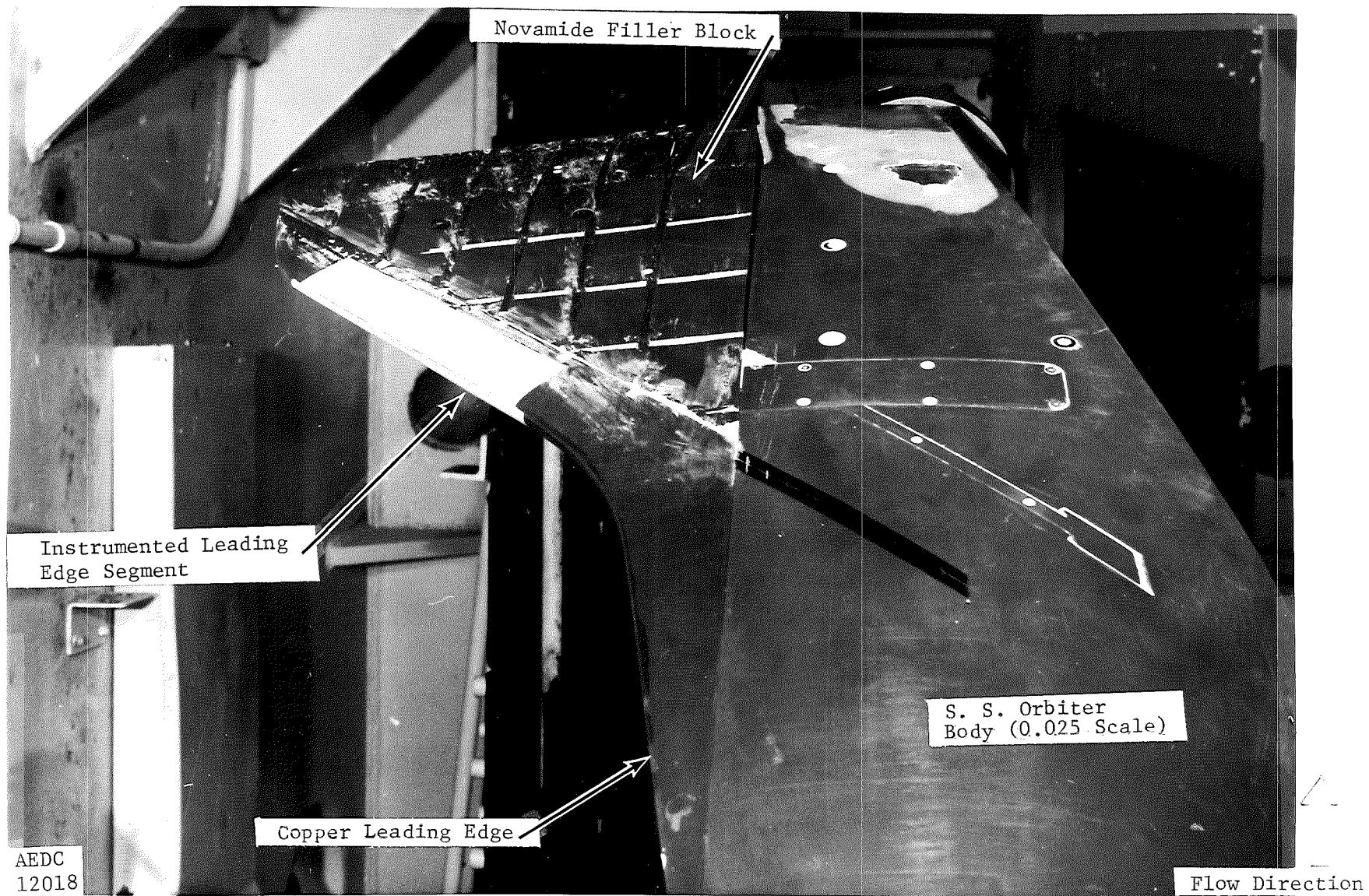


Figure 7.3 Instrumented Segment of the Orbiter Wing Leading Edge

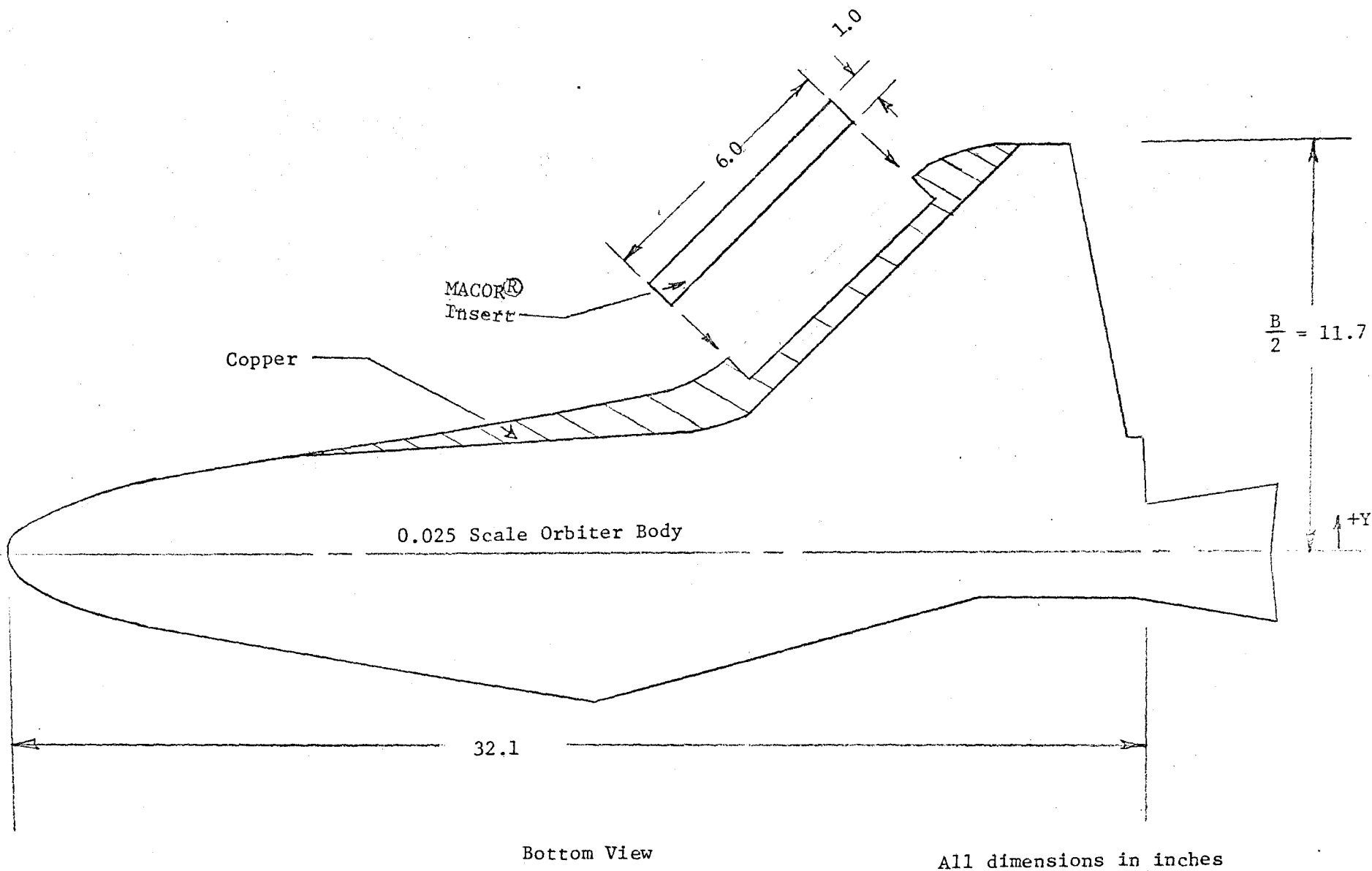
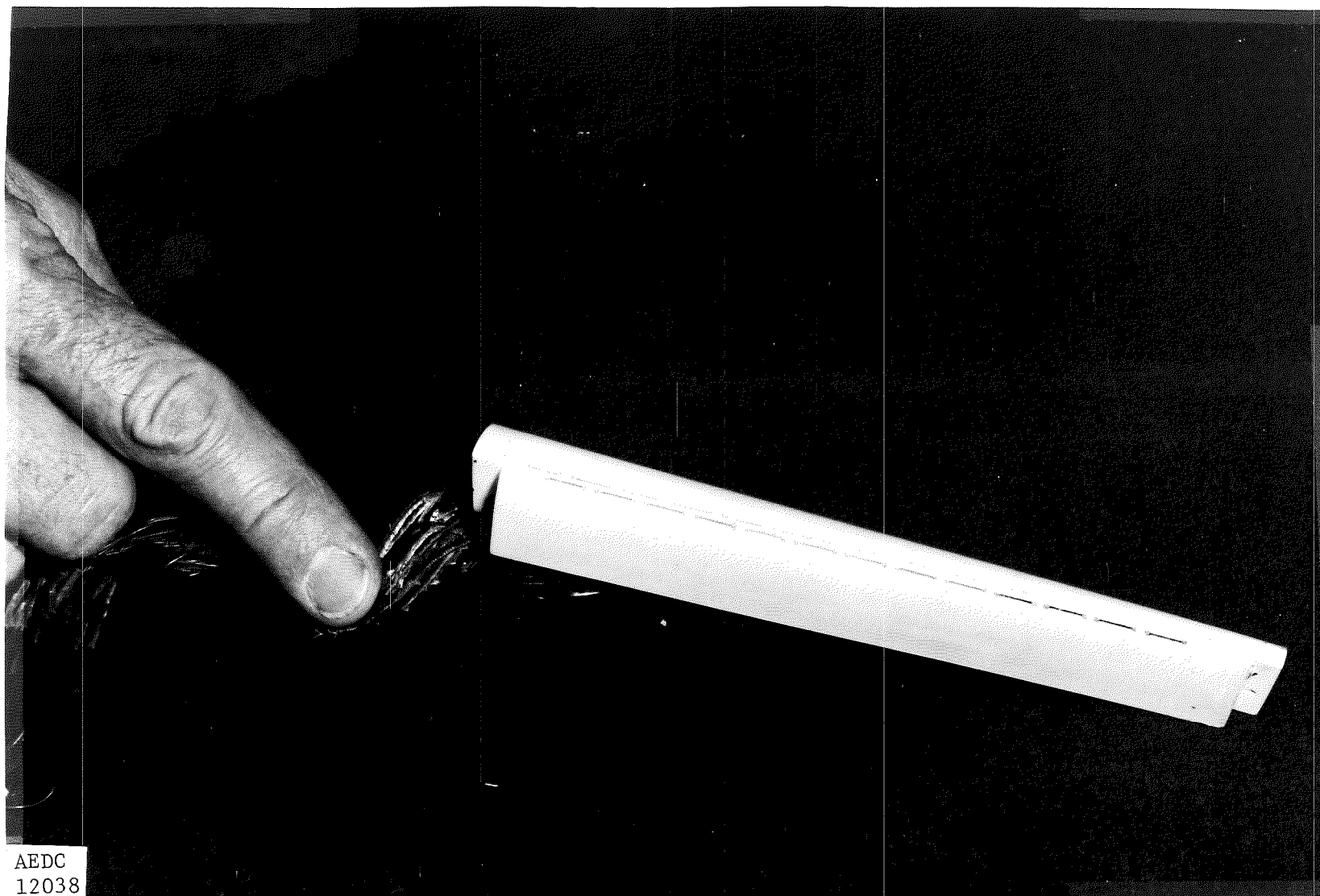
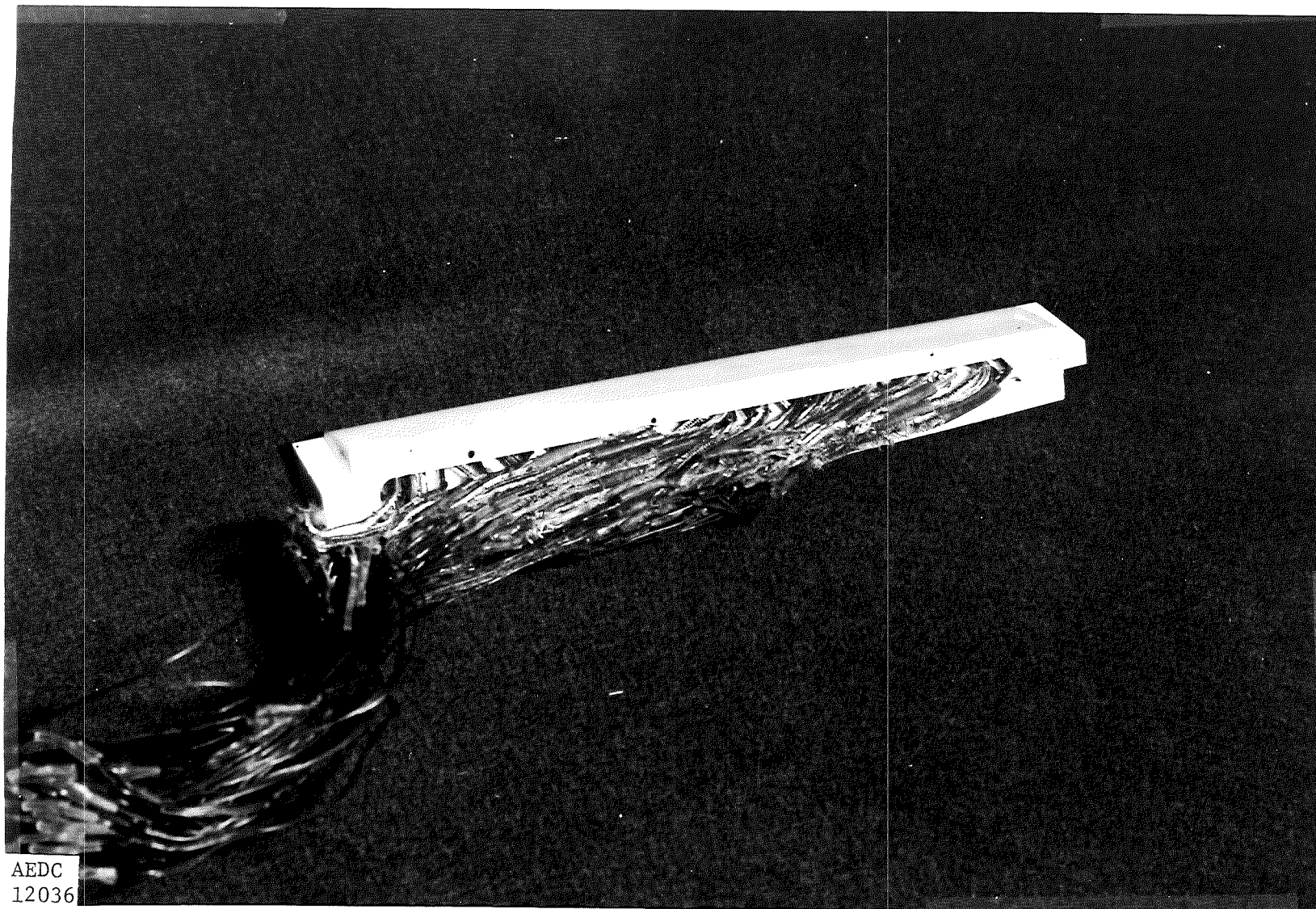


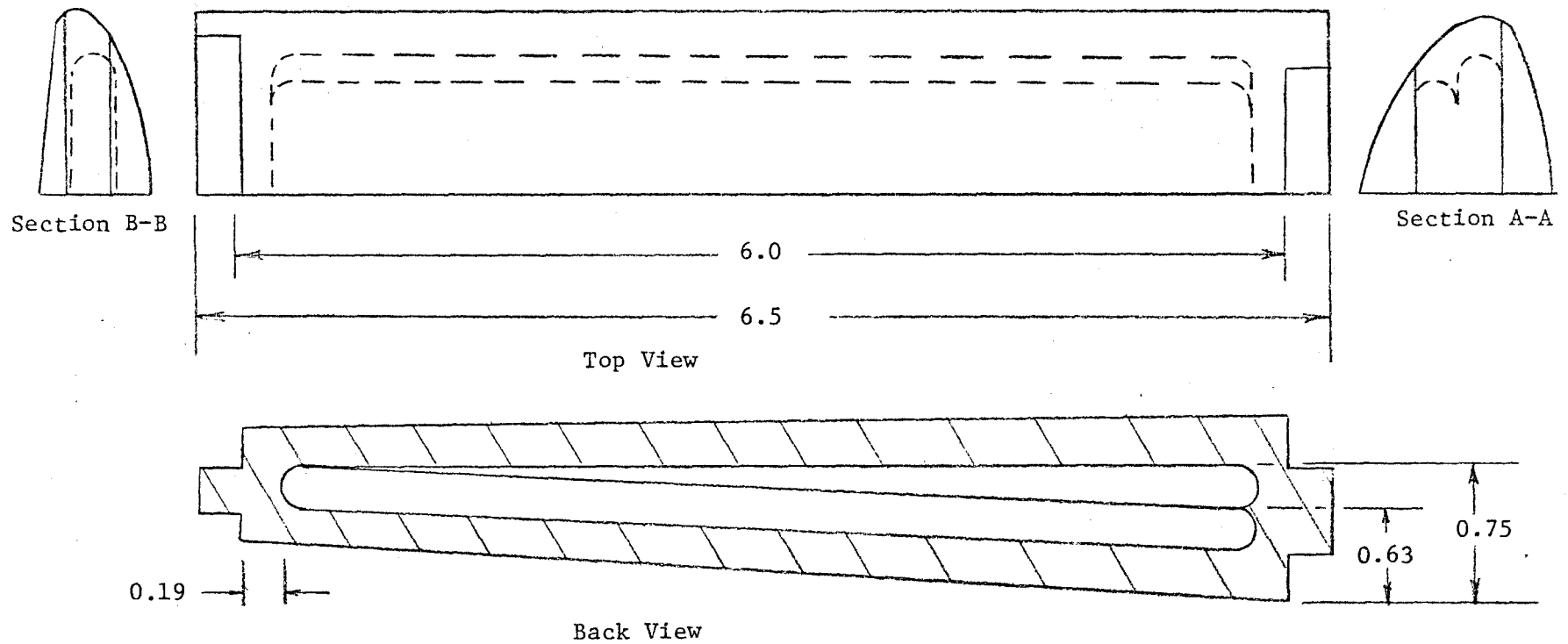
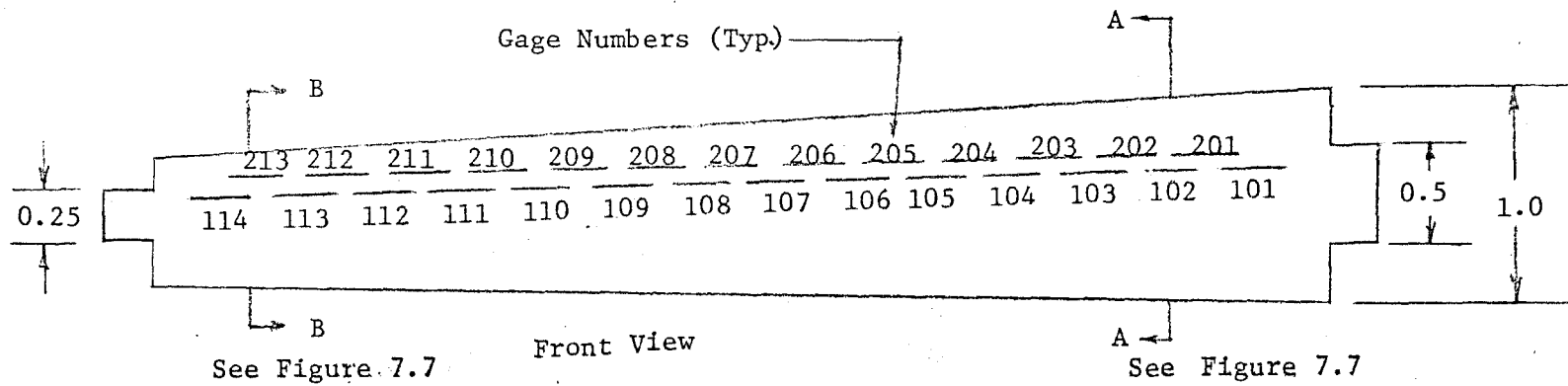
Figure 7.4 Basic Dimensions for the Wing Leading Edge Heating Test Article



a. Leading Edge View
Figure 7.5 Closeup of Wing Leading Edge MACOR® Insert



b. Backside View with Instrumentation Lead Wires
Figure 7.5 Concluded



All dimensions in inches

Figure 7.6 Basic Dimensions of the Wing Leading Edge Instrumented Insert with Gage Numbering Identification

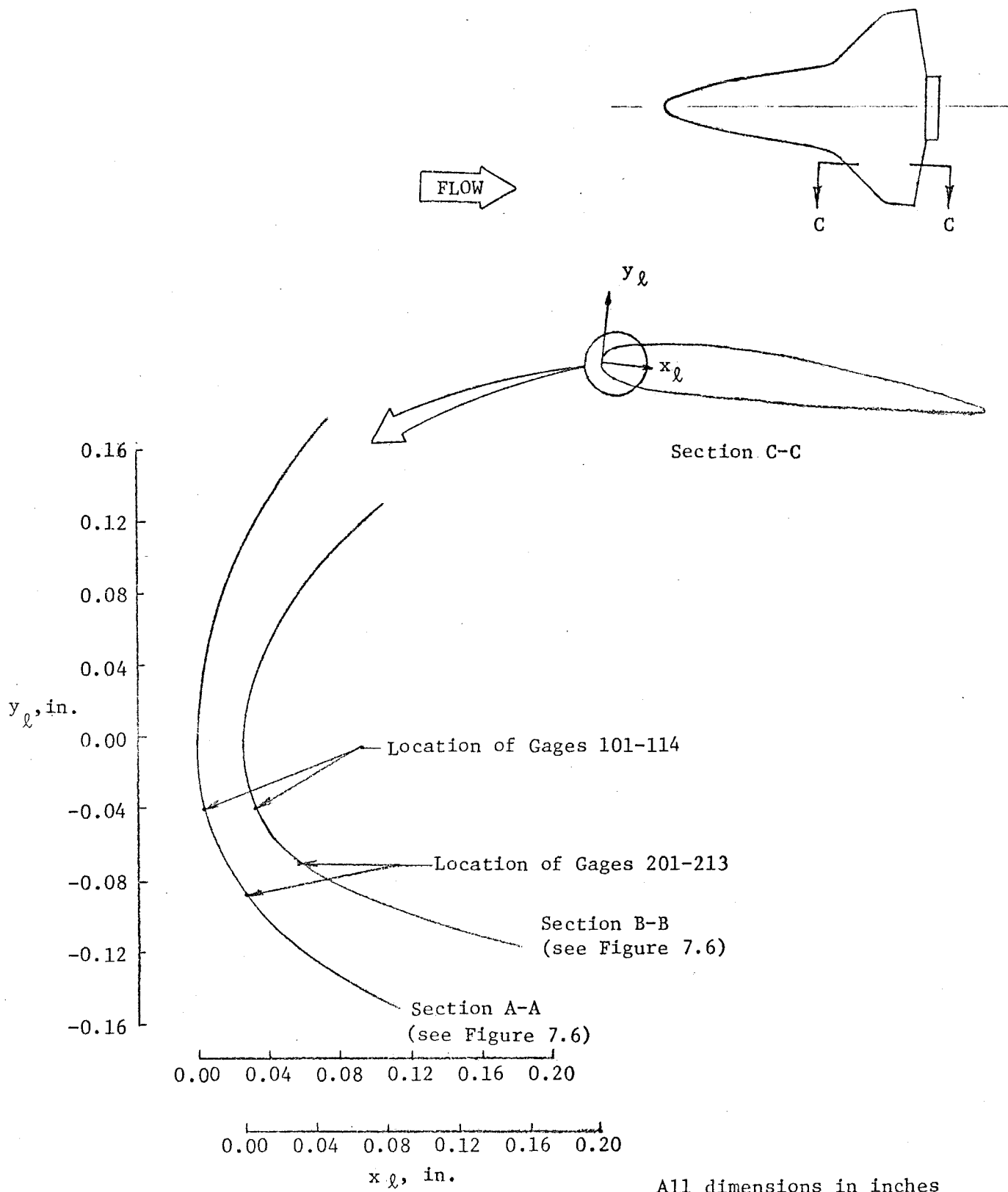


Figure 7.7 Measured Leading Edge Contours

TABLE 7.1 Thin Film Coordinates for the Wing Leading Edge
Heating Test Article

GAGE NO. *	2 Y/B Δ	DISTANCE FROM LEADING EDGE X_L , in.
101	0.56	.006
102	0.59	
103	0.61	
104	0.64	
105	0.65	
106	0.68	
107	0.70	
108	0.73	
109	0.75	
110	0.78	
111	0.80	
112	0.82	
113	0.85	
114	0.87	
201	0.57	.029
202	0.60	
203	0.62	
204	0.64	
205	0.67	
206	0.69	
207	0.70	
208	0.74	
209	0.76	
210	0.79	
211	0.81	
212	0.84	
213	0.86	

*See Figure 7.6 for gage locations.

Δ See Figure 7.4 for definition.

TABLE 7.2 Summary of Photographic Coverage for Wing Leading Edge Heating Test

	Camera Number	Camera Type	Camera View	Frame Rate	Run Number	Film ID
Phase IV - Leading Edge Heating	1	Varitron 70 mm shadowgraph stills	Side view of flow field through forward window	1 per run	1-19	917

TABLE 7.3 Summary of Leading Edge Heating Test (Phase IV)

Rex10 ⁻⁶ /ft	Orbiter Roll (PHII), deg	Angle of Attack (α), deg			
		25	30	35	40
0.56	0.0	1,6,16,17	2,18	3,5,19	4
	-90.0		7		
	-180.0		8		
1.50	0.0	9,14	10	11,13	12
	-90.0		15		

Run Number (TYP.)

ARVIN/CALSPAN FIELD SERVICES, INC.
AEDC DIVISION
VON KARMAN GAS DYNAMICS FACILITY
ARNOLD AIR FORCE STATION, TENNESSEE

DATE COMPUTED 1-FEB-83
TIME COMPUTED 09:12:16
DATE RECORDED 23-NOV-82
TIME RECORDED 21:46:12
PROJECT NUMBER V C-1L

RUN	ALP1 DEG	ALPHA DEG	PHI1 DEG	TIME SEC
1	5.00	25.00	0.00	1.50

HREF1 STREF1
(R= 0.0182) (R= 0.0182)
2.028E-02 6.239E-02

M	PT PSIA	T1 DEG R	T DEG R	P PSIA	Q PSIA	V FT/SEC	RHO LBM/FT3	MU LBF-SEC/FT2	RE FT-1	PT2 PSIA
9.89	377.83	1756.7	88.9	9.189E-03	0.63	4572.4	2.790E-04	7.153E-08	5.543E+05	1.167E+00

GAGE NO	2Y/B	T1 DEG R	TW DEG R	SRCK	QDOT BTU/FT2-SEC	H(TT) BTU/FT2-SEC-K	ST(TT)	H(TT)/HREF	ST(TT)/STREF
101	0.590	531.387	608.037	0.098	9.389E+00	8.174E-03	2.508E-02	4.030E-01	4.020E-01
103	0.630	536.123	614.018	0.098	1.242E+01	1.087E-02	3.336E-02	5.362E-01	5.346E-01
104	0.660	532.324	612.177	0.098	1.271E+01	1.111E-02	3.408E-02	5.476E-01	5.461E-01
105	0.680	532.175	614.230	0.098	1.323E+01	1.158E-02	3.553E-02	5.710E-01	5.694E-01
106	0.710	532.050	617.464	0.098	1.391E+01	1.221E-02	3.745E-02	6.020E-01	6.002E-01
107	0.730	531.375	619.279	0.098	1.465E+01	1.286E-02	3.950E-02	6.351E-01	6.331E-01
108	0.760	531.175	625.950	0.098	1.565E+01	1.384E-02	4.243E-02	6.824E-01	6.800E-01
109	0.780	531.655	627.824	0.098	1.624E+01	1.439E-02	4.410E-02	7.094E-01	7.069E-01
110	0.810	532.216	631.410	0.098	1.683E+01	1.496E-02	4.585E-02	7.376E-01	7.348E-01
112	0.860	529.301	640.978	0.098	1.960E+01	1.751E-02	5.383E-02	8.664E-01	8.627E-01
113	0.890	531.780	649.479	0.099	2.097E+01	1.894E-02	5.799E-02	9.338E-01	9.294E-01
114	0.900	526.085	652.425	0.099	2.239E+01	2.027E-02	6.207E-02	9.996E-01	9.948E-01
201	0.600	534.492	606.768	0.098	1.036E+01	9.011E-03	2.765E-02	4.443E-01	4.432E-01
202	0.620	536.024	612.816	0.098	1.248E+01	1.091E-02	3.347E-02	5.379E-01	5.364E-01
203	0.650	536.312	617.956	0.098	1.272E+01	1.117E-02	3.427E-02	5.510E-01	5.493E-01
204	0.670	525.132	606.584	0.098	1.271E+01	1.105E-02	3.390E-02	5.447E-01	5.434E-01
205	0.700	531.181	619.031	0.098	1.378E+01	1.212E-02	3.716E-02	5.975E-01	5.956E-01
206	0.720	532.236	627.074	0.098	1.568E+01	1.366E-02	4.256E-02	6.846E-01	6.822E-01
207	0.750	530.458	626.780	0.098	1.612E+01	1.426E-02	4.373E-02	7.033E-01	7.008E-01
208	0.770	524.152	624.704	0.098	1.608E+01	1.421E-02	4.356E-02	7.006E-01	6.982E-01
209	0.790	532.343	634.259	0.098	1.736E+01	1.547E-02	4.739E-02	7.626E-01	7.596E-01
210	0.820	531.980	631.349	0.098	1.734E+01	1.541E-02	4.722E-02	7.597E-01	7.568E-01
211	0.840	533.715	636.623	0.098	1.873E+01	1.672E-02	5.124E-02	8.245E-01	8.212E-01
212	0.870	522.964	635.867	0.098	2.007E+01	1.790E-02	5.486E-02	8.828E-01	8.792E-01
213	0.890	532.228	634.680	0.098	1.851E+01	1.649E-02	5.054E-02	8.133E-01	8.101E-01

Sample 7.1 Typical Tabulated Data on the Wing Leading Edge Heating Test

APPENDIX I

REFERENCE HEAT-TRANSFER COEFFICIENTS

In presenting heat-transfer coefficient results it is convenient to use reference coefficients to normalize the data. Equilibrium stagnation point values derived from the work of Fay and Riddell* were used to normalize the data obtained in this test. These reference coefficients are given by:

$$H_{REF}, H(REF) = \frac{8.17173(PT2)^{1/2}(MUTT)^{0.4} \left[1 - \frac{P}{PT2}\right]^{0.25} [0.2235 + (1.35 \times 10^{-5})(TT+560)]}{(RN)^{1/2}(TT)^{0.15}}$$

and

$$STREF = \frac{H(REF)}{(RHO)(V) [0.2235 + (1.35 \times 10^{-5})(TT + 560)]}$$

where

PT2	Stagnation pressure downstream of a normal shock wave, psia
MUTT	Air viscosity based on TT, lb _f -sec/ft ²
P	Free-stream pressure, psia
TT	Tunnel stilling chamber temperature, °R
RN	Reference nose radius, used to calculate H(REF) • (RN = 0.0175 ft)
RX	where X = 1,2, or 3 is the reference dimension used to calculate HREF and STREF for 2-D stagnation points. For Phase III, R1 = 0.0117, R2 = 0.0208, and R3 = 0.042. For Phase IV, R1 = 0.0182
RHO	Free-stream density, lbm/ft ³
V	Free-stream velocity, ft/sec

*Fay, J. A. and Riddell, F. R. "Theory of Stagnation Point Heat Transfer in Dissociated Air," Journal of the Aeronautical Sciences, Vol. 25, No. 2, February 1958.